To the Graduate Council:

I am submitting herewith a thesis written by Gary David Knox entitled "Combined Fluidization and Coal Feeding in a Model Fluidized Bed--Pipe Grid Feeder." I recommend that it be accepted in partial fulfillment of the requirements for the degree of Master of Science, with a major in Mechanical Engineering.

H. J. Wilkerson

H.J. Wilkerson, Major Professor

We have read this thesis and recommend its acceptance:

R. J. Edmondson

R. L. Maxwell

Accepted for the Council:

L Evans Roth

Vice Chancellor
Graduate Studies and Research

3

COMBINED FLUIDIZATION AND COAL FEEDING IN A MODEL FLUIDIZED BED--PIPE GRID FEEDER

A Thesis

Presented for the

Master of Science

Degree

The University of Tennessee, Knoxville

Gary David Knox

March 1981

ACKNOWLEDGMENTS

The author wishes to gratefully acknowledge the advice and assistance of many individuals during this investigation. He is particularly appreciative to Dr. H.J. Wilkerson, his major professor, who provided much guidance and support in this endeavor. Gratitude is also expressed to Dr. R.J. Krane, Dr. A.J. Edmondson, and Professor R.L. Maxwell who served on the author's graduate committee and reviewed this thesis.

Appreciation is also expressed to Mr. Rodney L. Henry and Mr. Reid L. Kress, fellow graduate students who worked on the project concurrently with the author. Messrs. Tim Lee, Hubert Black, Galen Bullock, and Brett Carpenter, undergraduate students, capably assisted in the design of the experimental system. Shop technicians Messrs. D.A. Johnson, Alfred West, James Hunley, Dennis Higdon, and Michael Howell deserve much credit for their excellent work in the construction of the experimental facility. The figures and graphs in this thesis were skillfully drawn by Jeff Bailey.

The greatest appreciation is expressed to the author's wife, Melissa. Her support, patience, understanding, and love sustained him through this undertaking. Gratitude is also extended to both sets of parents.

Financial support for this work was provided by the Tennessee Valley Authority under contract. Dr. Arnold Manaker, Mr. Henry Withers, and Mr. Clarence Andrews served as contract monitors.

ABSTRACT

Coal feeders for fluidized bed combustors must provide a uniform, regulated supply of coal to the combusting bed for efficient operation. Many of the fluidized bed coal feeders used in the past have suffered from plugging, maldistribution, and other problems. Thus, further coal feeder development work is necessary before the fluidized bed combustion process can become a viable alternative for power production. A project has been initiated for the development and evaluation of coal feeders which combine the fluidization and coal feeding functions. The combination of these two functions can potentially solve several of the problems experienced with past coal feeder designs.

An experimental ambient temperature atmospheric fluidized bed test facility has been designed and constructed for the evaluation of the combined function coal feeders. Methods were selected and developed to evaluate both the fluidization and coai feeding performance of the feeders. Fluidization evaluation was accomplished by measuring the expansion of the fluidized bed and the magnitude and frequency of the pressure drop fluctuations through it. The coal feeding distribution measurement system utilized a magnetically susceptible imitation coal material as a tracer. Specially designed sample probes were used to collect bed material samples during coal feeding tests. The samples were analyzed to determine the imitation coal distribution within the bed.

Basic performance tests were conducted on the experimental facility with a perforated plate air distributor. The fluidization produced by the distributor was characterized by large bubbles or slugs of air which caused significant displacements of the bed

material as they rose through it. An in-bed pipe grid combined coal feeder and air distributor was designed and tested. The initial configuration of this feeder did not give uniform fluidization, but a revised configuration did give uniform fluidization. Both feeder configurations distributed coal to all portions of the bed. Although the local coal concentrations varied from position to position within the bed and from test to test, the average variations were within reasonable limits.

FOREWORD

"So many of my best ideas have proven mistaken that I am now forced to maintain an attitude of humility with respect to fluid-bed art, clinging to what I know for sure, demanding strong proof of the untried, yet keeping flexible mind against the new surprises which are surely to come."

Arthur M. Squires

TABLE OF CONTENTS

CHAPTER PAGE

LIST OF TABLES

LIST OF FIGURES

LIST OF SYMBOLS

a arbitrary independent variable, dependent dimensions

A area, ft^2

Ar Archimedes number, dimensionless, $\frac{Re^2}{Fr_m} = \frac{\rho_g(\rho_s - \rho_g)D_p{}^3 g}{\mu^2}$, ratio of body-type forces to viscous forces

b pressure recovery factor, dimensionless, $\frac{(\rho V^2)_{actual}}{(\rho V^2)_{theoretical}}$, ratio of actual pressure to theoretical pressure

c speed of sound, ft/sec

C calculated result, dependent dimensions

d hole or orifice diameter, ft

D pipe or bed diameter, ft

f Blasius, Darcy, or Moody friction factor, dimensionless, $\frac{\Delta P}{\frac{L}{D}\frac{\rho V^2}{2g_c}}$, ratio of shear stress to inertia forces

F mass fraction, dimensionless, $\frac{\text{component mass}}{\text{total mass}}$, ratio of component mass to total mass

Fr Froude number, dimensionless, $\frac{V^2}{Lg}$ or $\frac{V^2}{D_p g}$, ratio of inertia forces to gravitational forces

Fr_m modified Froude number, dimensionless, $\frac{\rho_g}{\rho_s - \rho_g}\frac{V^2}{D_p g}$, ratio of inertia forces to gravitational forces multiplied by a density ratio

g acceleration of gravity, 32.174 ft/sec^2

g_c gravitational constant, 32.174 lbm ft/lbf sec^2

h piezometric head, ft

H bed diameter, ft

k specific heat ratio, dimensionless, $\frac{C_p}{C_v}$, ratio of specific heat at constant pressure (C_p) to specific heat at constant volume (C_v), 1.4 for air

K orifice flow coefficient, dimensionless, $\frac{Q}{A(2g\Delta h)^{1/2}}$

K' minor loss coefficient, dimensionless, $\frac{h}{V^2/2g}$

L length, ft

$\dot{m}$ mass flow rate, lbm/sec

M Mach number, dimensionless, $\frac{V}{c}$, ratio of inertia forces to elastic forces

n number of holes or orifices, dimensionless

P pressure, lbf/ft^2

q volumetric flow rate through a single hole or orifice, ft^3/sec

Q total volumetric flow rate, ft^3/sec

r cylindrical coordinate system radial component, ft

R gas constant for air, 53.34 ft lbf/lbm °R

Re Reynolds number, dimensionless, $\frac{\rho DV}{\mu} = \frac{DV}{\nu}$, ratio of inertia forces to viscous forces

s manometer pressure reading, ft or lbf/ft^2

SG specific gravity, dimensionless, $\frac{\gamma_{substance}}{\gamma_{water}}$, ratio of specific weight of a substance to the specific weight of water

t time, sec

T absolute temperature, °R

v component velocity, ft/sec

V velocity, ft/sec

$\forall$	volume, ft^3
w	uncertainty in an experimental measurement, dependent dimensions
W	weight, lbf
x	distance, ft
y	length, ft
z	cylindrical coordinate system axial component, ft
γ	specific weight, lbf/ft^3
Δ	denotes differential quantity
ε	voidage fraction, dimensionless
θ	cylindrical coordinate system tangential component, radians
μ	dynamic viscosity, lbf sec/ft^2
ν	kinematic viscosity, ft^2/sec
ρ	density, lbm/ft^3

Special Superscript

*	non-dimensional variable

Special Subscripts

a	air
b	bed
fl	fluidized
g	gas
i	inlet
mf	minimum fluidization
p	particle
r	cylindrical coordinate system component
s	solid
sf	superficial
sl	slumped

st	static
t	total
w	water
z	cylindrical coordinate system component
θ	cylindrical coordinate system component
∞	ambient condition
0	pipe inlet condition
1	orifice upstream pressure tap or bell mouth throat condition
2	orifice downstream pressure tap

CHAPTER 1

INTRODUCTION

Background

The New Source Performance Standards of 1978 [1][1], which superseded the Clean Air Act of 1971 [2], dictate that new coal fired steam generation facilities meet stringent standards in terms of sulfur dioxide (SO_2), nitric oxide (NO_x), and particulate emissions. Thus, power utilities and large industrial boiler users that burn coal are faced with a limited number of options to comply with the new regulations. Two major available choices are a switch from high sulfur eastern coal to low sulfur western coal or the implementation of a flue gas desulfurization system, i.e., scrubber, both of which are costly. Burning oil or natural gas in place of coal has occurred in the past, but this option is becoming prohibited by legislation and by the availability and cost problems associated with these fuels [3,4]. The remaining alternative for complying with the regulations is to develop new technologies. Three technologies with significant potential under current consideration are coal gasification or liquefaction with intermediate sulfur removal, coal beneficiation in the form of coal cleaning or solvent refined coal, and fluidized bed combustion [3,4]. The most promising of these technologies for a near term solution to the emissions problem is fluidized bed combustion, and this technology is the subject of this thesis.

---

[1]Numbers in brackets refer to similarly numbered references in the List of References.

A fluidized bed is a contained assemblage of particles which is suspended by a stream of fluid flowing upward through it. The weight of the particles is balanced by the buoyancy and drag forces of the fluid. The term "fluidized" is applied because in many ways the bed of particles behaves much like a fluid. The type of particles and fluidizing liquid or gas utilized in a fluidized bed vary from one application to another. In the case of fluidized bed combustion as referred to in this thesis, the fluidizing gas is air and the bed material is primarily limestone. Coal is most frequently burned in a fluidized bed combustor so the bed material also includes coal particles and ash. However, almost any combustible material can serve as the fuel including flammable liquids and gases. Two basic types of fluidized bed systems have been proposed--atmospheric and pressurized. Basically, atmospheric fluidized beds operate at pressures slightly above atmospheric, whereas pressurized fluidized beds operate at pressures several times the atmospheric value. Although both types have definite advantages [5], only atmospheric fluidized bed systems will be considered here as the development of this type is currently more advanced.

The fluidized bed concept is not new. Chemical engineers have been using the fluidization process for many years, particularly in operations requiring extensive mixing and maximum surface contact. In addition, metallurgists have used fluidization techniques for mineral and ore processing. The first documented report of fluidization associated with combustion is a patent by Fritz Winkler in 1921 [6]. Following Winkler's work further fluidization developments were made in Germany, Great Britain, and the United States; but fluidization work involving combustion was scattered and without direction for approximately four decades. During the early 1960's much of the fluidized bed combustion research was under the direction of the British Coal Utilization Research Association and the Central Electricity Generating Board in Great Britain. At about the same time fluidized bed combustion research was undertaken in the United States by the firm of Pope, Evans, and Robbins [7]. Fluidized bed combustion work soon expanded in the United States largely under funding from the Environmental Protection Agency and the Office of Coal Research of the Department of the Interior. During subsequent years fluidized bed combustion research has flourished in many countries under a large variety of organizations.

Several aspects of the fluidized bed combustion process make it an attractive alternative for boiler design. The major incentive to develop the fluidized bed combustion process in the United States is the low sulfur dioxide emission level characteristic of the process. Much of the sulfur released from the burning coal is captured by the calcium oxide (lime) from the calcined limestone bed material resulting in the production of calcium sulfate (gypsum) and thus the reduction of sulfur dioxide emissions. Unlike the wet sludge byproduct of a flue gas desulfurization unit, the spent limestone sorbent from a fluidized bed is in an easily handled dry solid particulate form. This latter byproduct can be used as a source of agricultural lime and trace minerals, a source of sulfur or sulfuric acid, a road base soil stabilization material, a wet scrubber sludge fixative, a cement set retarder, and an acid neutralizer for strip mine terrain [8]. In addition, because part of the heat transfer tubes for a fluidized bed combustor are placed within the bed material, high heat transfer coefficients can be obtained even with a relatively low bed to tube temperature differential due to the high heat flux from the bed material to the immersed tubes. The 1500 to 1600°F average fluidized bed temperature, which is low in comparison to the temperature of conventional furnaces, permits several advantages. Nitric oxide emissions resulting from combustion are reduced, fouling of the convection pass heat transfer tubes is lessened because the combustion temperature is below the coal ash softening temperature, the need for soot blowers is reduced or eliminated, and fewer heavy metal vapor contaminants are released from the bed [4,5]. Essentially any fuel with a net calorific value can be used in a fluidized bed. The reduction of the slagging and fouling problem allows many high ash fuels which are normally unsuitable for conventional furnaces to be burned in a fluidized bed combustor. Therefore, more plentiful and cheaper high ash, high sulfur coals can be utilized as a source of energy [5].

As would be expected, there are also several disadvantages associated with the fluidized bed combustion process. The combustion efficiencies achieved by fluidized beds are typically lower than those experienced with conventional furnaces [4]. This decreased efficiency is largely a result of the elutriation, or carryover, of unburned carbon particles in the exhaust gases. Potential solutions for the particle elutriation problem include recycling the unburned material, lowering the fluidization velocity, and increasing the bed material height. Fluidized bed combustors contain high dust loadings in the exhaust gases due to the attrition of the limestone and ash bed material and the previously mentioned elutriation of unburned fuel material. This particulate emission problem is normally dealt with through the installation of cyclone separators, baghouse fabric filters, and/or electrostatic precipitators [4]. The combustion air pumping power requirement for a fluidized bed is relatively high in comparison to a conventional boiler. However, this additional power requirement is partially offset by the savings in mill power because significantly less fuel crushing preparation is required for a fluidized bed unit than for a pulverized coal unit. This savings in mill power is based on present plans to utilize 0.25 inch top size coal in fluidized bed combustors [5] as compared to a sieve size of approximately 200 for pulverized coal. Load response with a fluidized bed boiler is somewhat more difficult to achieve than with a conventional unit as the fluidized bed temperature must be kept essentially constant for optimum emissions control and efficient combustion. Because the bed heat flux is essentially constant, the only way to change the heat absorption is to change the amount of submerged tube surface. It appears that this can best be accomplished by changing the bed height or by starting up or shutting down portions of the bed. The limestone sorbent required for a fluidized bed system entails additional transportation, storage, and materials handling costs. Also, the spent limestone removed from the bed contains a significant amount of sensible heat which should be recovered for efficient operation [4].

Both the attractive potential and the possible problems associated with fluidized bed combustion systems have sparked a great amount of detailed study covering many areas. These areas include the basic fluidization process, coal and limestone materials handling and distribution, combustion efficiency, heat transfer, boiler control and load following, erosion and corrosion of internal structures, and emissions control. Much of the current work in these areas is sponsored by the Department of Energy, the Electric Power Research Institute, the Environmental Protection Agency, and the Tennessee Valley Authority. Basic and applied research is being conducted by power utilities, universities, government research divisions, and numerous private companies [9; 10, p. 3-1].

Coal Feeding

A major problem with fluidized bed combustion systems is the difficulty encountered in feeding coal to the combustor. The coal feeding problem actually consists of two parts. First, the coal must be transported from storage to the fluidized bed, and then it must be injected into the bed. Attempts have been made to adapt conventional coal feeding methods to fluidized beds with only limited success. Several new coal feeding methods have been proposed, but these too exhibit problems.

A suitable fluidized bed coal feeding system must supply a controlled flow of coal to the bed in a uniform manner. Uniform coal distribution is prerequisite to the attainment of a uniform bed temperature. Without a uniform bed temperature, the heat transfer to the in-bed tubes is inefficient. Also, nonuniform combustion allows hot and cold regions to develop in the bed which cause the formation of oxidizing and reducing zones. The existence of these zones adversely affects the desired chemical reactions in the bed and thus leads to a decrease in sulfur capture and an increase in nitric oxide emissions. The oxiding and reducing zones also contribute to heat transfer tube corrosion.

The first part of the coal feeding problem is the transport of the coal from the storage location to the fluidized bed. In the case of an overbed feed system, the transport problem is not too difficult as conventional methods such as belt or screw conveyors or gravity feed from overhead bins can be used. However, most other coal feed systems utilize the pneumatic transport process for the conveyance of the coal from storage to the fluidized bed. Three specific problems are involved with pneumatic transport systems. First, the material to be conveyed must be introduced into the transporting air system. Rotary valves and gate locks are frequently used to get particulate material into pressurized transport lines [11]. Considerable experience has been gained in the pneumatic transport of pulverized coal with Fuller-Kinyon pumps in conventional systems. Currently, efforts are being made to adapt the Fuller-Kinyon pump idea to larger particles such as would be used in fluidized beds, but initial operational problems are possible with these large particles [12, pp. 22-25, App. 6-9; 13]. Because multiple feed points are required in all but the smallest fluidized bed combustors, a second problem arises in the division of the pneumatically conveyed feed material into individual supply lines for the coal injection points. Caldwell [14] describes some flow splitting methods which have been developed, and additional methods are outlined by Combustion Engineering [15, pp. 112-121]. A third problem common to all pneumatic transport systems is the particle degradation which occurs in conjunction with the erosive wear on the system components [16,17].

The second part of the coal feeding problem concerns the injection and distribution of the coal into the fluidized bed. A summary of several proposed coal feeding methods is contained in design reports by Combustion Engineering [15, pp. 107-121] and the Fluidized Combustion Company [18]. One of the first coal feeder concepts tested in a sizeable fluidized bed combustor was the so-called needle design. A needle is basically a slanted pipe projecting into the bed region from one of the side walls through which coal is pneumatically transported. Coal feeding needles were utilized in the multicell fluidized bed boiler designed by Pope, Evans, and Robbins and Foster Wheeler Energy Corporation which was built at Rivesville, West Virginia [19; 20, pp. 101-110]. Even after several modifications were made to the original needle design, the devices continued to suffer from plugging which occurred when the coal softened as it came into contact with the hot needle walls or when oversized lumps or wet coal bridged in the needles [12, pp. 13-15; 21]. The overbed spreader feeder arrangement is being utilized in the industrial size fluidized bed combustor being operated at Georgetown University [22]. With an overbed feeder it is difficult to service a large bed effectively. Also, unless the coal is double screened, a significant amount of the coal fines are elutriated before reaching the bed surface. Some of these fines do burn above the bed, but the sulfur which is released cannot be captured by the limestone bed material. Those fines which do not burn contribute to the exhaust gas dust loading and cause a decrease in the combustion efficiency. Many of the coal feeder devices which are currently being used or considered contain some type of nozzle injectors through which coal is fed by a pneumatic transport system. The cold model fluidized bed described by Fraas and Holcomb [23] utilized four coal feeding nozzles each in the form of a cross at the top of a pipe. The fluidized bed boiler at the Babcock Renfrew Works in Great Britain contains nine T-shaped feed injectors which are supplied by a pneumatic transport system [24]. The "six by six" fluidized bed combustion test facility of Babcock and Wilcox at Alliance, Ohio, also utilizes underbed coal distributors supplied by a pneumatic transport system [25]. In addition to the three pneumatic transport problems described previously, nozzle-type feeders also experience problems with coking and plugging, coal maldistribution in the bed, and bed weeping or draining when the fluidizing air is turned off.

Coal Feeder Evaluation Project

More work needs to be done on fluidized bed coal feeders as evidenced by the overview in the preceding section. Thus, this project was conceived with the purpose of developing, designing, and testing innovative coal feeding methods. The project has also included the design and fabrication of an experimental test facility and the development and implementation of fluidization and coal feeding evaluation methods.

All coal feeding methods considered in this project combine the coal and its transport air with all the fluidization air prior to entry into the fluidized bed. In previously reported work utilizing pneumatic transport of the coal to the fluidized bed feeding points, only a fraction of the total bed air flow passed through the coal injection points. However, several potential advantages exist when the coal feed and fluidization processes are combined. First, one of the major problems experienced in past fluidized bed operation has been nonuniform combustion which leads to the problems with nonuniform temperature distribution discussed previously. This combustion non-uniformity occurs primarily because a proper mixture of coal and air is not distributed throughout the bed. By combining the coal with all the fluidization air, both of these combustion ingredients will be present together in the fluidized bed. Thus, if essentially uniform fluidization can be achieved, then it follows that the coal distribution has the same degree of uniformity. In these combined coal and air feeding schemes, a small amount of initial transport air containing the coal in a moderately dense mixture is combined with the balance of the fluidization air closely upstream of the bed injection points. This late combination is desirable because the fluidization air in an operating fluidized bed combustor is preheated to approximately 600°F. Due to the extremely dilute mixture of the coal in the fluidization air, the possibility of coal agglomeration in the transport lines or feeding devices is small.

For a coal feeder of this type to operate successfully, it must provide good bed fluidization as well as uniform coal feeding. Thus, methods must be available to evaluate both aspects of the coal feeder performance. The fluidization evaluation methods used in this project were essentially adopted from the work of other fluidized bed researchers. In addition, a large part of the fluidization evaluation was performed visually with the assistance of video recordings. However, considerable time and effort were expended in the development of an original coal feeding evaluation method. This method was used to analyze the resulting coal feed distribution in the fluidized bed of limestone. The coal/air stream splitting and erosion aspects of the pneumatic transport part of the coal feeding process discussed previously were not investigated in detail in this study.

A large amount of work has been invested in the design, fabrication, and shakedown of the experimental test facility. This facility is a cold model atmospheric fluidized bed incorporating much flexibility so that a variety of different coal feeding devices can be evaluated in it.

A pipe grid feeder was chosen as a representative in-bed coal feeder combining the coal feeding and fluidization functions. Some analysis was performed on this feeder concept prior to the design and fabrication phases. Then the feeder was evaluated in the experimental test facility. The results of the tests with this coal feeder and a summary of its performance characteristics are included.

Limited theoretical analysis has been performed in this project. Some analysis was required in the design of the experimental facility and the pipe grid coal feeder. Also, a chapter is included on the scaling or modeling aspects of such an experimental system, but the comments contained therein are mostly a summary of information from the literature.

Several conclusions are drawn from the results obtained and the experiences gained in this thesis project. These conclusions are supplemented with recommendations for future work with the present experimental facility and for coal feeder design and testing of a similar nature.

The work presented in this thesis is only a part of a more comprehensive coal feeder evaluation project. The in-bed pipe grid coal feeder referred to is one of several coal feeders which have been or will be tested in the experimental facility. The basic philosophy of the total project has been to spend a moderate amount of time, effort, and money developing and testing coal feeders combining the fluidization and coal feeding functions which exhibit a reasonable likelihood of success. These coal feeder evaluations serve as a culling process, so that extensive development effort will be spent only on those coal feeders which exhibit significant promise. At a later time the more promising candidates can be tested in a hot fluidized bed.

This coal feeder evaluation project is supported by the Tennessee Valley Authority (TVA). The TVA, as the nation's largest electric power utility, is actively involved in the research, development, and design of a commercially viable fluidized bed combustion facility. This project has been in support of the TVA's 20 megawatt pilot plant scheduled for operation in 1982. Further plans of the TVA are to have a 200 megawatt demonstration unit in operation by 1985.

CHAPTER 2

FLUIDIZATION EVALUATION METHODS

Introduction

Fluidization evaluation for comparative purposes is difficult. Many fluidization quality indexes and measurement methods have been proposed, but none of these are universally acceptable or applicable. The major problem is that there is no general agreement as to what constitutes good fluidization. In fact, the desired qualities vary greatly depending on the application being considered. For example, in some applications a quiescent bed with minimal bubbling is preferred, while other applications are best served by a relatively violent bed with extensive bubbling. Bubble formation is detrimental to gas-solids contacting because the gas within the bubbles bypasses the solid phase. However, bubble passage through the bed is primarily responsible for the mixing which occurs in a fluidized bed. Although bed design is not too difficult when only one of the two effects is desired, fluidization processes such as fluidized bed combustion require a combination of both effects. Gas-solids contact is important both in the coal combustion process and in the limestone utilization as a sorbent. At the same time, extensive mixing is desirable so that the coal combustion and thus the bed temperature will be somewhat uniform across the bed for maximal heat transfer and for minimal in-bed tube corrosion. Therefore, in such a case, not only is the evaluation of the fluidization a problem, but the specification of the type of fluidization to be attained is not very clear-cut.

Fluidization Quality

Many different methods for evaluating fluidization quality have been developed. Some of these methods are enumerated by Orr [26, pp. 209-215] and by Romero and Johanson [27]. They include the measurement of pressure fluctuations, light beam transmission, capacitance changes, alpha and gamma ray absorption, x-ray attenuation, and apparent viscosity. Essentially all of these methods are an attempt to quantify the fluidized bed density. They can be divided into two basic classes. First, some of them measure local bed densities while the balance measure gross or overall bed densities. Second, part of the methods require some type of probe or instrumentation within the bed, while the remainder utilize measuring equipment which is completely external to the bed.

Morse and Ballou [28] used a capacitometer to measure local bed densities. Their system was based on a small probe containing three parallel vertical plates which was placed in the bed. The probe measured the capacitance changes between the plates caused by the presence or absence of bed material. A "uniformity index" was derived which was calculated by dividing the percent deviation in the bed density by the frequency of the density fluctuations. Romero and Johanson [27] also used an internal probe to detect local changes in bed density. Their probe consisted of a bubble collector nozzle containing a specially constructed hot-wire anemometer. They collected density data by recording bubble passage at the bed surface.

External fluidization quality measurements include the work of

Shuster and Kisliak [29] who used the magnitude and frequency of pressure drop oscillations across a section of a fluidized bed to calculate a "quality index." This index was calculated by dividing the average pressure drop deviation by the frequency of these pressure drops. Grohse [30] used x-ray absorption to measure bed density profiles in an effort to characterize fluidization. Similarly, Bailie et al. [31] used gamma ray attenuation to produce data from which an "index of instability" was calculated. This index is purported to measure bed stability as well as uniformity.

In all of these studies, the experiments were performed with small (1.75 to 4 inch diameter) columns. The parameters varied were the bed height and the fluidization velocity. Some of the tests also compared the effects of different gas distributors, particle sizes and size ranges, and bed geometries. All of the fluidization quality evaluation methods appeared to produce meaningful results as long as the range of bed behavior tested was sufficiently great. In every case, the actual fluidization quality was determined by visual observation in order to validate or invalidate the measured results.

A limited amount of effort has been devoted to the development of a theoretically based fluidization quality standard. Rice and Wilhelm [32] investigated fluidization quality by performing a stability analysis of the interface between the emulsion phase and the particle free, fluid phase of a fluidized bed. Their theoretical results agreed reasonably well with experimental ones. Romero and Johanson [27] extended the work of Rice and Wilhelm by developing four dimensionless groups to characterize the uniformity of fluidization.

These groups include the Froude and Reynolds numbers and density and geometry ratios defined respectively as

$$\frac{V_{mf}^{2}}{g\,D_p}\ , \quad \frac{D_b V_{mf} \rho_g}{\mu g_c}\ , \quad \frac{\rho_s - \rho_g}{\rho_g}\ , \text{ and } \frac{H_{mf}}{D_b}\ . \tag{2.1}$$

If the product of these groups is less than 100, then the fluidization is termed particulate, whereas fluidization yielding a product greater than 100 is referred to as aggregative. These two terms are essentially arbitrary designations of fluidized bed behavior. However, in general, fluidized beds using water as the fluid are particulate while those utilizing air are aggregative. Normally, the fluidization quality decreases as the product of the groups increases. Seki et al. [33] developed a modified Froude number to characterize fluidization. They treated particle-fluid motion as two phase flow and established a wavelength based on the physical properties of the fluid and particles in the bed. Then they used their theoretical results to predict a discriminating criterion between particulate and aggregative fluidization which they verified by comparison to experimental results.

Measuring Fluidization Quality

As discussed in Chapter 1, a two-fold evaluation is performed on the coal feeders tested in this project. The coal feeders must be able to fluidize the bed and uniformly distribute coal into it. Because it was expected that visual observation would be a large part of the fluidization evaluation, the majority of time and development effort were spent on the coal feeding evaluation. Also, at the outset it was believed that a given coal feeder either would or would not fluidize the bed, although this was found not to be the case. Rather, it has been learned that a wide variety of gas distributing devices will fluidize the bed, and the degree of difference in the resulting fluidization quality is often not readily apparent.

Numerous fluidization quality measurement methods, including those described in the previous section, were considered for use in this project. Almost all of the available methods require a sizeable investment of money and/or time for the acquisition or development of the necessary equipment and for the tedious calibration processes required. Also, many of these methods measure very localized bed performance, which while satisfactory for the small beds in which they were developed, makes then unsuitable for the larger bed of the present experimental facility. Essentially, the only fluidization evaluation methods which do not fall in these categories are the use of bed pressure fluctuations and frequencies and the measurement of bed expansion characteristics. These methods are attractive from an equipment standpoint because pressure transducers and a strip chart recorder were readily available.

Bed pressure drop fluctuations and frequencies have been used by numerous fluidized bed researchers in an attempt to quantify the bed behavior. The work of Shuster and Kisliak [29] was mentioned previously in which pressure measurements were used to calculate a fluidization quality index. Lirag and Littman [34] studied the pressure fluctuations and frequencies in a small (2.5 inch diameter) fluidized bed in an effort to determine the effects of gas velocity, bed height, particle size, and particle density on these parameters. They applied statistical analysis to the data and were able to identify a periodic component in the fluctuations. Verloop and Heertjes [35] considered periodic pressure fluctuations from a theoretical viewpoint and developed a critical bed height based on the pressure frequency and wave velocity in the bed. Above this critical height the pressure fluctuations change significantly and bubbling or slugging ensues. More commonly, the relative magnitude, fluctuations, and frequencies of overall bed pressure drops have been used to characterize the flow behavior within the bed [36, 37, 38, 39, 40]. As described by Orr [26, pp. 200-202], the pressure drop through the bed increases as the gas velocity is increased from zero to the minimum fluidization velocity. After this point, in a uniformly fluidized bed, the pressure drop remains essentially constant or increases only slightly as the fluidization velocity is increased. However, in a channeling bed this pressure drop decreases with fluidization velocity increases beyond the minimum, while in a slugging bed the pressure drop increases significantly with a fluidization velocity increase. Canada et al. [39] concluded from their studies with a bed very similar to the present experimental facility that for the range of fluidization velocities being considered for combusting beds these pressure drops have a definite frequency and amplitude and are quite repeatable. They compared pressure fluctuations and frequencies for several configurations and were able to characterize the flow regimes represented.

The primary problem with the pressure drop measurements is the difficulty in interpreting the results for conditions which do not span several flow regimes. It may be that the value of such measurements is less in the present study which utilizes several consistent parameters, e.g., bed size, particle size and density, and fluidization velocity range, as compared to other studies in which these parameters are varied significantly.

The fluidized bed expansion is an indication of the fluid phase distribution within the solid phase of the bed. It is related to the average bed density or equivalently the average bed void fraction which are both characteristic of the flow regime, the particle properties, and the bed geometry. Cranfield and Geldart [41] utilized bed expansion measurements in their study of a fluidized bed very similar to the present one. They attempted to predict mean bubble diameters using bed expansion data but did not have much success. However, Canada et al. [39] were able to correlate bed expansion data in a form by which they could predict significant changes in the bed flow regimes. Babu et al. [42] reviewed many of the published bed expansion correlations and then developed a more inclusive one which compares well with published bed expansion data.

While numerous theories have been developed to predict bed expansion, and several correlations have been derived to relate experimental results, it appears that this parameter actually has been used for very few purposes other than the characterization of bed flow regimes. Thus, the same difficulties may be encountered with the use of bed expansion measurements as were discussed in relation to the pressure drop measurements.

Flow Regimes

The fluidization quality which can be achieved in a fluidized bed is closely related to the flow regime in which the bed is operating. The flow regimes also appear to be important in the scaling concepts discussed in Chapter 4. These flow regimes have been defined in various manners by several researchers.

Geldart [43] made one of the first attempts to define bubbling fluidized bed flow regimes. His classification system is based on the properties of the solids and gases composing the bed. Four groups are identified based on the relative average particle size and the particle-gas density difference. Briefly, Group A, aeratable materials, are fine solids which fluidize with good bubble distributions. Group B, sandy solids, are larger particles in which the bubbles grow and coalesce. Group C, cohesive solids, are either very small or cohesive and are difficult to fluidize. Group D, spoutable solids, are coarse particles which are capable of forming a spouted bed.

Later flow regime classifications for gas-solid systems are also based on particle size. Yerushalmi et al. [44] classified small particle regimes on the basis of the slip velocity and the volumetric solid concentration in the system. The slip velocity is the difference between the gas velocity and the solid velocity. The four regimes defined are a particulate regime, a bubbling/slugging regime, a fast fluidization regime, and a dilute phase flow regime. A fifth regime, the turbulent regime, may exist between the bubbling/slugging and fast fluidization regimes. These regimes will not be described as the particle size range for which they are applicable is below that of the present system. More representative particle sizes are the basis of flow regimes proposed by Canada et al. [39] and Canada and McLaughlin [45]. These regimes are defined for large particle beds over a wide range of gas velocities. The flow regimes, in terms of increasing fluidization velocity, are bubbly flow, apparent slug flow, plug flow, and turbulent flow. In bubbly flow the characteristic small bubbles remain discrete as they rise through the bed. In apparent slug flow the bubbles coalesce into large voids which rise through the bed and produce large oscillations of the bed material. Plug flow is a type of apparent slug flow in which the voids formed completely span the bed cross section. Turbulent flow is characterized by smaller voids, extensive lateral mixing, and milder oscillations of the bed material in comparison with the previous regimes.

Catipovic et al. [46] obviated the need for two sets of flow regimes by categorizing all fluidized bed behavior in terms of the particle diameter and the fluidization velocity. They qualitatively define four fluidization regimes while acknowledging the need for more experimental data to quantify these regimes. The fast bubble regime is characteristic of fine or small solids. It exists in a bed in which the bubbles move upward through the dense phase more quickly than the interstitial gas moves through the bed. The slow bubble regime is characteristic of larger particles. In this regime bubbles move upward through the dense phase more slowly than the interstitial gas moves through the bed. The rapidly growing bubble regime encompasses a wide particle size range at velocities greater than those of the slow bubble regime. In this regime large pressure drop oscillations exist within the bed and may develop into slugging if the bed is sufficiently deep. The turbulent regime appears to cover the full range of particle sizes and exists at higher velocities than any of the other regimes. This regime is characterized by smaller pressure drop oscillations than the previous regime while still possessing superior solids mixing characteristics. This four regime scheme has been modified by van Deemter [47] to include a homogeneous fluidization regime at the lowest velocities and a fast fluidization regime at the highest velocities. He notes that the boundaries between the flow regimes depend on the density ratio of the fluidized solid to the fluidizing gas, and he includes the minimum fluidization velocity and particle terminal velocity in his flow regime mapping.

As briefly discussed in Chapter 6, the experimental fluidized bed has been determined to operate in the apparent slug flow regime or its equivalent, the rapidly growing bubble regime. Both the average particle size and the velocity range used in the tests correlate with the conditions which distinguish these two regimes. The most significant characteristic of these regimes in terms of the experimental fluidized bed behavior is the large bed pressure drop oscillation or slugging which occurs. This slugging phenomenon is discussed extensively in the literature [26, 35, 36, 37, 38, 39, 40, 41, 44, 45, 46, 47, 48, 49, 50]. The slugging caused considerable initial concern until an examination of these references revealed that it is to be expected for the conditions under which the experimental fluidized bed is operated.

Bed Internals

One of the primary ways to reduce slugging in a fluidized bed without changing the basic design and operational parameters is to install internal structures within the fluidization zone. These bed internals serve either to restrict the bubbles from coalescing into slugs or to break up the slugs once they have been formed.

A moderate amount of information exists in the literature concerning the design and function of fluidized bed internals. Kunii and Levenspiel [51, pp. 251-254] briefly describe both horizontal and vertical bed internals arrangements. In his comparison of small particle and large particle fluidized beds, Squires [52] points out the need for internals in tall beds to redistribute the vertical bubble paths at successive levels. Volk et al. [53] describe a specific fluidized bed application in which bed internals were necessary to achieve successful operation. One of the best overviews of fluidized bed operation with internals is that of Harrison and Grace [54]. They consider all the major types of internals which have been proposed and discuss the manner in which these internals affect the bed operation.

Bed internals in the form of heat transfer tubes were selected for the experimental fluidized bed facility as internals of this type would be present in an actual hot bed. A physical description of the heat transfer tube assembly which was fabricated is contained in Chapter 5.

CHAPTER 3

COAL FEEDING EVALUATION METHODS

Background

A key requirement for the development of coal feeders for a fluidized bed is to have a reliable and efficient method for evaluating the performance of the feeders. The primary criterion to be judged is whether or not a feeder provides a uniform distribution of the coal throughout the bed. In a hot bed (i.e., one in which combustion is occurring) the degree of uniformity can be established in terms of the combustion process by utilizing thermal or chemical sensors. However, in a cold (ambient temperature) bed, the coal or other feed material must be analyzed directly to determine the degree of its distribution. Thus, there must be a detectable difference, albeit natural or artificial, between the feed material and the bed material. A natural difference can be due to color, chemical reactivity, specific gravity, conductivity, magnetic susceptibility or any other measureable property of the two materials. An artificial difference is produced through some alteration of the feed material by creating one or more characteristics which make it more easily distinguished from the bed material. Or, an imitation material with properties similar to the feed material, but which can be easily distinguished from the bed material or detected in it, can be substituted for the actual feed material of interest. In both of these latter cases, the altered or substitute material is referred to as a tracer.

Many different methods have been developed to study fluidized bed behavior using these natural and tracer materials. Generally, the methods for evaluating solids mixing are the ones which can be applied to material feeding studies. Donlevy [55] suggests that these latter evaluation methods can be grouped into three basic types. Samples can be taken from a slumped or settled bed, samples can be removed from an operating bed, or measurements can be made on an operating bed.

Removing samples from a slumped bed after the fluidization air has been turned off is the method which seems to have been used the longest. This method is inherently somewhat inaccurate because the particles in the bed move in relation to one another during slumping. After defluidization the bed must be dissected in some manner to evaluate the dispersion of the feed material throughout the bed material. Rowe et al. [56] describe the use of a solidifying liquid such as paraffin to freeze the bed so that it may be sliced into layers to be analyzed. Sutherland [36] dissected the bed by hand and visually analyzed the dispersion of colored feed particles in uncolored bed particles. He described the process as "very tedious," and seemingly the only attractive aspect of his process was the ability to dissolve the color with acetone and then reuse the same material. Cranfield [57] slumped the bed and removed successive layers for analysis by carefully vacuuming the material. Rowe and Sutherland [37] also used suction to remove 2 inch layers from the bed. Both of these latter two studies utilized the magnetic response of the feed material to separate it from the unresponsive bed material. Babu et al. [58] vacuumed off layers of their bed material containing sodium tripolyphosphate particles mixed with glass beads, dissolved the sodium tripolyphosphate with hot water, and measured the change in weight to arrive at their results. Rowe et al. [56] used adhesive sheets of heavy plastic to remove successive layers of the bed material in one set of experiments. They state that photography or optical scanning methods can be used to analyze the samples after the bed is dissected. They also claim that electrically charged particles can be separated from uncharged particles following mixing in the bed by passing the mixture through an electric field.

Removing samples from an operating bed is a more accurate evaluation method than sample removal from a slumped bed. However, removing samples from an operating bed without disturbing the solids dispersion which is being measured is rather difficult. Then, too, once the samples are removed they must be analyzed in a manner such as those described previously. Tailby and Cocquerel [59] describe experiments in which material was removed from an active bed through tubes projecting through the base of the bed. They used colored and uncolored particles, dissolved the color coating with chloroform, and then analyzed the resulting colored liquid with a spectrophotometer by comparing this liquid with solutions of known concentration. Highley and Merrick [60] used sample probes projecting into the bed which, when opened, discharged a continuous flow of material from the bed. They had tagged the feed material with a radioactive tracer which they subsequently analyzed with a scintillation counter. Sutherland [36] also used a radioactive tracer, but he removed material from the bed bottom with a screw conveyor, passed it by a scintillation counter, and then reinjected it into the bed.

Taking measurements on an operating bed without disturbing the bed should provide the best results. The primary difficulty encountered with such techniques is the interpretation of the data. Weiner et al. [61] used the common method of sequentially photographing the positions of colored particles in a fluidized bed with transparent walls. A major drawback of this method was that information was only gathered at the bed walls. Also, the analysis of the many photographs was quite time consuming. Hayakawa et al. [62] used an electrical resistance probe to detect the passage of conductive tracer material between two electrodes. The probe caused minimal distrubance in the bed due to its small size, but the data collected was difficult to analyze. Grohse [30] detected silicon powder tracer movement in a fluidized bed by means of x-ray absorption. Rowe et al. [56] also used x-rays to detect a lead-glass ballotini tracer. In both cases the results were somewhat difficult to interpret because the x-ray pictures taken were two dimensional silhouettes of a three dimensional phenomenon. In addition, as with the radioactive tracer technique discussed previously, x-ray techniques require expensive equipment and proper shielding structures for operating personnel. Donlevy [55] developed an inductance probe which he used to detect the presence of ferrite tracers in a fluidized bed. Results obtained with this probe are also presented by Fitzgerald et al. [63]. This method of measurement presented two problems. First, the inductance probes were relatively large to be placed in a fluidized bed, but this problem was solved by placing the probes in simulated heat transfer tubes. The major problem encountered was that the data collected were difficult to interpret.

These examples of evaluation methods are by no means a comprehensive survey of the field, although they do include many of the more common methods. Other methods are described in previously cited references, especially those of Sutherland [36], Donlevy [55], Rowe et al. [56], and Hayakawa et al. [62]. Also, Potter [64] mentions many evaluation methods in his fluidized bed mixing overview.

Integrated Evaluation Method

Introduction

The most accurate results from coal feeding tests in a fluidized bed are achieved when actual coal is fed into limestone bed material. However, coal is dirty, has explosive dust, and is difficult to detect in or separate from limestone. Thus, for the purpose of the coal feeder evaluation project, a coal substitute material was desired which possessed the same physical properties as coal, but which could be effectively used to quantify coal feeding performance. The evaluation method utilizing this substitute material needed to be reasonably quick and easy to perform due to the large number of coal feeding tests required. Also, because of the limited storage space available, it was desirable to be able to separate the feed material from the bed material after each test for reuse. Primary consideration was given to taking samples from an operating bed rather than making measurements on an operating bed due to the difficulties often encountered with the latter method.

To achieve all of these ends, a coal feeding evaluation method was sought which integrated the various functions. It was concluded that a magnetically susceptible coal substitute material would best serve as the basis of this method. The potential ability to use magnetism to concentrate the substitute feed material in the collected sample was considered important because local coal/limestone concentrations during coal feeding tests would be in the range from less than one percent to about five percent as that is typical of an actual fluidized bed. Also, because limestone is not magnetically susceptible, a magnetic separation process could be used to separate the two materials between feeding tests.

The utility of magnetic sampling methods has been demonstrated by several researchers. Cranfield [57] and Geldart and Cranfield [65] performed mixing studies with alumina particles, part of which were impregnated with iron. Following each test they dissected the bed and passed samples of the material through a magnetic separator to determine the proportions of the particle types in a given bed region. Sutherland [36] and Rowe and Sutherland [37] used a bed of copper shot with nickel shot as the magnetic tracer material. They too dissected the bed and magnetically separated the samples to determine mixing results. Bowling and Watts [66,67] produced magnetically susceptible char particles which they used to study particle residence time in a fluidized bed. They analyzed the material which overflowed the bed for the concentration of the magnetically tagged particles. Several other researchers allude to the use of magentic sampling methods, but few details are given.

Imitation Coal

A substitute material or tracer should have properties and physical characteristics which reproduce those of the actual material as closely as possible. Thus, to produce a material which models coal requires a determination of those coal characteristics which are important in the feeding experiments.

The primary coal characteristics chosen to be modeled were the particle size and shape, durability, and specific gravity. The particle size selected was 0.25 inches by 0 because this was the size frequently specified in various fluidized bed combustion design reports [15, p. 98; 20, p. 178; 68, p. 3-8]. Ideally, the particle shape should be angular like coal, although spherical or random particles were not out of the question. A wear and fracture resistant durability was desired as this is typical of coal and would be helpful in keeping the particle sizes from decreasing significantly in the abrasive environment of the limestone fluidized bed. The primary difficulty arose in selecting the coal specific gravity to be modeled. Bituminous coal was chosen for modeling because it is the primary type being considered for use in fluidized bed combustors, particularly in the Tennessee Valley. Clean bituminous coal has a specific gravity in the range of 1.1 to 1.5 [69,70], although the specific gravity of bituminous coal actually used for combustion ranges from 1.3 to 2.7 due to moisture and impurities such as ash and slate [71]. Because the amount and type of impurities in coal vary so widely, it was decided to duplicate the specific gravity of clean bituminous coal only. However, actual coal feeders must be designed to transport the heavier impurities in the coal to prevent plugging by such material.

Obtaining a substitute coal material with the proper specific gravity which exhibits magnetic response is difficult because the specific gravities of ferromagnetic materials range from approximately 5 for ferrites to almost 8 for iron [72]. The obvious solution is to mix the ferromagnetic material with a low specific gravity binder material to yield a product with an intermediate specific gravity. The difficulty in using such materials to produce a mixture with the proper specific gravity can be illustrated by a simple example. Assume that iron and plastic are the component materials of the mixture. If F is the mass fraction of iron used, then 1-F is the mass fraction of plastic required. Letting SG represent the specific gravity, the mass fraction equation is

$$(F)(\text{SG iron}) + (1-F)(\text{SG plastic}) = (1)(\text{SG mixture}). \qquad (3.1)$$

The relation between the various specific gravities is best seen by solving for F to get

$$F = \frac{\text{SG mixture} - \text{SG plastic}}{\text{SG iron} - \text{SG plastic}} \qquad (3.2)$$

To obtain a material with the greatest magnetic susceptibility, the iron fraction, F, must be maximized. Because the specific gravities of the mixture and the iron are fixed, the only option is to decrease the plastic specific gravity. Consider specific gravities of 1.35 for the mixture, 7.9 for iron, and 1.0 for the plastic. This combination of specific gravities yields a mass fraction of 0.05 (or 5 percent) for this iron. It is doubtful whether such a small amount of iron in the material mixture would yield sufficient magnetic susceptibility for detection and separation purposes.

A few attempts to produce a magnetically susceptible feed material have been reported. Donlevy [55] and Fitzgerald et al. [63]

used a ferrite tracer which contained polyester casting resin, but it was denser than most coals. Rowe et al. [56] report that glass spheres have been made magnetic by coating them with a thin film of high permeability iron and suggest that porous particles can be made magnetically responsive by precipitating iron into the pores. The process of metallizing plastics has been used on occasion to obtain materials with certain desired properties [73, 74]. The metallizing can take the form of a metallic coating or of incorporating metal inserts in the plastic when it is molded. Conductive plastics are a form of metal coated plastics which have been used in the electronics industry [75, 76]. Many thermoplastic or thermosetting engineering plastics are particularly suitable as a binder for a ferromagnetic material because they are easily fabricated and have specific gravities as low as 0.9 [77].

Preliminary attempts to produce a coal substitute material, subsequently termed imitation coal, in the laboratory met with only limited success. However, the prototype imitation coal batches, which contained iron powder in polystyrene, did demonstrate that the concept of dispersing a ferromagnetic material in a plastic to produce a magnetically susceptible product was feasible. Thus, a specialty plastics manufacturer, Vernay Products of Yellow Springs, Ohio, was contacted about the possibility of developing an imitation coal material. After experimentation with several trial batches, Vernay Products was able to develop a technique for uniformly mixing iron powder with a curing polyester resin. The mixture was cast in 0.5 inch thick slabs, and a black pigment was added to make it look like real coal. The final imitation coal material contained 15 percent iron powder. This relatively high amount of iron could be added to a polyester resin with a specific gravity of 1.1 because very tiny hollow thin walled glass spheres were added to the mixture. These microspheres entrap very tiny bubbles of air in the material during formation and thus reduce the overall specific gravity.

The true, or particle, density of the imitation coal slabs was determined by a variety of water displacement methods. The average of all the results indicated a true density of 87 lbm/ft^3 (specific gravity of 1.4). Then the material was ground up in a hammermill crusher containing a 0.25 inch screen. The resulting material is shown in Figure 3.1, and a sieve analysis of it is shown in Table 3.1. Table 3.2 illustrates a comparison of the imitation coal sieve analysis with that of a 0.25 inch by 0 real coal sample. These sieve analyses, as well as others referred to later, were performed according to the appropriate ASTM standards [78]. It is apparent from Table 3.2 that real coal yields finer particles when crushed than imitation coal. Several measurements were made of the bulk density of the imitation coal and the average was found to be 47 lbm/ft^3 (specific gravity of 0.75). This value agrees well with the 50 lbm/ft^3 bulk density quoted for bituminous coal of the same size range [79].

Coal Sample Probes

The primary qualifications of a fluidized bed sampling device are that it collects reproducible samples from determinate locations in the bed and has a minimal effect on the bed behavior. Many variables exist such as the number and size of the samples to be taken and the locations at which they will be taken. In theory, a high number of samples is best, but in practice this number is limited

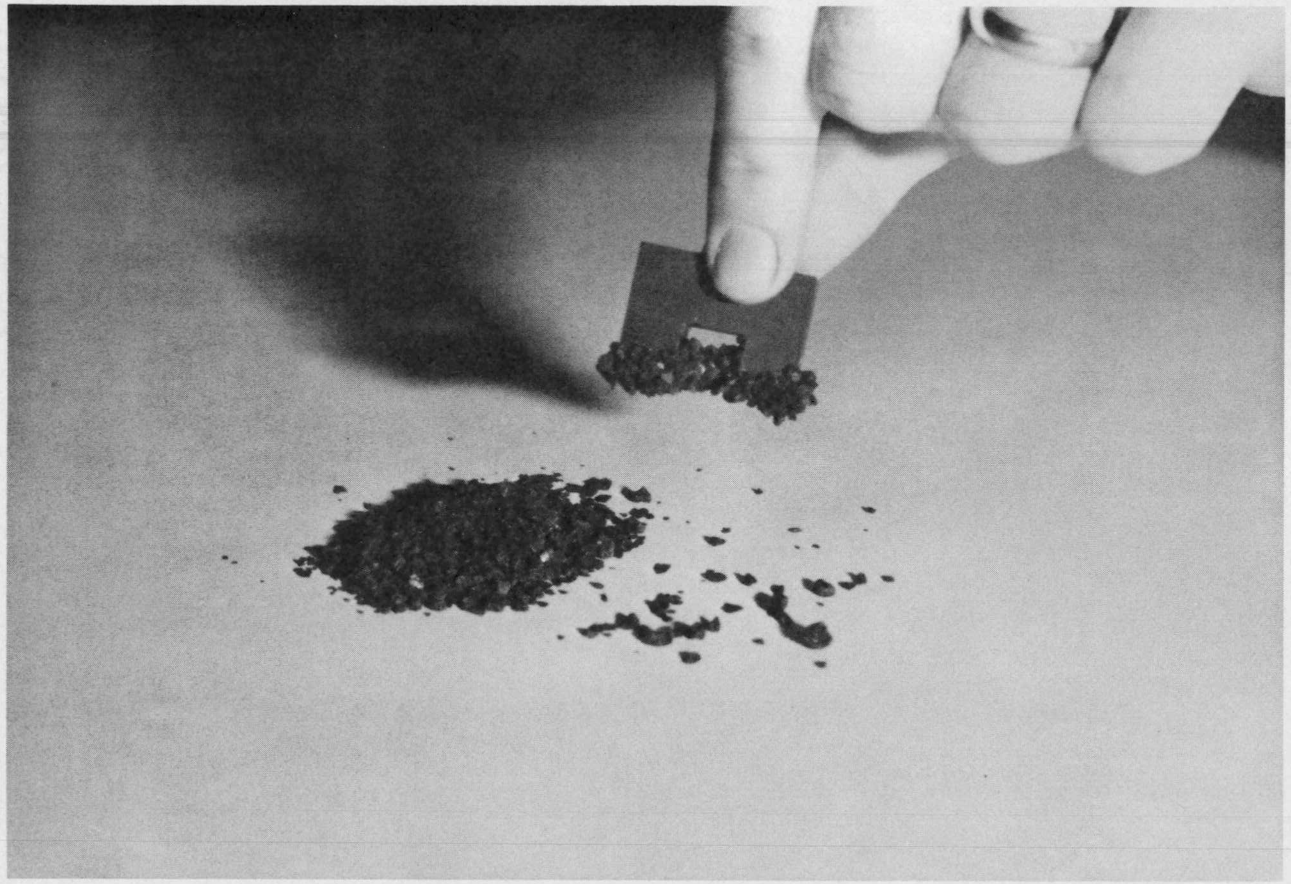

Figure 3.1. Crushed Imitation Coal

TABLE 3.1

IMITATION COAL SIEVE ANALYSIS

Sieve[1]	Sieve Opening[2]	Percent Retained	Cumulative Percent Retained
3/8 in.	0.3750	0.0	0.0
1/4 in.	0.2500	0.0	0.0
4	0.1870	0.3	0.3
8	0.0937	33.7	34.0
16	0.0469	33.6	67.6
30	0.0234	16.6	84.2
50	0.0117	7.6	91.8
100	0.0059	4.0	95.7
200	0.0029	2.4	98.2
325	0.0017	1.2	99.4
Pan	0.0000	0.6	100.0

[1]U.S.A. Standard Series.

[2]Approximate opening diameter in inches.

TABLE 3.2

SIEVE ANALYSIS COMPARISON OF IMITATION COAL AND REAL COAL

Sieve[1]	Sieve Opening[2]	Percent Retained	
		Imitation Coal	Real Coal[3]
3/8 in.	0.3750	0.0	0.0
1/4 in.	0.2500	0.0	0.2
4	0.1870	0.3	2.1
8	0.0937	33.7	13.1
16	0.0469	33.6	26.7
30	0.0234	16.6	22.5
50	0.0117	7.6	15.6
100	0.0059	4.0	9.2
200	0.0029	2.4	4.4
325	0.0017	1.2	2.6
Pan	0.0000	0.6	3.6

[1] U.S.A. Standard Series.

[2] Approximate opening diameter in inches.

[3] Babcock and Wilcox, Series 8, Test 4 sequence, April 1979, average of four sieve analyses from unpublished results.

by the tolerable disturbance to the bed, the experimental system geometry, the time required to collect and analyze samples, and sampling device costs. The size of the samples is determined by the amount of total material required to give statistically satisfactory concentration data as well as by the geometry of the experimental system and sampling probes themselves. The sampling locations are dictated primarily by the above factors and by symmetry considerations.

Very limited information exists in the literature concerning fluidized bed sampling devices. Orr [26, p. 91] describes a "sampling thief" which consists of one or more container cells built into a pipe which can be opened and closed to entrap and remove a sample from the bed. Sutherland [36] discusses the use of an electrically actuated automatic sample probe of this type in mixing studies, but he gives very few details about its construction or operation. The sample probe of Highley and Merrick [60] mentioned previously was different in that it extracted a continuous sample rather than a discrete one.

Quite a multitude of ideas and methods were considered during the selection and design of the sample devices, which became known as coal sample probes. Although the idea of using a mechanical collection scheme in the gritty environment of the limestone bed material was viewed with reluctance, it was concluded that the potential advantages of this method outweighed those of other methods considered. Because the only normal bed internals within a combusting fluidized bed are heat transfer tubes, excepting the mechanisms which inject air, coal, and limestone, the coal sample probes were fashioned in the form of heat transfer tubes. The recommended diameter of such tubes varies from approximately 1 to 2 inches, so bed sampling and geometry factors were also considered in sizing the coal sample probes.

The basic coal sample probe configuration chosen was an arrangement of two rotating concentric tubes. With sets of rectangular holes cut in both tubes, material could be allowed to pass perpendicularly through the tubes or it could be trapped in the tubes by changing the hole alignments. Also, by keeping the outer tubes immobile and rotating the inner tube only, a minimal amount of the moving part of the probe would be in contact with the abrasive bed material.

A schematic of a coal sample probe is shown in Figure 3.2. The aluminum outer tube has an outside diameter of 2.25 inches while that of the inner tube is 2.125 inches. Each rectangular hole represents a 60 degree sector of the tube and is 1.125 inches long. These holes are on 8 inch centers with either end hole being 4 inches from the adjacent wall when the probe is installed in the bed. Disks are positioned at the hole edges to form three compartments in each coal sample probe. These compartments can be seen in Figure 3.3. Only two coal sample probes were fabricated due to the time and costs involved.

Because the concentration of imitation coal in the bed during coal feeding tests would be small, the incorporation of electromagnets in the coal sample probes for the purpose of sample enhancement was evaluated. Suitable electromagnets were not readily available, so they were designed and manufactured. The electromagnet cores were made in-house and the coil winding was performed by Tennessee Armature

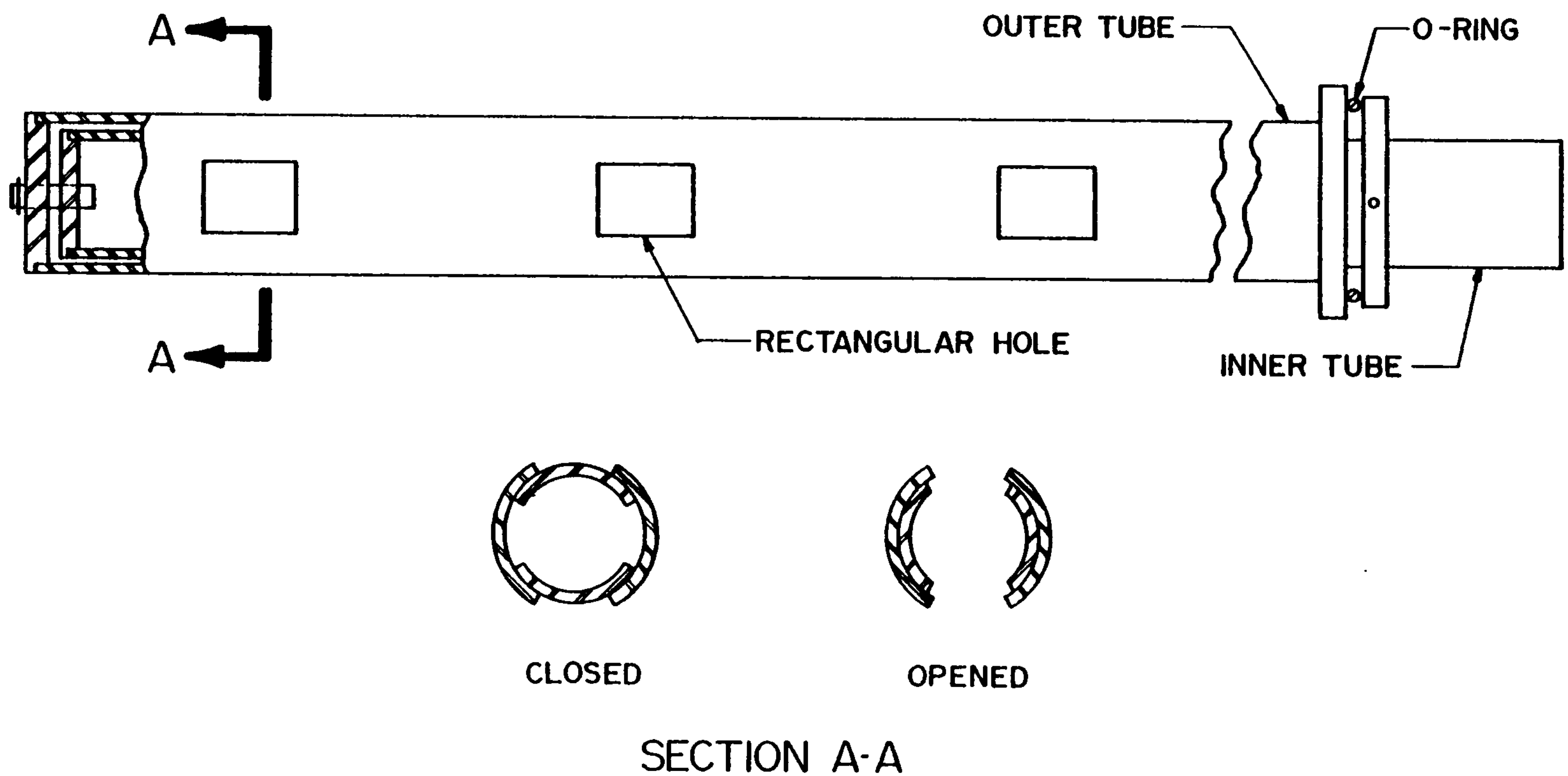

Figure 3.2 Coal Sample Probe Details.

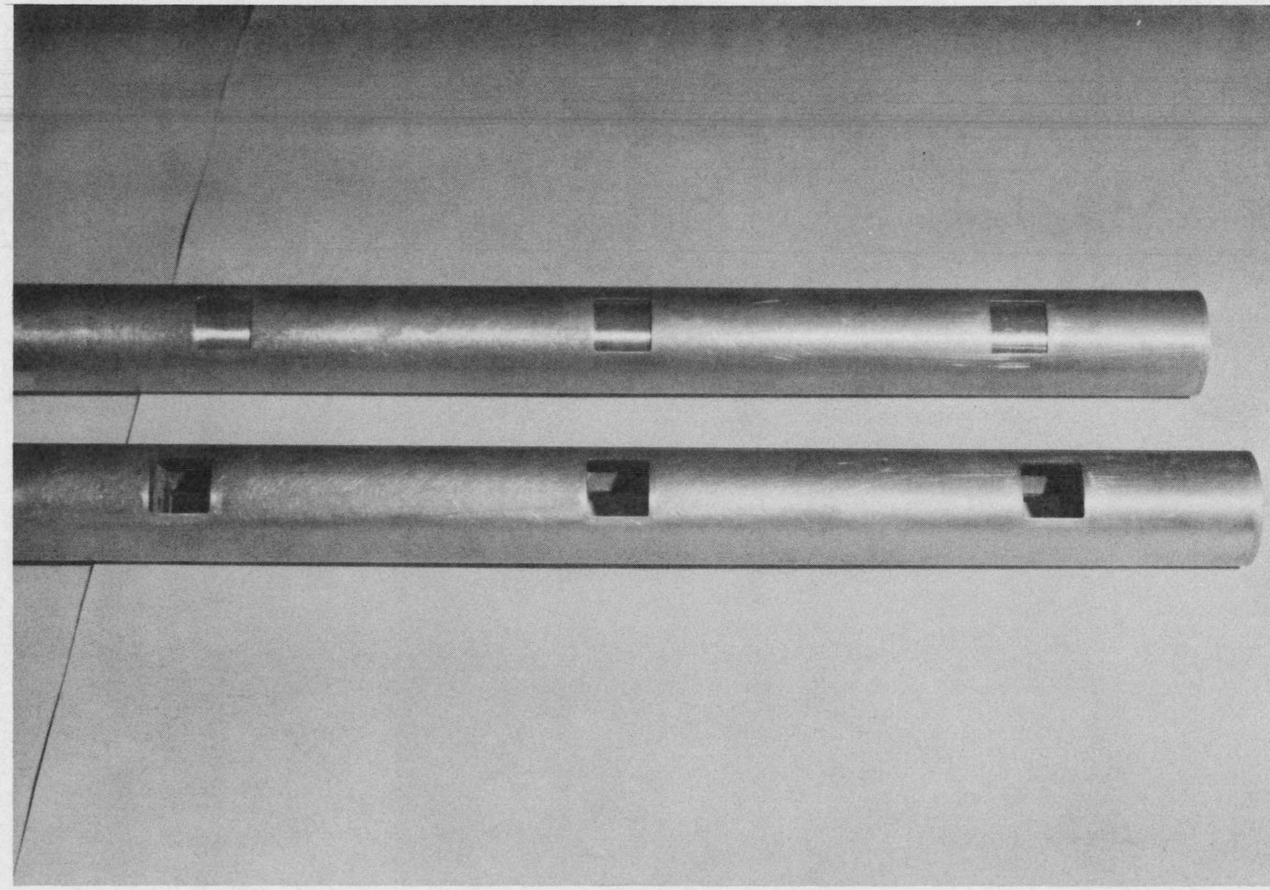

Figure 3.3. Coal Sample Probes with Opened and Closed Compartments.

and Electric Company of Knoxville, Tennessee. One of the six electromagnets is shown in Figure 3.4. Each one contains 2025 turns of 30 gage wire wrapped around a 0.480 inch diameter steel core. The average coil resistance is 51 ohms.

The plexiglass bed test section, which is described in Chapter 5, contains 12 ports into which the coal sample probes can be inserted for sample collection. The probes project through the ports into the bed region without any internal support. They are supported outside the bed by thick aluminum sleeves clamped to a support frame as shown in Figure 3.5. The square plates on the support sleeves visible in the figure contain index marks so that the opened or closed positions of the coal sample probes can be easily set.

Magnetic Separator

Within the scope of the integrated evaluation method, the mixed feed material and bed material must be separated following each test by some type of magnetic separator. Several researchers mention the use of a magnetic separator for this purpose, but they do not describe the type used. However, there is some information in the literature concerning magnetic separation, particularly in relation to ore and mineral processing. Pryor [80] introduces the theory of magnetic separation and then proceeds to describe the basic types of separators used industrially. Taggart [81] gives a similar, but briefer, treatment to the subject. Moskowitz [82] descirbes several interesting methods and applications involving magnetic separators, but he only considers those containing permanent magnets. Fitzgerald [83], who performed work with the inductance probes and ferrite tracer material mentioned previously, experimented with

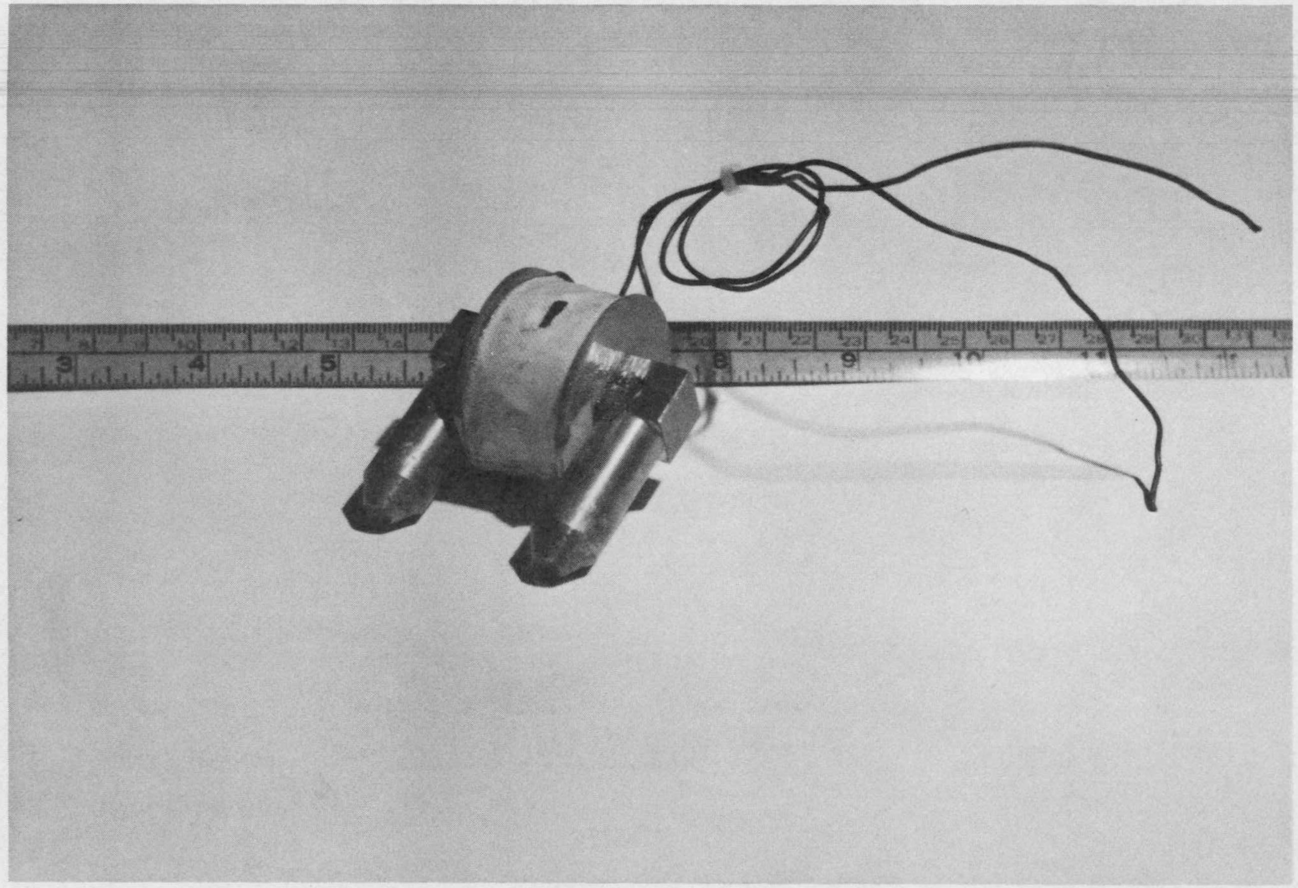

Figure 3.4. Electromagnet Removed from a Coal Sample Probe.

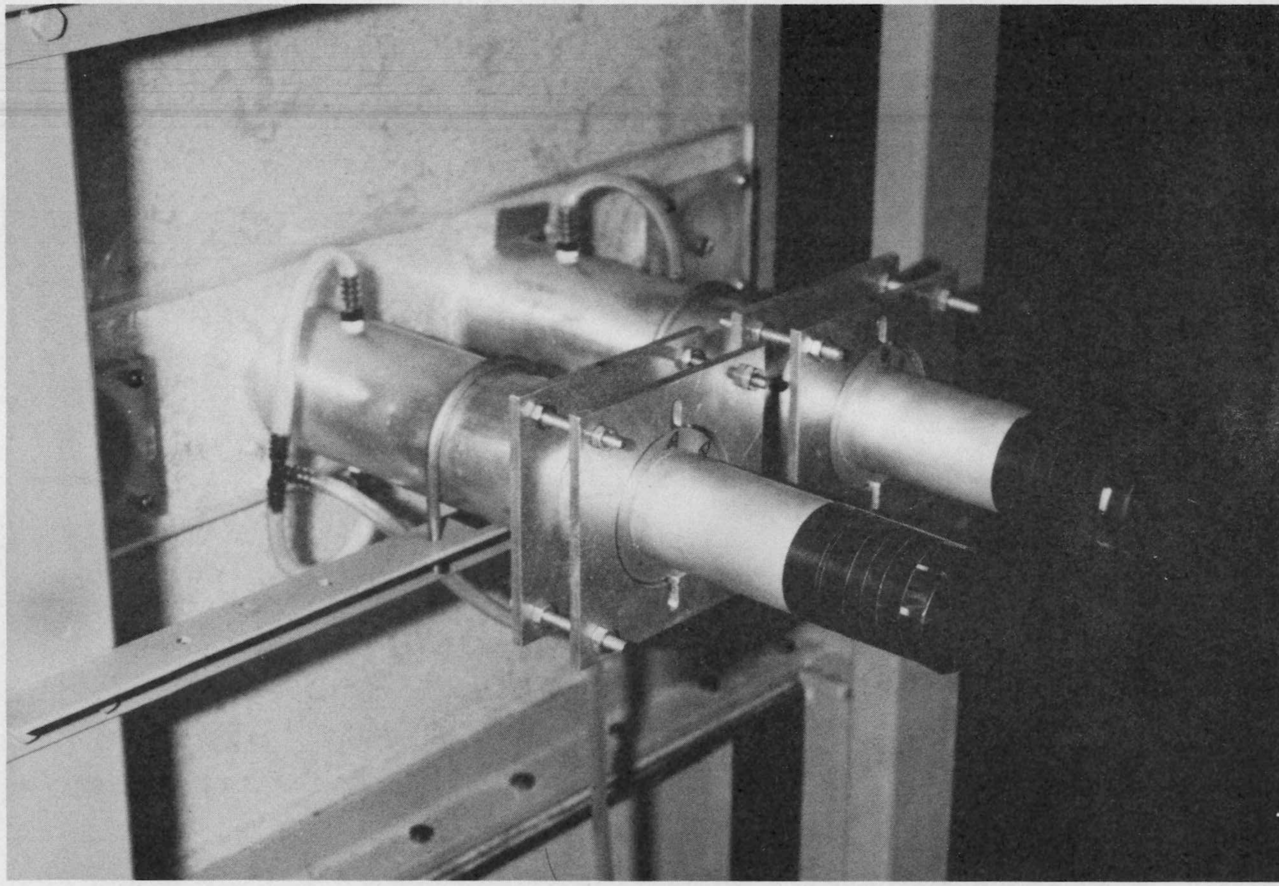

Figure 3.5. Coal Sample Probe Support Structure and Sleeves.

several methods of magnetic separation. He first tried immersing an energized electromagnet into the bed material and then removing it to a collection bin where it was de-energized, but this method was too time consuming. Next he used a fixed permanent magnet in front of a moving belt carrying the bed material, but this configuration experienced numerous mechanical difficulties due to jamming. The third and most successful method employed a conveyor belt carrying the bed material which passed over a magnetic pulley. The magnetically susceptible particles were attracted to the pulley and drawn out of the stream of unsusceptible particles.

Either a magnetic pulley or a magnetic drum separator could be utilized for the present application. The latter type of separator contains a rotating cylinder surrounding a magnet onto which the material to be separated is gravity fed. As shown in Figure 3.6, magnetically unsusceptible material drops off the cylinder edge whereas magnetically susceptible material is held to the drum until it passes out of the magnetic field and then drops to a different location.

A Model 1212, Series 520, permanent magnetic drum separator, manufactured by Stearns Magnetics of Cudahy, Wisconsin, was selected. A magnetic drum separator was chosen over a magnetic pulley arrangement because the former can be easily incorporated into a closed system. This characteristic is important because of the large amount of limestone dust which is generated in a fluidized bed.

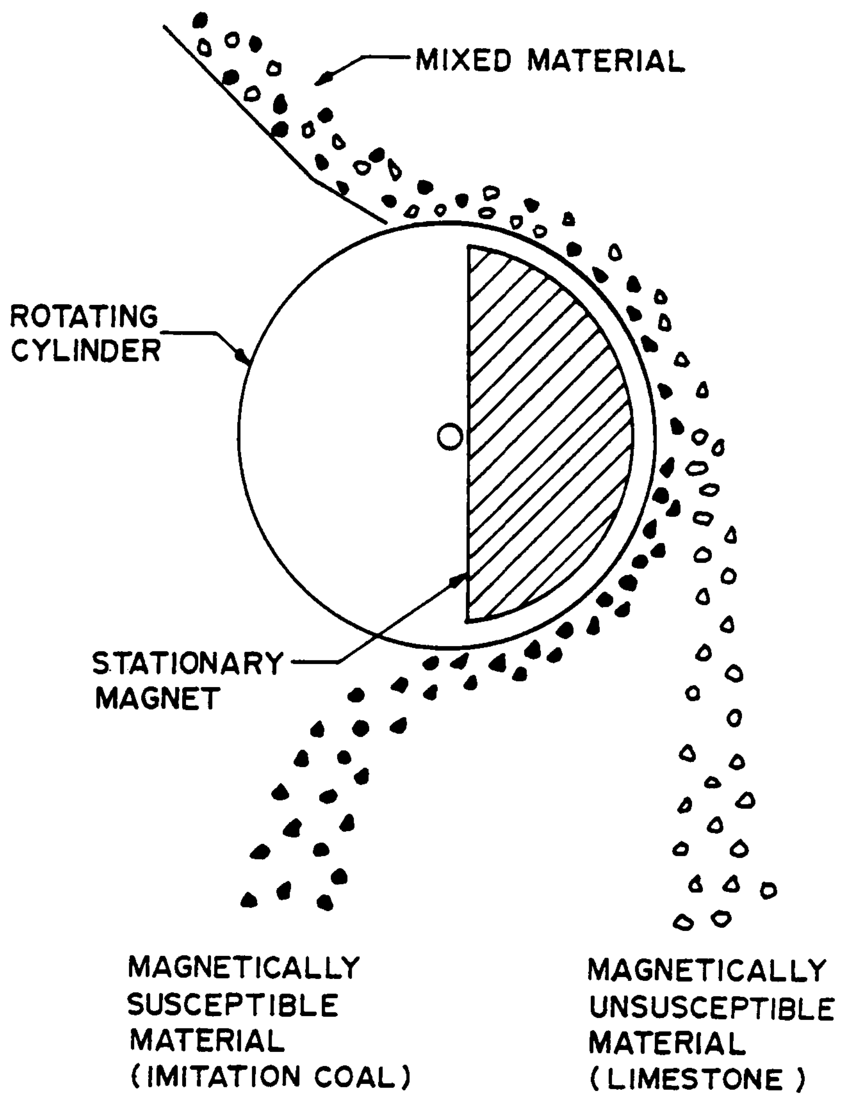

Figure 3.6 Magnetic Separation Principle.

CHAPTER 4

FLUIDIZED BED SCALING

Overview

Scaling, or modeling, is used to predict the operational characteristics of a full scale prototype from those of a reduced scale model. The scaling of a fluidized bed combustor is a very complex problem. In fact, it is not only beyond the scope of this thesis, but apparently comprehensive fluidized bed scaling has not been accomplished to date. However, qualitative aspects of scaling are discussed and pertinent developments in this field are reviewed with the intention of providing a basis for future scaling work.

Many factors contribute to the difficulty encountered in fluidized bed scaling. First, geometric scaling, or similitude, relates the bed and particle dimensions between the model and the prototype. The effects of the bed walls and internals on the fluidization behavior are important here. Second, dynamic, or kinetic, similitude concerns the forces in a fluidized bed system. Because a fluidized bed is a constantly changing array of particles in a fluid, the equations of motion for such a system are extremely complex. Also, the conditions which exist in the dilute phase pneumatic transport system used for many fluidized bed coal feeders are quite different from those existing in the dense phase mixture of the bed. Third, when a fluidized bed combustor is being represented by an ambient temperature model, thermal similitude is required. This poses a problem because the fluidization and coal transport air at ambient conditions are preheated to approximately 600°F and then raised to 1500 - 1600°F in the fluidized bed. Thus, three sets of thermal conditions should theoretically be modeled. Furthermore, the chemical reactions occurring in a combusting fluidized bed significantly affect the bed behavior, and these chemical reactions are virtually impossible to model in an ambient temperature bed. Finally, the flow regimes discussed in Chapter 2 appear to be important in fluidized bed scaling. There is some uncertainty as to whether a scale model fluidized bed always operates in the same flow regime as a full scale prototype at equivalent operating conditions. The correspondence of flow regimes is important because fluidized bed behavior varies dramatically among the various flow regimes which have been observed.

Numerous fluidized bed researchers have recognized the need for the application of scaling techniques. Cranfield and Geldart [41] question the value of a large volume of fluidized bed data because it was generated in small diameter beds. They examined the results of several researchers on the subject of wall effects and concluded that a minimum bed diameter of 8 inches is necessary to ensure three dimensional behavior. In addition, acknowledgement is made that the mechanism of fluidization must be better understood for scaling rules to be developed. Wen and Dutta [84] state that scaling is probably the most challenging and difficult job in the field of fluidization, and then they summarize several problems pertinent to fluidized bed scaling which support this claim.

Traditionally, the most common approach to fluidized bed scaling has been the development of correlations, often in non-dimensional form, from available data. The intent is that the parameters represented by these correlations based on small fluidized beds can be extrapolated to larger beds. Lapple [85] made one of the early attempts to develop a non-dimensional correlation for all fluid-particle systems. He was able to represent all such systems excepting gas fluidization in terms of a modified drag coefficient and a modified Reynolds number for the data which he analyzed. The general graphical presentation of multiphase flow systems which Lapple developed relating the slip velocity (gas velocity minus solid velocity) to the pressure drop per unit length is still useful in the study of two phase flow behavior. Babu et al. [42] surveyed much of the available fluidized bed data and many correlations in an attempt to develop improved correlations for the minimum fluidization velocity and the fluidized bed expansion ratio. They utilized the Reynolds and Archimedes numbers, which are discussed later, and a bed height ratio in the correlations. Catipovic et al. [46] correlated the fluidization regimes for large particle systems in dimensional form using the fluidization velocity, particle diameter, and bed height. Horio and Wen [86] describe and compare many of the currently used fluidized bed modeling correlations. They emphasize the often neglected admonition that the range of applicability of a given model must be determined and adhered to if dependable results are to be obtained.

The Buckingham π theorem, also known as the Rayleigh method, has been applied to fluidized bed scaling. This method is used to develop pertinent non-dimensional parameters by applying certain rules to groupings of the important variables. Broadhurst and Becker [48] demonstrate the application of this method by developing sets of independent and dependent variables representing fluidized bed geometry and behavior. The independent variables include the Archimedes number, the particle sphericity, and ratios of the particle to fluid density, particle to fluid pressure, particle to bed diameter, and particle diameter to bed height. The dependent variable set contains the Froude number, discussed later, and the bed voidage fraction. In the same paper, statistical analysis and the theory of dimensionless groups are applied to the results of many experiments in the development of minimum fluidization, bubbling, and slugging velocity correlations to determine the significance of each of the non-dimensional variables on these parameters.

A more recent analytical modeling technique involves scaling the governing differential equations of a system to develop non-dimensional parameters. Actually, a form of this method was used several years ago in fluidized bed work by Romero and Johanson [27], who solved linearized Navier-Stokes equations for certain simple cases. They concluded that pertinent non-dimensional groups for gas fluidized beds are the Froude and Reynolds numbers and several particle and bed geometry ratios. One of the problems encountered with this scaling method is the development of the proper governing differential equations for fluid-particle systems. Jackson [87] provides an overview of current fluid mechanical theory which treats a fluidized bed system as two interpenetrating and interacting continua. By deriving continuity and momentum equations for fluid-particle systems and developing constitutive relations, Jackson was able to find the solutions for certain simplified cases and then relate the results to fluidized bed stability and bubbling phenomena. Boothroyd [88] considers this scaling method for the dilute phase suspension flow of fine particle systems. He points out several factors which apply to the scaling of both pneumatic transport systems and to fluidized beds. For particle-fluid relative velocities outside the region in which Stokes' law is applicable, exact dynamic similarity of the particle trajectories cannot be attained if different gas flow velocities are used in the model and the actual system. Also, scaling becomes very difficult for systems containing large particles in dense phase mixtures where collisions are frequent, certainly a description of a fluidized bed. Boothroyd makes the important point that partial modeling, a method of simplification utilizing a selected number of the non-dimensional groups which are applicable to a system, is useful in reducing a complex system to one that can be handled. Glicksman [89] claims to have used the scaling of the governing fluid dynamical equations to develop a set of scaling factors, but he provides no details about the method. He does state that the Froude number, particle Reynolds number, bed geometry ratio, particle to bed dimensions ratio, and the particle shape and size distribution must be utilized to produce dynamic similarity between two fluidized bed systems.

None of the previous work cited, excepting that of Glicksman, considered the thermal scaling of fluidized beds. This seeming oversight is reconciled by the recognition that many fluidized beds utilized in the chemical industry are operated at approximately ambient temperatures. However, this is certainly not the case for fluidized bed combustion systems in which the air temperature increases from the ambient to the bed combustion temperature. Due to this temperature increase, the air density decreases by almost a factor of four as it passes through the system. Glicksman [89] proposes to account for the hot bed density effect in an ambient temperature fluidized bed model by increasing the particle density while keeping air as the fluid. It is also possible to use a lower density fluidizing gas in the model if the actual bed material is to be used. Lackey and Withers [90] thermally scaled a cold model fluidized bed for partial slumping experiments. Unlike Glicksman, they did not utilize exact dynamic similarity, but rather varied the parameters in their quarter scale model to approximate a range of Archimedes and Reynolds numbers which had been calculated for the full scale unit.

Example

The method of scaling the governing differential equations of a system to produce non-dimensional parameters is illustrated. The analysis is very simplified in that the continuity and momentum equations for single phase flow are used. Also, the energy equation is not considered. Yet, some insight can be gathered into the origin of some of the non-dimensional parameters used in fluidized bed modeling.

Consider a cylindrical fluidized bed of diameter D_b and height H as shown in Figure 4.1. For single phase flow, the application of the law of conservation of mass to the control volume represented in the figure gives the continuity equation in cylindrical coordinates as

$$\frac{\partial \rho_g}{\partial t} + \frac{1}{r}\frac{\partial}{\partial r}(\rho_g\, r\, v_r) + \frac{1}{r}\frac{\partial}{\partial \theta}(\rho_g\, v_\theta) + \frac{\partial}{\partial z}(\rho_g v_z) = 0. \qquad (4.1)$$

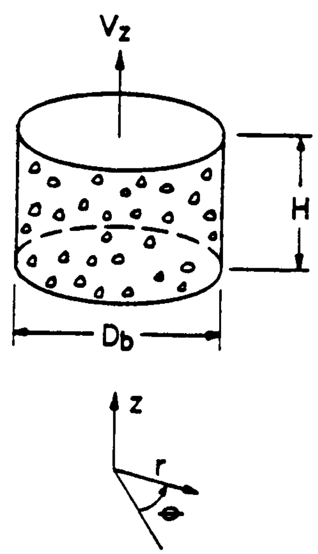

Figure 4.1. Fluidized Bed Geometry.

Similarly, the application of Newton's second law to the control volume gives the three momentum equations in cylindrical coordinates for single phase flow. Only the z - component equation will be considered, and it is

$$\rho_g\left(\frac{\partial v_z}{\partial t} + v_r \frac{\partial v_z}{\partial r} + \frac{v_\theta}{r}\frac{\partial v_z}{\partial \theta} + v_z \frac{\partial v_z}{\partial z}\right) = -\frac{\partial P}{\partial z}$$

$$+ \mu\left(\frac{1}{r}\frac{\partial v_z}{\partial r} + \frac{\partial^2 v_z}{\partial r^2} + \frac{1}{r^2}\frac{\partial^2 v_z}{\partial \theta^2} + \frac{\partial^2 v_z}{\partial z^2}\right) + \rho_g\, g. \qquad (4.2)$$

In this development it will be assumed that the velocity in the circumferential direction, v_θ, is negligible, and that by symmetry the derivative of any variable with respect to θ, i.e., $\frac{\partial(\ )}{\partial\theta}$, is zero.

Thus, Equation (4.1) becomes

$$\frac{\partial \rho_g}{\partial t} + \frac{1}{r}\frac{\partial}{\partial r}(\rho_g r v_r) + \frac{\partial}{\partial z}(\rho_g v_z) = 0 , \tag{4.3}$$

and Equation (4.2) becomes

$$\rho_g\left(\frac{\partial v_z}{\partial t} + v_r \frac{\partial v_z}{\partial r} + v_z \frac{\partial v_z}{\partial z}\right) = - \frac{\partial P}{\partial z}$$

$$+ \mu\left(\frac{1}{r}\frac{\partial v_z}{\partial r} + \frac{\partial^2 v_z}{\partial r^2} + \frac{\partial^2 v_z}{\partial z^2}\right) + \rho_g g. \tag{4.4}$$

The first step in this scaling method is to define certain non-dimensional variables based on the characteristic dimensions of the system. The guidelines used for this process are beyond the scope of this development. For this example the following non-dimensional variables are chosen:

$$r^* = \frac{r}{D_b} \qquad v_r^* = \frac{v_r}{V_z} \qquad t^* = \frac{t}{H/V_z}$$

$$z^* = \frac{z}{H} \qquad v_z^* = \frac{v_z}{V_z} \qquad P^* = \frac{P}{(\rho_s - \rho_g)gH} \ . \tag{4.5}$$

These choices are based on physical reasoning. In particular, the non-dimensional pressure is based on the definition of the pressure drop through a fluidized bed, which is

$$\Delta P = (\rho_s - \rho_g)\,(1 - \varepsilon)\, g H \ . \tag{4.6}$$

The voidage fraction term, which is dimensionless, is omitted in the non-dimensionalized variable.

Substituting the appropriate non-dimensional variables into the continuity equation, Equation (4.3), gives

$$\frac{V_z}{H}\frac{\partial \rho_g}{\partial t^*} + \frac{V_z}{D_b}\frac{1}{r^*}\frac{\partial\left(\rho_g r^* v_r^*\right)}{\partial r^*} + \frac{V_z}{H}\frac{\partial\left(\rho_g v_z^*\right)}{\partial z^*} = 0 \;. \tag{4.7}$$

After this equation is multiplied by H/V_z and rewritten in physical variables it becomes

$$\frac{\partial \rho_g}{\partial t} + \left(\frac{H}{D_b}\right)\frac{1}{r}\frac{\partial(\rho_g r\, v_r)}{\partial r} + \frac{\partial(\rho_g v_z)}{\partial z} = 0 \;. \tag{4.8}$$

The dimensionless parameter which results is

$$\frac{H}{D_b} = \text{bed geometry ratio.} \tag{4.9}$$

In the same way, the non-dimensional variables of Equations (4.5) can be substituted into the z - component momentum equation, Equation (4.4), to yield

$$\frac{\rho_g V_z^{\,2}}{H}\left(\frac{\partial v_z^*}{\partial t^*} + \frac{H}{D_b} v_r^*\frac{\partial v_z^*}{\partial r^*} + v_z^*\frac{\partial v_z^*}{\partial z^*}\right) = -\,(\rho_s - \rho_g)g\,\frac{\partial P^*}{\partial z^*}$$

$$+\,\mu\frac{V_z}{H^2}\left(\frac{H^2}{D_b^{\,2}}\frac{1}{r^*}\frac{\partial v_z^*}{\partial r^*} + \frac{H^2}{D_b^{\,2}}\frac{\partial^2 v_z^*}{\partial r^{*2}} + \frac{\partial^2 v_z^*}{\partial z^{*2}}\right) + \rho_g g \;. \tag{4.10}$$

When the equation is multiplied by $H/\rho_g V_z^2$, it becomes in physical variables

$$\frac{\partial v_z}{\partial t} + \left(\frac{H}{D_b}\right) v_r \frac{\partial v_z}{\partial r} + v_z \frac{\partial v_z}{\partial z} = - \frac{(\rho_s - \rho_g)\, Hg}{\rho_g V_z^2}$$

$$+ \left(\frac{\mu}{\rho_g V_z H}\right) \left[\left(\frac{H}{D_b}\right)^2 \frac{1}{r} \frac{\partial v_z}{\partial r} + \left(\frac{H}{D_b}\right)^2 \frac{\partial^2 v_z}{\partial r^2} + \frac{\partial^2 v_z}{\partial z^2}\right] + \frac{Hg}{V_z^2} . \qquad (4.11)$$

The dimensionless parameters which result are

$\frac{H}{D_b}$ = bed geometry ratio, as before, (4.9)

$\frac{\rho_s - \rho_g}{\rho_g} \frac{Hg}{V_z^2}$ = inverse Froude number modified by a density ratio, (4.12)

$\frac{\mu}{\rho_g V_z H}$ = inverse of the conventional Reynolds number, and (4.13)

$\frac{Hg}{V_z^2}$ = inverse of the conventional Froude number. (4.14)

With the exception of the first Froude number, these are the non-dimensional parameters which would result for flow in a cylindrical pipe without a solid phase of particles. This is true, of course, because the single phase forms of the continuity and momentum equations were used. The major fluidized bed parameter which does not appear in these non-dimensional groups is the particle diameter. However, for large diameter beds of sufficient height, the particle diameter can be used as the characteristic length parameter in Equations (4.5) rather than the bed diameter and height. Thus, for positions away from the walls the non-dimensional parameters now take the more common form of

$$Fr_m = \frac{\rho_g}{\rho_s - \rho_g} \frac{V_z^{\,2}}{D_p g} \quad \text{for the modified Froude number,} \tag{4.15}$$

$$Re = \frac{\rho_g D_p V_z}{\mu} \quad \text{for the particle Reynolds number, and} \tag{4.16}$$

$$Fr = \frac{V_z^{\,2}}{D_p g} \quad \text{for the conventional Froude number.} \tag{4.17}$$

Sometimes the viscosity used in the Reynolds number is the bed viscosity, which is the average viscosity of the two phase mixture existing in the fluidized bed. Several attempts have been made to measure this viscosity, but it is not an easily determined value. In addition, some researchers claim that one of several combinations of the solid density and particle velocity should be used in the Reynolds number rather than the equivalent values for the fluid. The actual problem here is that the true form of the continuity and momentum equations for a fluidized bed system have not yet been determined.

There appears to be a conflict between the Froude numbers of Equations (4.15) and (4.17). The latter one is normally defined in fluid mechanics where the majority of flow systems in which the Froude number is used involve the flow of water adjacent to a free surface of air. In such a case the Froude number is actually defined as

$$Fr = \frac{V^2}{(\Delta\gamma/\rho)L} = \frac{V^2}{(\Delta\rho/\rho)Lg} = \frac{\rho_w}{\rho_w - \rho_a} \frac{V^2}{Lg} \approx \frac{V^2}{Lg} \quad , \tag{4.18}$$

where L is a characteristic length of the system. The simplification occurs because $\rho_w >> \rho_a$. Both forms of the Froude number have been used for fluidized bed modeling, although this simple analysis indicates that the modified form should be used as the appearance of the gas density in the numerator prevents a simplification of the above type. The difference in the two cases is that in the conventional one the density of the flowing phase is greater than that of the second phase, while in the fluidized bed case the reverse is true.

The Archimedes number for fluidized bed systems is defined as

$$Ar = \frac{Re^2}{Fr_m} = \frac{\rho_g(\rho_s - \rho_g) D_p^3 g}{\mu^2} . \tag{4.19}$$

It should be noted that this combination of groups eliminates the velocity parameter. This is desirable because the characteristic velocity in a fluidized bed could be the gas phase velocity within the bed, the bubble velocity, the solid phase velocity, or the commonly used superficial velocity.

As noted before, the preceding analysis is very simplistic, and it is not intended to serve as a guide for utilizing the analytical scaling method. Much more work remains to be done in the area of fluidized bed scaling. A few recommendations concerning this work are included in Chapter 8.

CHAPTER 5

EXPERIMENTAL FACILITY

Introduction

An experimental atmospheric fluidized bed test facility has been designed and built for use in coal feeder evaluations. It is a cold, i.e., ambient temperature, facility for studying the fluidization and feeding characteristics of the feeders. The facility is not scaled but rather represents a section of a full size fluidized bed. Because the geometries of the coal feeders to be tested varied considerably, a prominent concern during the design was to build as much flexibility into the facility as possible to allow for future changes and additions. Thus, numerous extra access ports, flanges, and mounting points were included in the basic structure.

The total facility, shown in Figure 5.1, is essentially a vertically oriented system which is located on three adjacent levels of Dougherty Hall on The University of Tennessee, Knoxville, campus. The facility requires an average of less than 100 square feet of area on each level. The fluidization air supply system and the material transport and storage systems are located on the first floor. On the second floor are the fluidized bed test section, the transport air and control air distribution systems, and the instrumentation and control panel. The third level contains the exhaust air filter. The various components of each system are described below and also by Henry [91], who shared in the experimental facility design. Detailed procedures for operating the experimental facility are contained in Appendix A.

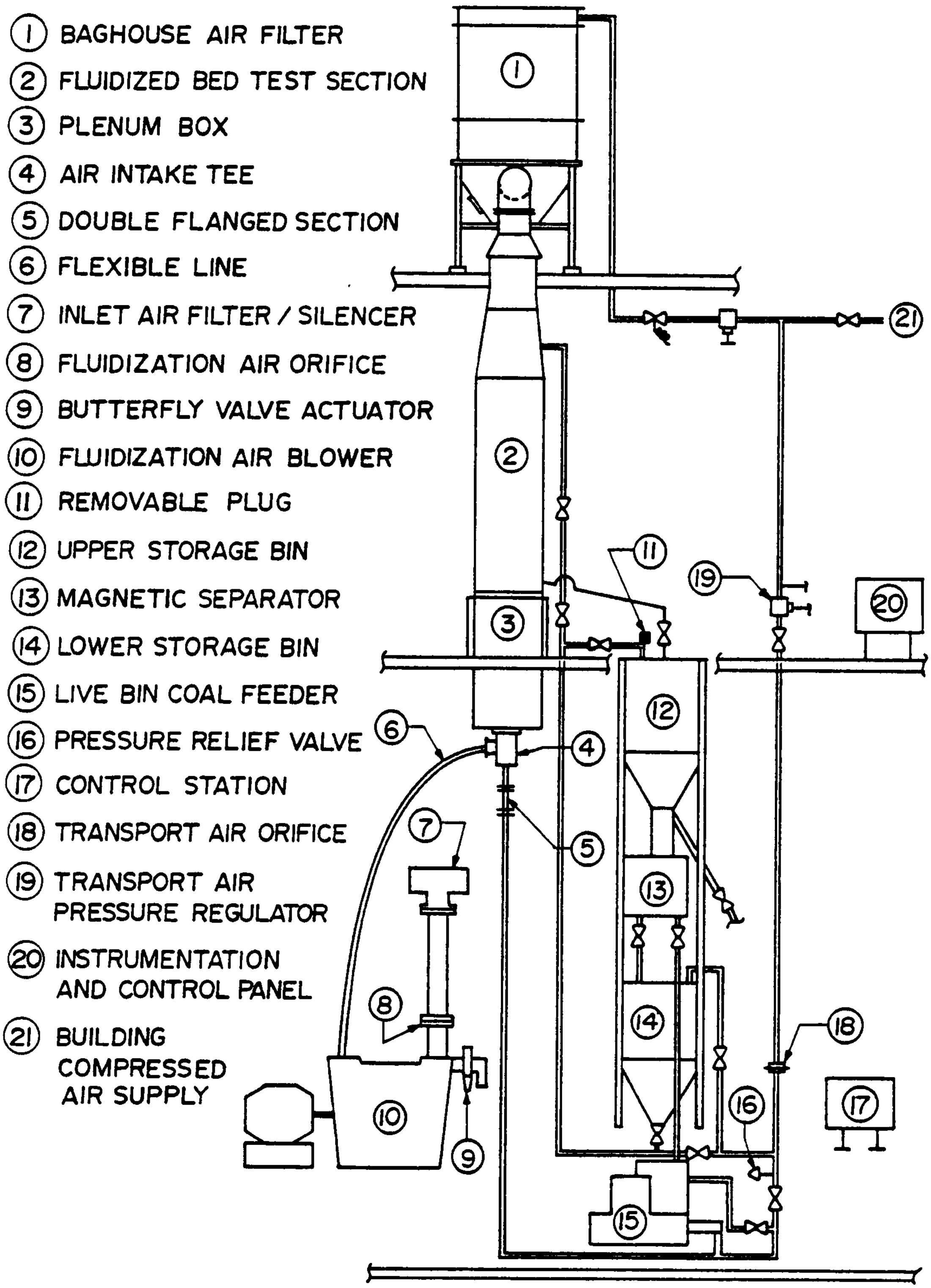

Figure 5.1 Experimental Facility.

Primary Systems

The primary systems of the facility are those systems which are basic to any fluidized bed. These systems include the fluidized bed containment and support structures, the fluidization air supply, the air distribution chamber below the bed (referred to as the plenum box), and the exhaust air filter.

The heart of the experimental facility is a 2 feet by 2 feet square and 7 feet high fluidized bed test section which is shown in Figure 5.2. It is formed from 0.5 inch thick plexiglass sheets which are permanently bonded in the corners and surrounded by a steel frame of vertical corner angles and horizontal support members for structural integrity. Each side or wall of the fluidized bed has one or more holes as shown in Figure 5.3. The plugs or panels which are normally installed in these holes are so designed that they are flush with the interior bed walls. Two opposing sides of the plexiglass bed have removable plywood panels at the base for access into the bed and for the placement of certain coal feeders. A third side of the plexiglass bed contains a matrix of twelve holes or ports into which the coal sample probes can be inserted. These ports are sealed with plexiglass plugs when the coal sample probes are not installed in them. Four of these plugs in turn contain small holes through which a hot-wire anemometer probe can be inserted for bed air velocity measurements. The fourth side of the plexiglass box contains a 6 inch diameter hole which provides easy access to the bed interior. Beneath the access hole is the 2 inch diameter bed drain hole. This side of the bed also contains two pressure taps and two thermocouples as shown in Figure 5.3. The plexiglass bed is

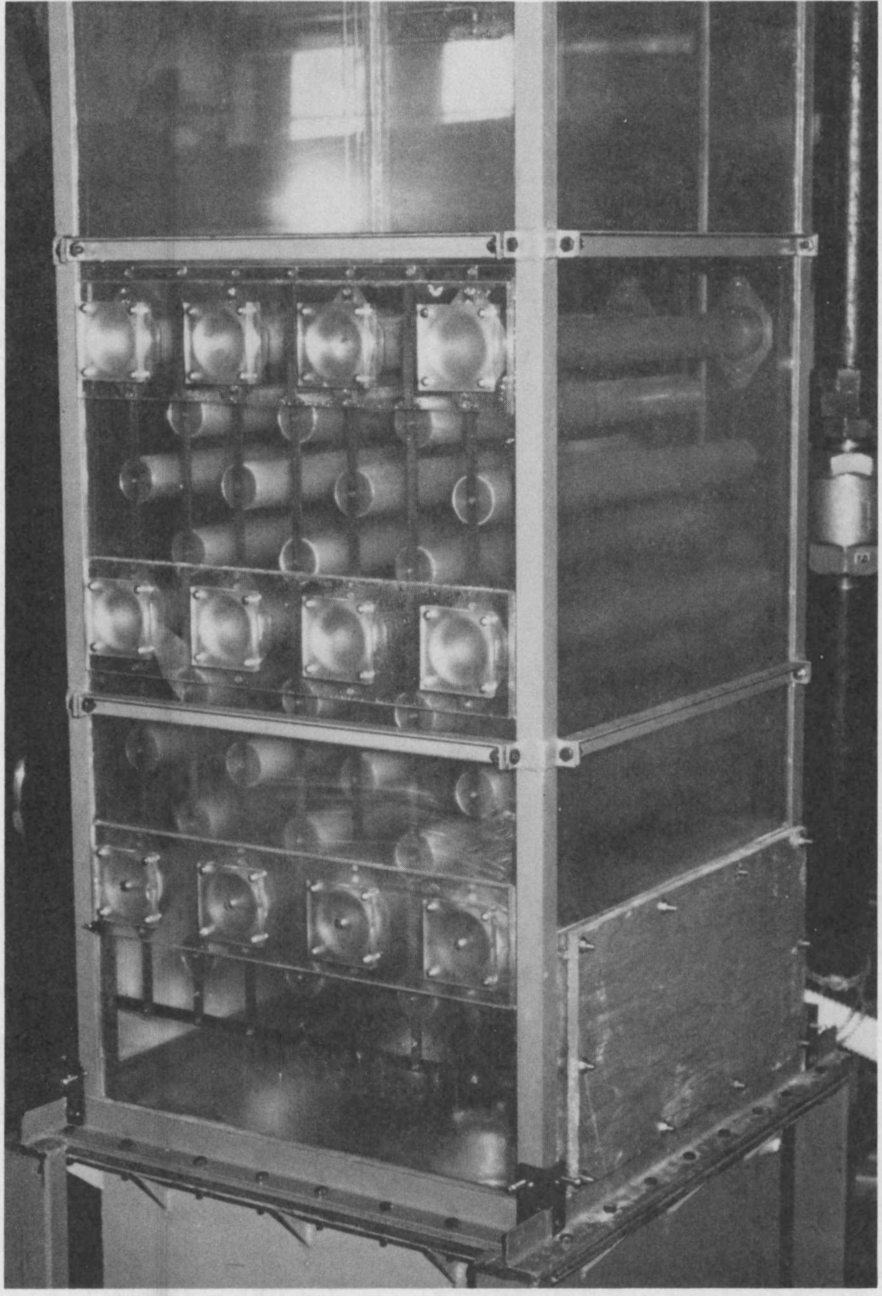

Figure 5.2. Fluidized Bed Test Section.

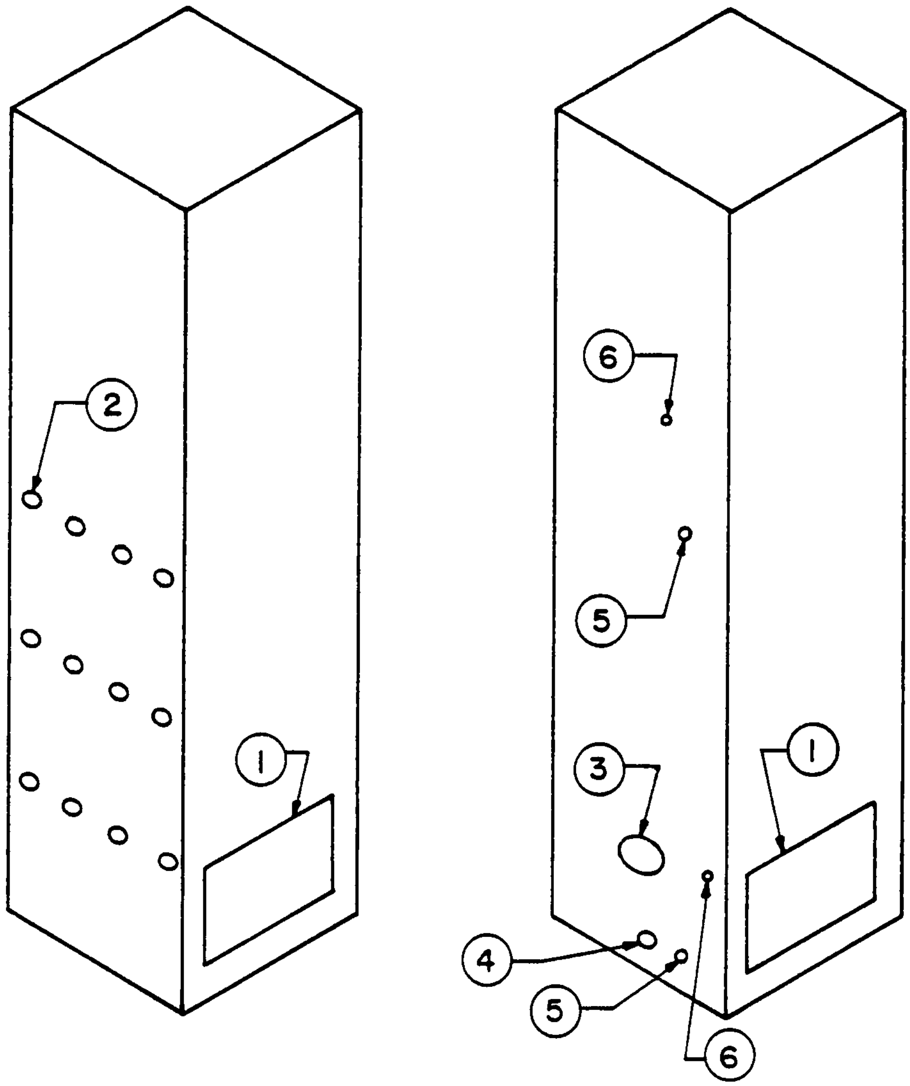

(1) RECTANGULAR OPENING
(2) COAL SAMPLE PROBE PORT
(3) ACCESS HOLE
(4) DRAIN HOLE
(5) PRESSURE TAP
(6) THERMOCOUPLE

Figure 5.3. Plexiglass Bed Walls.

rigidly supported at the base by a steel frame of channels and angles. All other connections to the bed are either flexible or semiflexible so that thermal expansion and vibration problems are minimized.

The fluidization air for the system is supplied by a seven stage Hoffman centrifugal blower located on the first floor. It is driven by a 60 horsepower single speed electric motor. Inlet air to the blower passes through a filter/silencer combination and an in line flow measuring orifice. Flow control is provided by a 6 inch pneumatically actuated butterfly valve on the inlet flange. The air exhausted from the blower passes through a 6 inch flexible line upwards into the plenum box.

The plenum box is a 2 feet by 2 feet by 4 feet high rectangular metal enclosure which is bolted to the support structure directly beneath the plexiglass bed test section. When a perforated plate air distributor is being used, the plenum box serves as an air expansion chamber between the 6 inch flexible line from the blower and the plexiglass bed test section. It is used as an airtight containment vessel for below-bed coal feeders, such as the valve cap feeder described by Henry [91], which are not designed to withstand differential pressures. Also, it serves as the mixing chamber for the fluidization air and the coal and transport air for most of the coal feeders tested. The plenum box contains five flanged ports covered by removable plexiglass disks which are pipe connection points for some of the coal feeders.

Bolted to the bottom of the plenum box is the air intake tee, shown in Figure 5.4. This is a specially made 90 degree tee consisting of a 6 inch diameter horizontal run joined to an 8 inch diameter

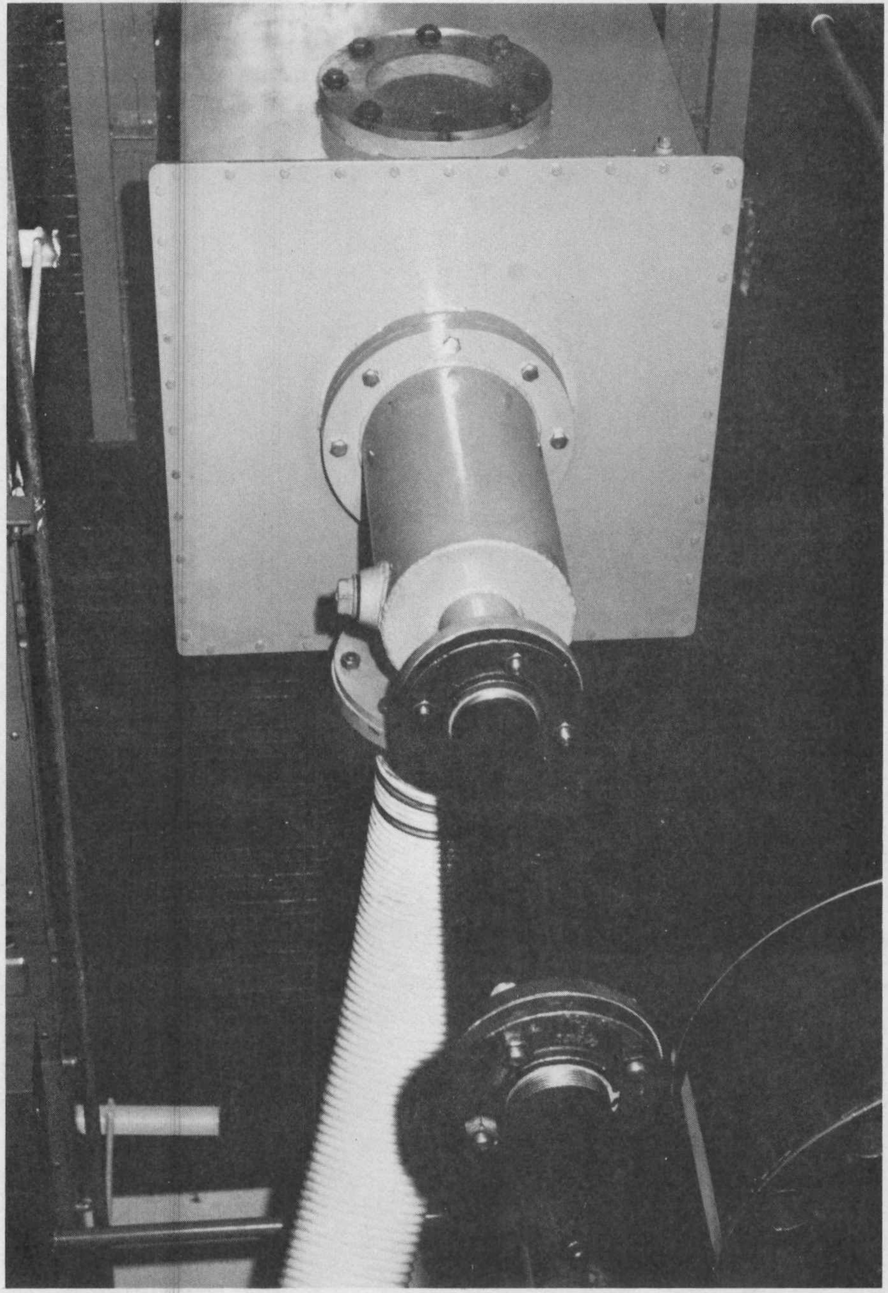

Figure 5.4. Air Intake Tee.

vertical run. The horizontal run is connected to the 6 inch flexible line from the blower, while the vertical run surrounds a concentric 3 inch pipe which is a section of the coal transport line. Near the bottom of the tee is a removable pipe plug to allow drainage of limestone which might leak out of the bed when the perforated plate air distributor or certain coal feeders are installed.

The plenum box and air intake tee assembly can be unbolted from the bed frame and lowered. Four wheels mounted on the plenum box drop into tracks, and the whole assembly can be rolled out from under the bed, as shown in Figure 5.5. Prior to lowering the plenum box, the 1 foot long double flanged section of 3 inch pipe visible in Figure 5.4 must be removed from the coal transport line directly beneath the air intake tee. The plenum box is lowered or raised through the simultaneous operation of two manual scissors jacks on opposite sides of the box. The flexible line from the blower does not have to be disconnected from the air intake tee during this movement of the plenum box. The easy disassembly and reassembly processes allow coal feeders to be installed or removed from the system with minimal amounts of labor and time.

The air which leaves the fluidized bed of limestone contains an appreciable dust loading. Thus, it is exhausted through a baghouse air filter located on the roof of the building above the plexiglass bed test section. The air filter contains 36 fabric bags which are cleaned automatically by reverse pulses of high pressure air. The dislodged dust falls to the bottom of the air filter housing where it collects and is subsequently removed.

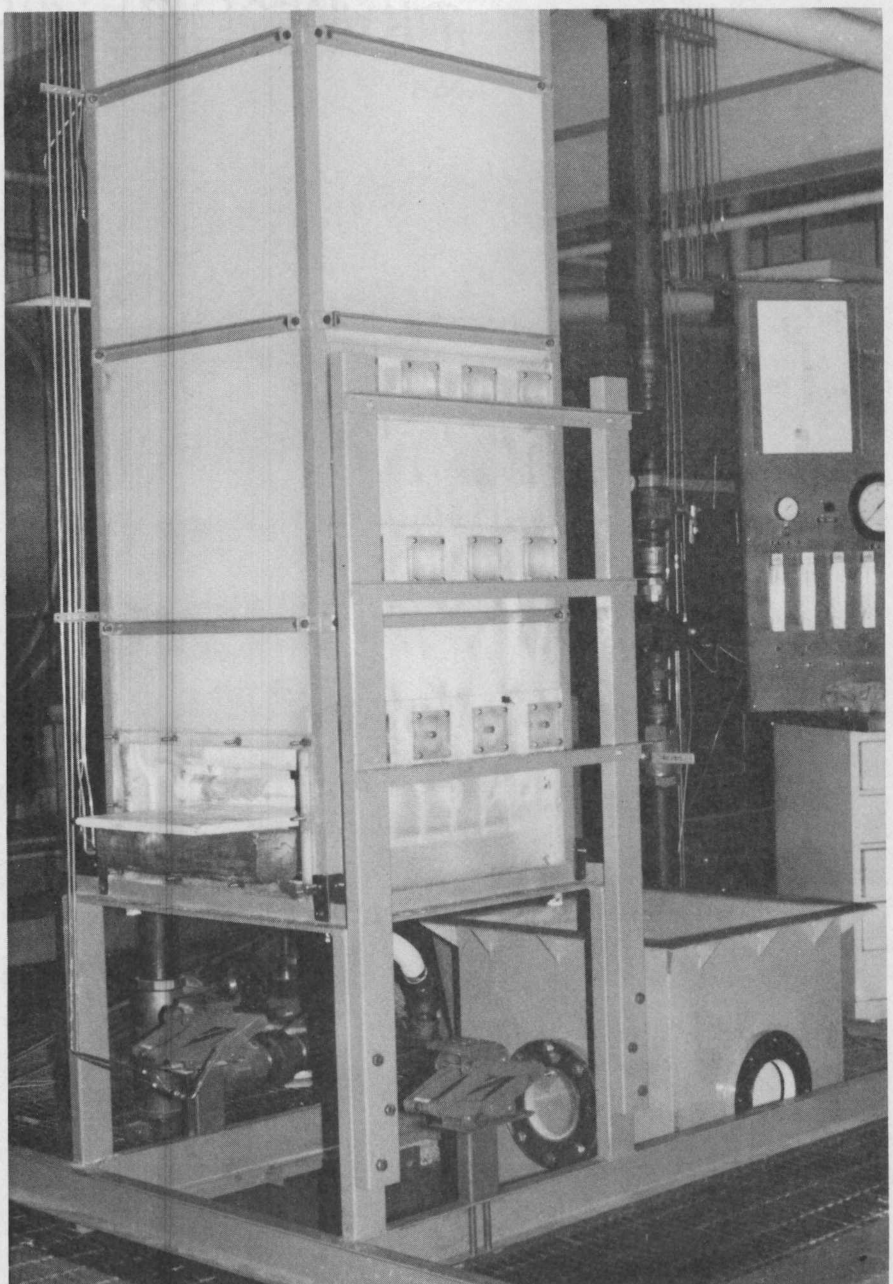

Figure 5.5. Plenum Box Removed from the Bed Section.

Secondary Systems

In addition to the primary systems of the experimental facility, there are four secondary systems which support the operation of the basic fluidized bed. These secondary systems are the coal transport system, the limestone transport system, the bed drain system, and the separation-recycle system. The components of these systems are shown schematically in Figure 5.1 on page 59.

The coal transport system delivers imitation coal at a specified rate to the coal feeder being tested. The primary component of this system is a volumetric live bin screw feeder manufactured by Vibra Screw Incorporated of Totowa, New Jersey. The live bin feeder contains a 5 cubic foot capacity hopper which is vibrated to ensure a continuous flow of coal into the screw conveyor which leads to the coal transport line. After exiting the screw conveyor, the coal is pneumatically transported through a 3 inch line approximately 5 feet horizontally and then 15 feet vertically through the air intake tee and into the plenum box where it enters the coal feeder being tested. All sharp elbows in the material transport lines are actually standard pipe tees which have one leg plugged. The tees are oriented so that the dead end leg containing the plug is in the path of the material entering the tee. Material accumulates in the plugged leg and tends to wear on itself, rather than on the fitting.

The limestone transport system fills the bed with the desired amount of limestone prior to a fluidization or coal feeding test. A major component of this system is the lower storage bin which has a capacity of approximately 18 cubic feet. The bin is designed to withstand a pressure of 10 lbf/in^2 gage, although normally the pressure does not exceed 2 lbf/in^2 gage unless the transport line becomes plugged with limestone. The limestone flows out of the bin by gravity and into the 3 inch transport line. It is pneumatically conveyed 25 feet vertically to the top of the plexiglass bed from whence it free falls approximately 7 feet to the bed base.

The bed drain system removes the limestone, and imitation coal if present, from the bed following a test. This system contains a flexible 2 inch drain hose connecting the base of the plexiglass bed to the upper storage bin. The original intent was to use the pressure due to the weight of the fluidized bed material to cause this material to drain into the bin. However, due to the small downward slope of the drain hose and the friction within the hose, the drainage rate proved to be too slow. The solution has been to use an industrial vacuum cleaner to draw the bed material through the drain hose by putting a vacuum on the upper storage bin. By keeping the bed fluidized during draining, the surface of the bed remains level. Thus, the bed can be drained down to a 2 inch height of material, which, for structural reasons, is the height of the bed drain line above the bed base. When necessary, the remaining bed material can be vacuumed into the upper storage bin by connecting a short flexible hose to the inside of the 2 inch drain hole.

The separation-recycle system separates the limestone from the imitation coal after a coal feeding test. The system components include the upper and lower storage bins and the magnetic separator. The upper storage bin has a capacity of approximately 21 cubic feet and is larger than the lower storage bin primarily because it must contain more imitation coal than the lower bin due to the separation process between the bins. The upper bin is airtight, but is not built to withstand any significant differential pressure. The material flow from the upper bin into the magnetic separator immediately below it is regulated by a manually operated sliding gate valve at the base of the bin. The imitation coal is extracted from the limestone by the magnetic field of the separator. The imitation coal then passes through a flexible hose to the live bin coal feeder hopper and the limestone falls into the lower storage bin. Because all of the imitation coal is not separated from the limestone in a single pass through the magnetic separator, the material in the lower storage bin is returned or recycled to the upper storage bin for additional passes through the separator. This material is moved to the upper bin by a pneumatic transport process very similar to that used for limestone transport into the bed.

The transport air utilized by the above secondary systems is supplied by an air compressor which services the building. A small amount of the incoming air is used for control pressures and for the baghouse cleansing cycle. The majority of the air is used for pneumatic transport purposes, and its flow is remotely controlled with a pressure regulator. The transport air flow branches into one line supplying the limestone transport and separation-recycle systems and another line serving the coal transport system. A pressure relief valve is installed in the transport air line to protect the lower storage bin and the live bin coal feeder from overpressurization.

Instrumentation

Because the fluidized bed is an experimental facility, a reasonably large amount of instrumentation has been incorporated into the system to allow efficient data collection. The measurements which are made during tests consist primarily of pressures and temperatures at various locations and coal feeding measurements made with the coal sample probes.

The fluidization air volume is measured with an orifice in the 6 inch inlet line to the blower. This orifice does not conform to ASME design codes because it has a diameter ratio of 0.85 to give a lower than normal pressure drop, and the upstream straight pipe length is less than that recommended. The transport air volume is measured by an orifice in the 3 inch supply line. This orifice does conform to ASME design codes and has a diameter ratio of 0.60 and an upstream straight pipe length of approximately 10 feet.

Three important pressures are measured during each fluidization or coal feeding test. The pressure taps for these measurements are specially constructed because two of the pressures are measured in two phase regions, i.e., regions containing both air and solid materials. The principal idea behind these two phase pressure taps is that a small purge flow of air is necessary to insure that the pressure lines, which are 0.25 inch copper tubes, do not become plugged with solids. High pressure air is regulated to 60 lbf/in^2 gage and then split into three separate lines, one for each pressure tap. The air in each line passes through a needle valve and rotameter upstream of the pressure taps. The needle valve is used to achieve a sonic flow condition such that a constant purge flow of 9 standard cubic feet per hour is maintained despite variations in the downstream pressure. The pressure in each purge line is measured approximately 1 inch from the outlet of the line. This pressure is not the actual pressure which exists at the line outlet due to the effect of the purge flow, but a differential pressure between two such taps is the true differential pressure because each pressure tap is constructed identically. One pressure tap is located in the plenum box approximately 1 foot from its top and at the center of one side. A second pressure tap is located 2.5 inches above the base of the bed approximately 7 inches from the nearest corner. This tap is not closer to the base plate partly due to structural reasons and also so that it will be above the jet formation region of the perforated plate air distributor. The third pressure tap is located in the bed 4 feet directly above the second tap so that it will be above any bed height which is tested.

The three pressure lines to the plenum box and the bed are connected to pressure transducers which convert the mechanical pressure signal to an electrical signal. Each pressure tranducer contains a diaphragm connected to a strain gauge. The electrical signal from the strain gauge is amplified and used to drive a pen on a Gould Brush 2400 strip chart recorder. Thus, both the magnitude and frequency of the three pressures are recorded in analog form on the chart.

The three pressures mentioned above, the two pressures from each orifice, and the inlet and exhaust pressures of the blower are recorded in digital form by a device known as the scanivalve unit.

This instrument is a teletype to which a microprocessor, a transducer, and a scanivalve have been attached. The scanivalve is a mechanism which consecutively connects each of as many as 48 pressure ports to a single transducer under the control of the microprocessor. The microprocessor interprets the pressure signal at each port and causes the teletype to print it. The scanivalve unit is programmed to read and record the nine pressures listed above within repeating 30 second cycles.

The above nine pressure lines can be connected individually or in differential sets to a bank of six 30 inch water manometers or a single 60 inch water manometer located at the control panel. The actual connections to the manometers vary from test to test. The lower bed pressure line and the transport air pressure line are connected to gauges on the control panel. These pressures are observed and recorded manually as desired during the tests.

Despite the fact that the experimental fluidized bed is a cold, or ambient temperature, facility, various temperatures must be monitored. Five type J (iron-constantan) thermocouples are used for the temperature measurements. A digital thermocouple reader is used in conjunction with a special thermocouple switch to display the five temperatures individually. Also, the fourth channel of the previously mentioned strip chart recorder is used to record the in-bed temperature in analog form.

The blower inlet air temperature and the in-bed air temperature are measured so that the volume of air through the system can be determined by correcting the inlet fluidization air flow for the expansion caused by the temperature rise across the blower. The inlet transport air temperature is also measured so that the transport air flow can be corrected to the in-bed conditions. The temperature of the air exiting the blower is monitored because the 6 inch flexible hose softens at excessively high temperatures. The temperature of the plexiglass near the base of the bed is also monitored for a similar reason.

A Sony portable video camera and video tape recorder are used to record the visible fluidization characteristics of selected tests. The tapes can be replayed on a television monitor to review and compare the performance of the various coal feeders tested.

Auxiliary Components

Two auxiliary components which do not fit into any of the above classifications are the perforated plate air distributor and the heat transfer tube assembly. These components can be installed in or removed from the experimental facility depending on the test configuration required.

The perforated plate is a basic air distributor containing a square matrix of holes and is shown in Figure 5.6. It was fabricated from a 29 inch by 29 inch high strength aluminum plate of 0.25 inch thickness and contains 2809 holes in a 53 by 53 array. The holes are 0.1094 inches in diameter and are spaced 0.453 inches center-to-center in the square array. The area factor (ratio of hole area to plate area) of this plate is 0.046. On the bottom side of the plate each hole has a 90 degree countersink of 0.25 inches diameter. The design of the perforated plate distributor is outlined in Appendix B.

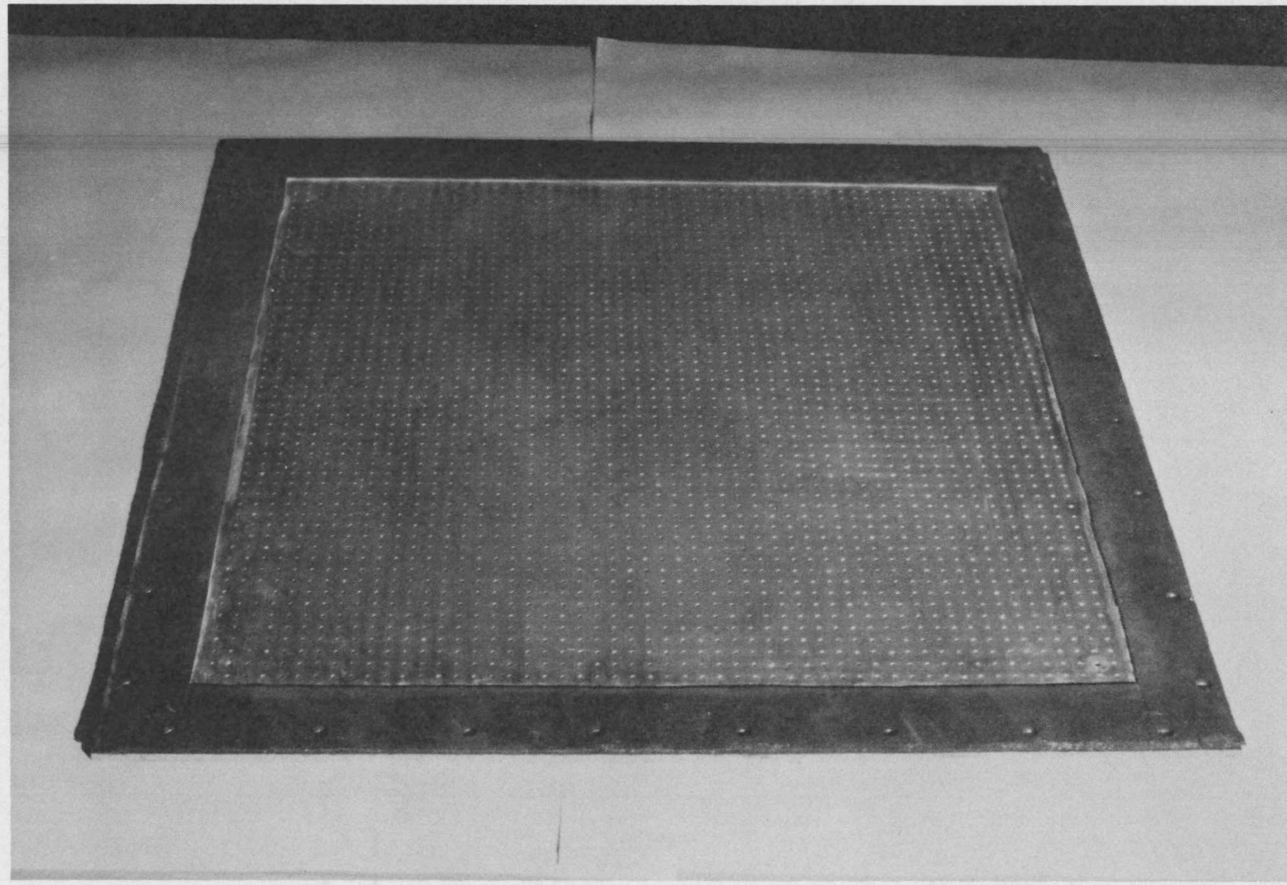

Figure 5.6. Perforated Plate Distributor.

The heat transfer tube assembly, shown in Figure 5.7, is a matrix of 35 straight tubes which simulate the heat transfer tube configuration of a hot bed. The tubes themselves are 2 inch aluminum thin wall tubes. The tubes are in a triangular array as shown in Figure 5.8 with a horizontal center-to-center spacing of 6 inches and a vertical distance of 3 inches between the centerlines of each row of tubes. Twelve of the tubes can be removed through the ports in one wall of the bed and replaced by the coal sample probes when coal feeding samples are to be taken. The tubes are held in place at either end by a frame of vertical bars attached to two cross pieces which in turn are attached to vertical angles in the bed corners as can be seen in Figure 5.7. The frame can be installed in or removed from the bed when the plenum box is moved to the side. When the assembly is installed, it is held in place by four screws which secure the frame to the base plate.

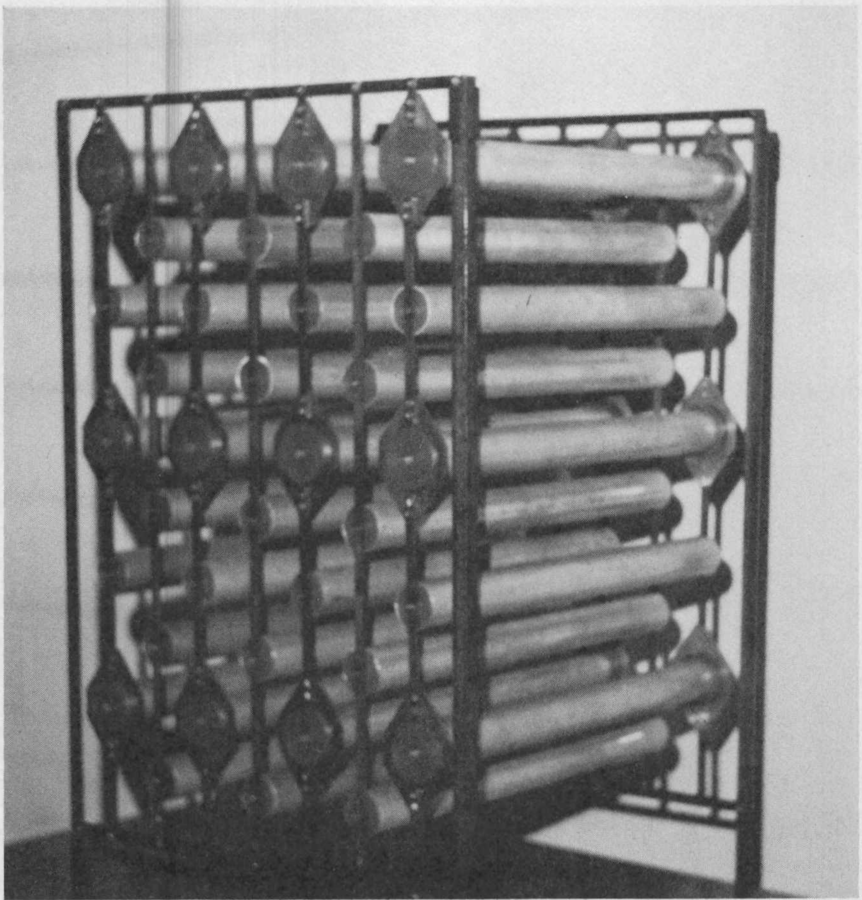

Figure 5.7. Heat Transfer Tube Assembly.

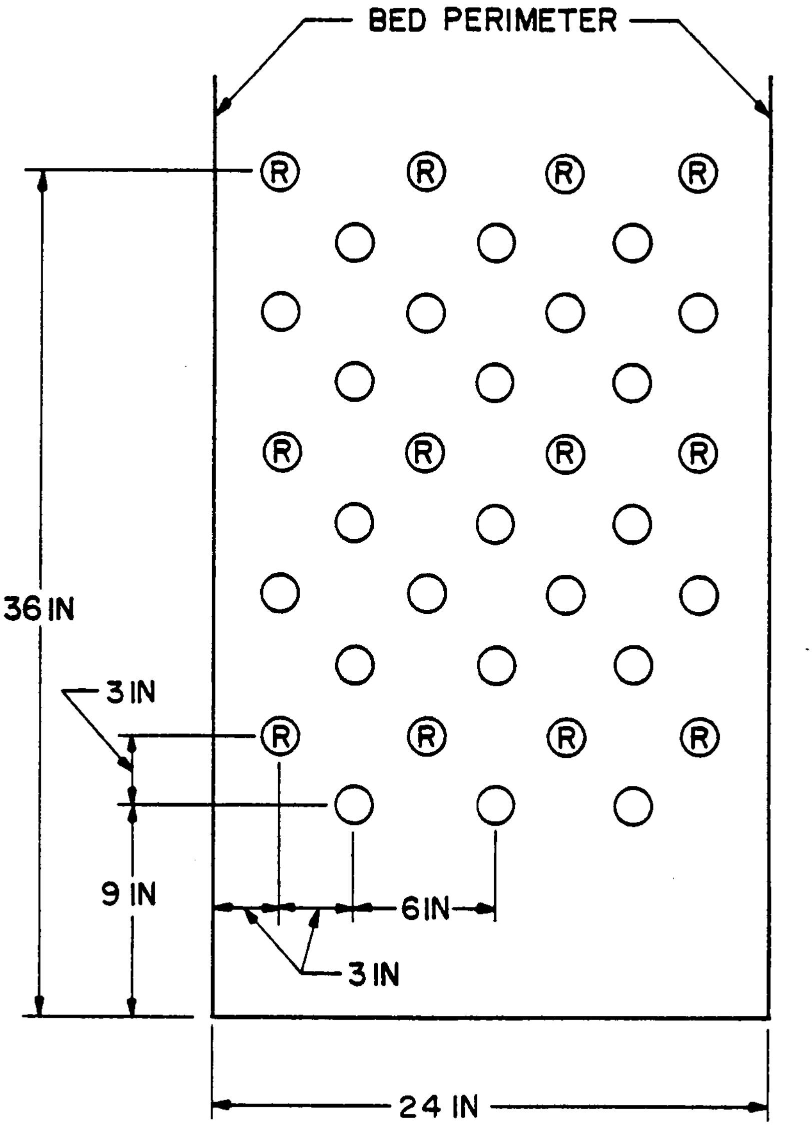

R - DENOTES TUBES WHICH CAN BE REMOVED

Figure 5.8. Heat Transfer Tube Assembly Dimensions.

CHAPTER 6

BASIC FACILITY PERFORMANCE AND EXPERIMENTAL METHODS

Introduction

The basic performance of the experimental fluidized bed test facility is discussed in conjunction with a description of the experimental methods employed because the facility performance often guided the development of these experimental methods. At the outset it was uncertain whether or not some of the methods developed during past fluidized bed research would yield useful results with the present experimental facility. Thus, while several of these older methods were in fact adopted for use, it was also found necessary to modify some of these methods and to even develop new ones during the basic performance tests.

Air Handling Systems

Fluidization Air System

The fluidization air system consists of the blower inlet air filter/silencer combination, the flow measurement orifice, the butterfly control valve, the blower, the flexible hose at the blower outlet, the air intake tee, the plenum box, the plexiglass bed test section, and the baghouse air filter. Initial tests revealed that no air leaks existed in the system and that all the components were functioning as expected except for the air filter/silencer combination and the blower.

The inlet air filter/silencer combination exhibited a higher pressure drop than appeared reasonable. Although this problem might seem minor, every loss in the system was significant because the blower performance was found to be marginal. A series of tests were performed with various combinations of the air filter element, the silencer housing, and the silencer housing top removed from the blower inlet. It was found that the air filter/silencer combination had a pressure drop of 19 inches of water (0.7 lbf/in^2) while that of the filter element alone was 11.5 inches of water (0.4 lbf/in^2). Thus, with the concurrence of the blower manufacturer, the air filter element was removed from the silencer housing for all testing.

The geometry and location of the fluidization air flow measurement orifice deviate significantly from recommended practice, so it was necessary to calibrate the orifice in place. The original intent was to perform velocity measurements in the bed with a hot-wire anemometer and then use a simple velocity-area-integration method in conjunction with corrections for the temperature rise across the blower to determine the flow rate. This method is performed by dividing the flow area into several regions, measuring the velocities in each of these regions, and then summing the individual flow rates using the equation

$$Q = \Sigma(VA) \; . \tag{6.1}$$

The cross section of the fluidized bed test section was divided into 16 equal square regions of 0.25 ft^2 area, and the velocity was measured at the center of each of these regions. Thus, the bed flow rate could be calculated by modifying Equation (6.1) to become

$$Q = (\Sigma V)(.25\ ft^2) \; . \tag{6.2}$$

Numerous tests were conducted at different flow rates and with the velocity traverses being taken at different heights in the bed. The measured velocities varied by as much as 90 to 120 feet per minute (1.5 to 2.0 feet per second), and, in addition, no symmetry was ever evident in the velocity profiles. A typical set of average velocity readings for an air test at full blower flow is shown in Figure 6.1. For this case the velocity-area-integration method measured a flow of 1825 ft^3/min, whereas a more accurate method measured a flow of 2075 ft^3/min. In several comparisons of the two methods, the velocity-area-integration method yielded flow rates which were 10 to 20 percent lower than those measured by the more accurate method.

The more accurate flow measurements were obtained by using a bell mouth inlet device. Quite fortuitously, a bell mouth with the required base diameter of 6 inches was available. It was fastened to a short pipe on the blower inlet for a series of tests. The method developed by Wilkerson [92], outlined in Appendix C, was used to calculate the flow rate from the static pressure measured at the bell mouth throat.

The bell mouth inlet was thus used as the flow measuring device for calibrating the fluidization air orifice. The resulting calibration curve for this orifice is shown in Figure 6.2. The uncertainty analyses performed on these and other experimental data presented subsequently are outlined in Appendix D. To determine the actual flow rate within the bed test section, the inlet volumetric flow rate indicated by the orifice must be corrected to the bed conditions due to the changes in the air temperature and pressure which occur. Letting the subscript i represent the inlet quantities and b represent the in-bed quantities, the continuity

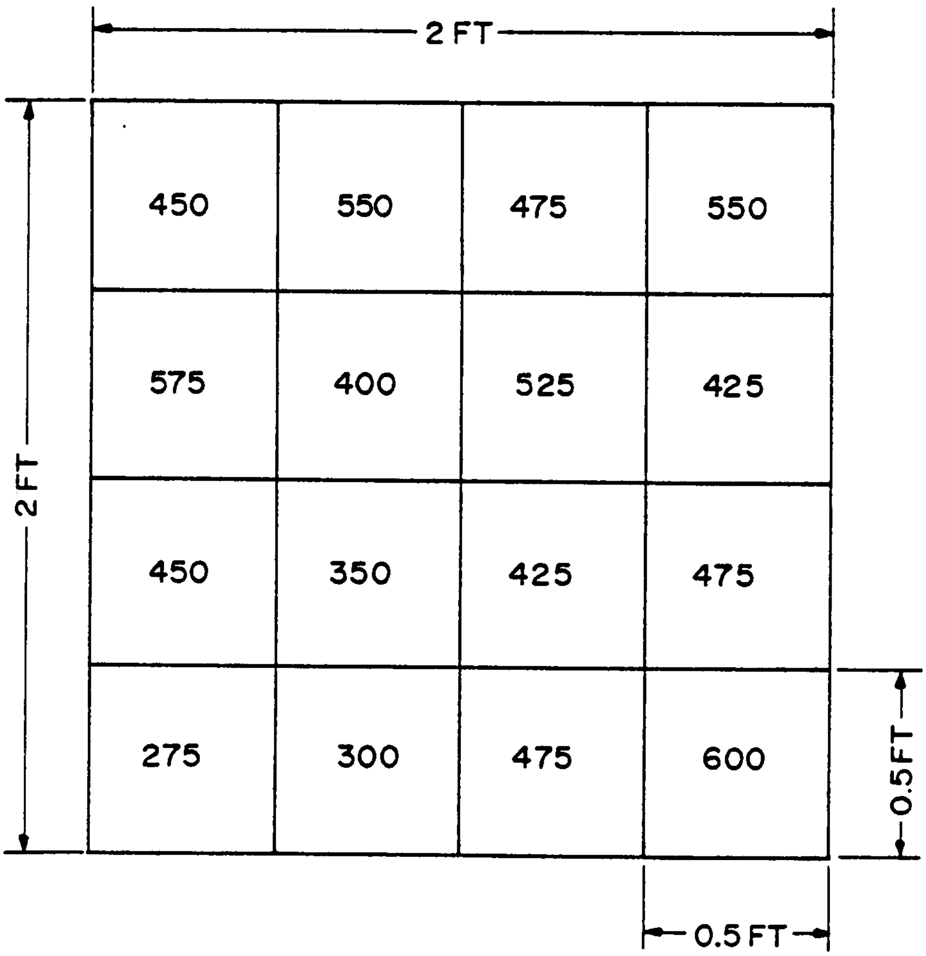

Figure 6.1. Typical Bed Air Velocity Profile Measured With the Hot-Wire Anemometer. Average velocities are in ft/min.

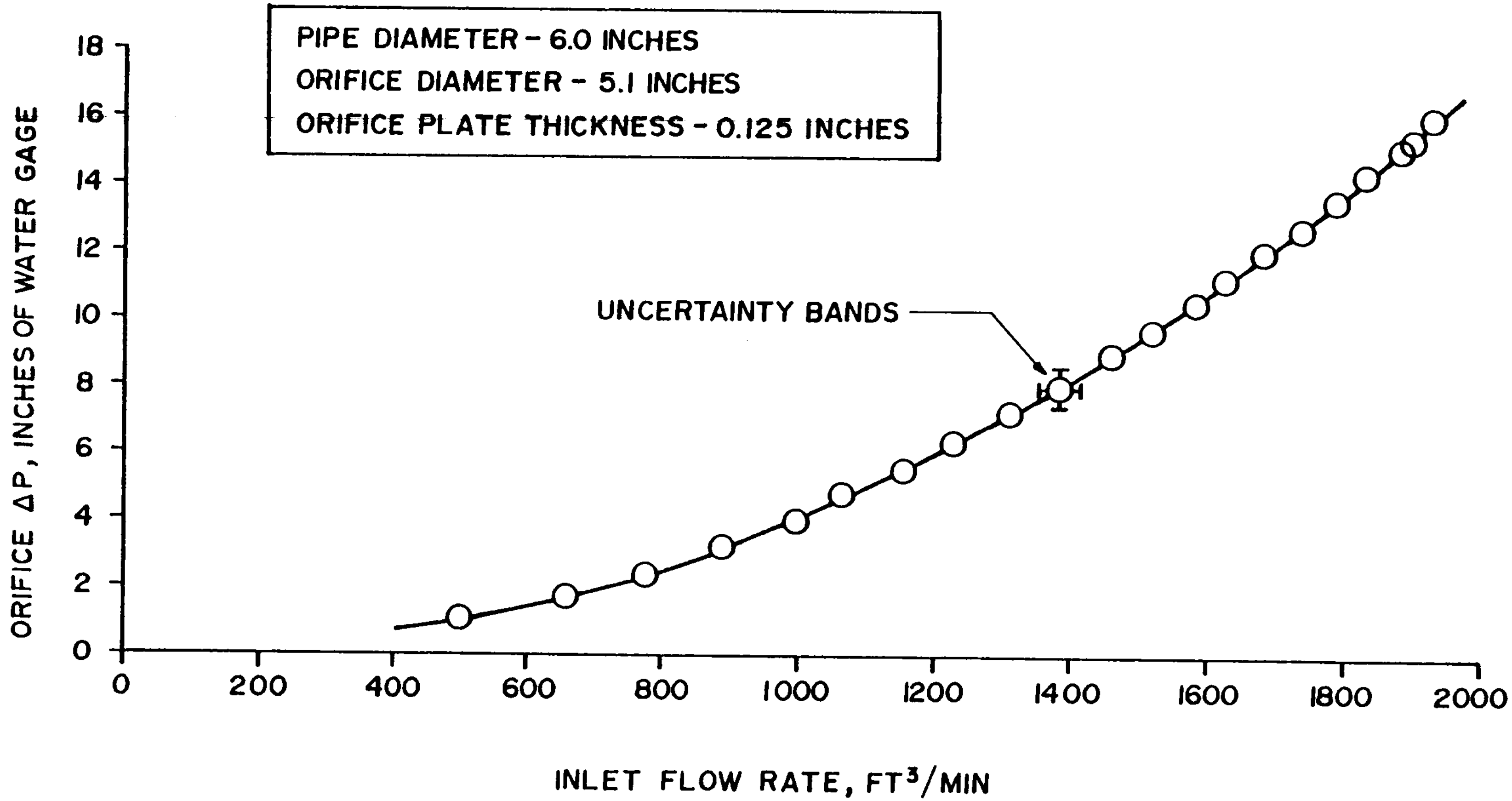

Figure 6.2. Fluidization Air Orifice Calibration Curve.

equation and ideal gas equation give the in-bed flow rate in terms of the inlet flow rate as

$$Q_b = Q_i (T_b/T_i)(P_i/P_b) \tag{6.3}$$

where the temperatures and pressures are absolute quantities.

Another series of measurements were taken with the bell mouth inlet to determine the blower performance curve. During initial tests the blower output appeared to be somewhat below the specifications, so data were taken to generate the discharge pressure versus inlet volume curves shown in Figure 6.3. In this figure the discharge pressure has been corrected to ambient conditions of 14.7 lbf/in^2 and 68°F. During these tests the pneumatically actuated butterfly control valve was on the inlet of the blower and a manually actuated butterfly valve was bolted to the outlet flange of the flexible line on the blower exhaust. Measurements were made primarily to determine the blower performance with a fully open inlet valve, although some measurements were made with this valve at the intermediate positions shown in the figure. The blower performance was indeed found to be below the specifications, but it was adequate for the tests which were subsequently conducted.

Transport Air System

The transport air system consists of the 1.5 inch pressure regulator, the pressure relief valve, the flow measurement orifice, and the necessary control elements. All the components in this system performed essentially as expected.

No convenient means was available by which the 3 inch orifice could be calibrated, so it was assumed that the design orifice flow

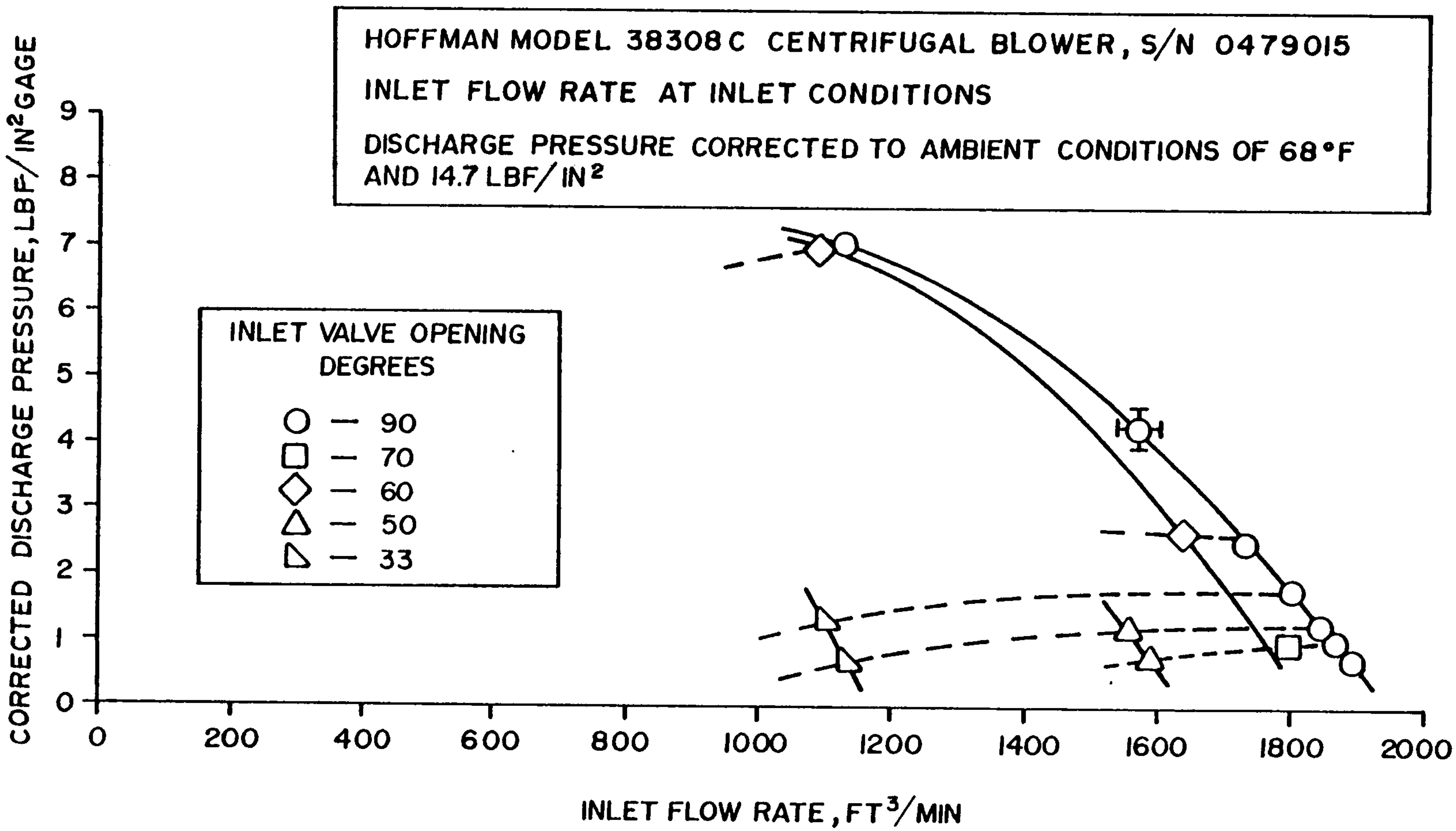

Figure 6.3. Experimental Blower Performance Curves.

coefficient of 0.65 is reasonably accurate. The source of this coefficient is discussed by Henry [91]. Some error in the calculation of the transport air flow rate can be tolerated because at most it is only 20 percent of the total bed flow. The equation used to calculate the transport air flow, derived in Appendix E, is

$$Q = 7.66(T_a \Delta s/P_a)^{1/2} \ . \qquad (6.4)$$

In this equation the transport air flow is in ft^3/min for the air temperature in degrees Rankine, the manometer deflection in inches of water gage, and the air pressure in lbf/in^2 absolute. Figure 6.4 illustrates the manometer deflection versus flow relationship for average inlet air conditions during the tests of 83°F and 17.5 lbf/in^2 absolute. As with the fluidization air calculations, Equation (6.3) on page 83 must be used to correct the transport air inlet flow to the bed conditions.

Two Phase Pressure Measurement System

The system for measuring pressures in two phase regions, i.e., regions in which both solid particles and air are present, was checked for proper operation during the air system test series. Although the three pressure taps were constructed as similarly as possible, the base pressures were not equal when measured with identical purge flows through the lines but with no air flow or solids in the bed test section. The base plenum box pressure was 0.3 inches of water, while the base lower bed pressure and upper bed pressure were 0.1 inches of water. However, this difference in base values was considered negligible because the pressures were only read to

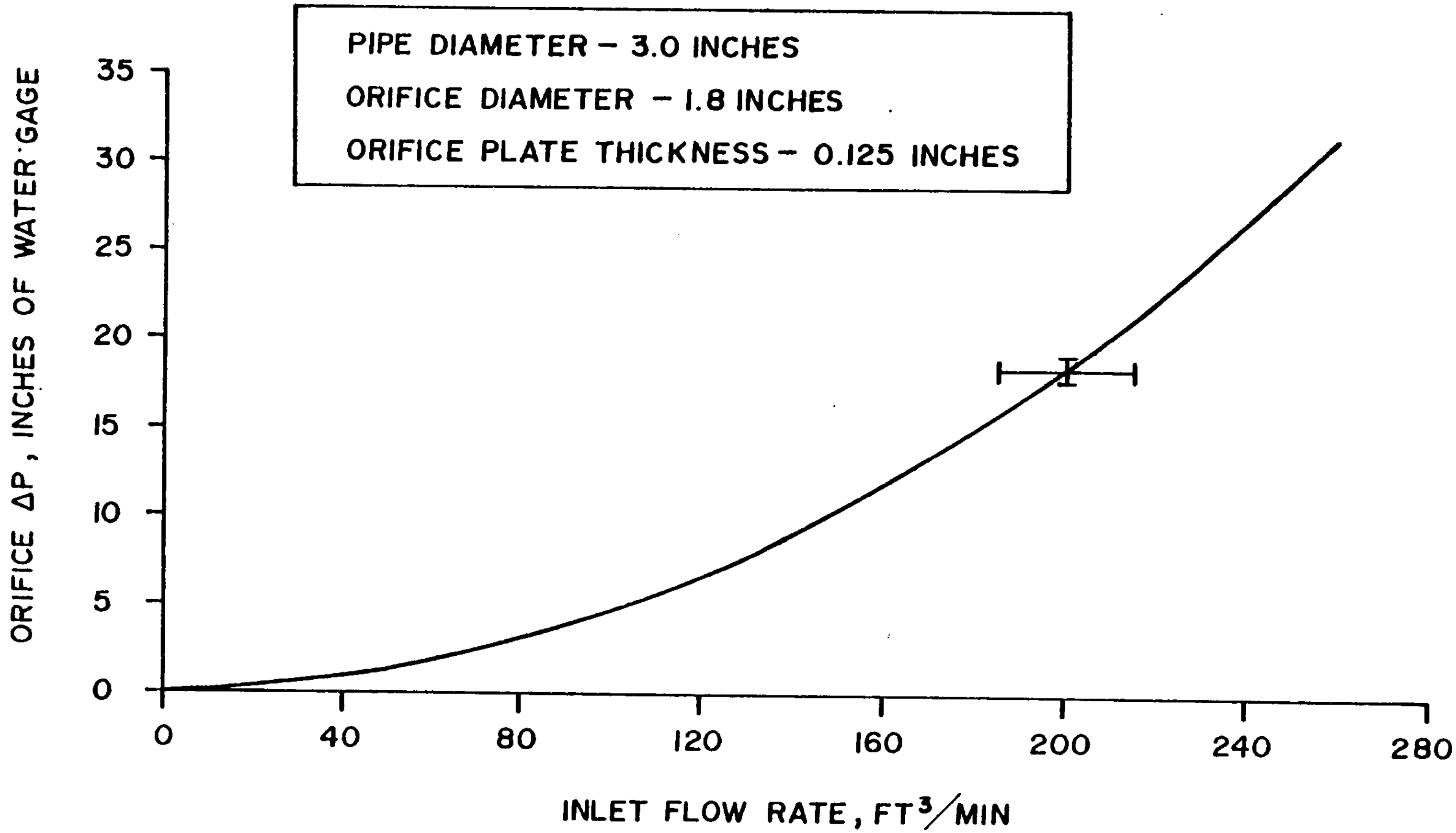

Figure 6.4. Transport Air Orifice Discharge. For average inlet air conditions of 83°F and 17.5 lbf/in^2 absolute.

an accuracy of ± 0.2 inches of water. The base values for the plenum box and upper bed pressure taps remained essentially constant during subsequent tests, but that of the lower bed pressure tap did not. During tests with the pipe grid coal feeder, described in Chapter 7, the base value for this latter tap varied from 0.0 to 2.0 inches of water. As verified by the rotameter indications, this pressure line never became plugged during the tests. However, at times a few particles were seen in the end of the pressure line when the bed material was drained. The presence of these particles may account for the variations in the base pressure values.

Perforated Plate

The perforated plate air distributor was installed in the facility for air tests while the fluidization and transport air systems were being tested. The pressure drop across the perforated plate as a function of the bed superficial velocity is shown in Figure 6.5. The pressure drop measured at the design velocity of 7.5 ft/sec was approximately half of that predicted by the equations developed in Appendix B. This discrepancy between the theoretical and experimental values occurred because the actual orifice flow coefficient was 0.89 while the design coefficient was 0.61. Evidently the countersinks on the hole inlets performed well.

Because the perforated plate pressure drop was lower than predicted and due to slugging problems discussed in the next section, after several tests the perforated plate was modified to increase the pressure drop across it. This modification consisted of covering alternate holes in the plate with strips of heat resistant plastic tape. In the modified version, referred to as the taped perforated plate,

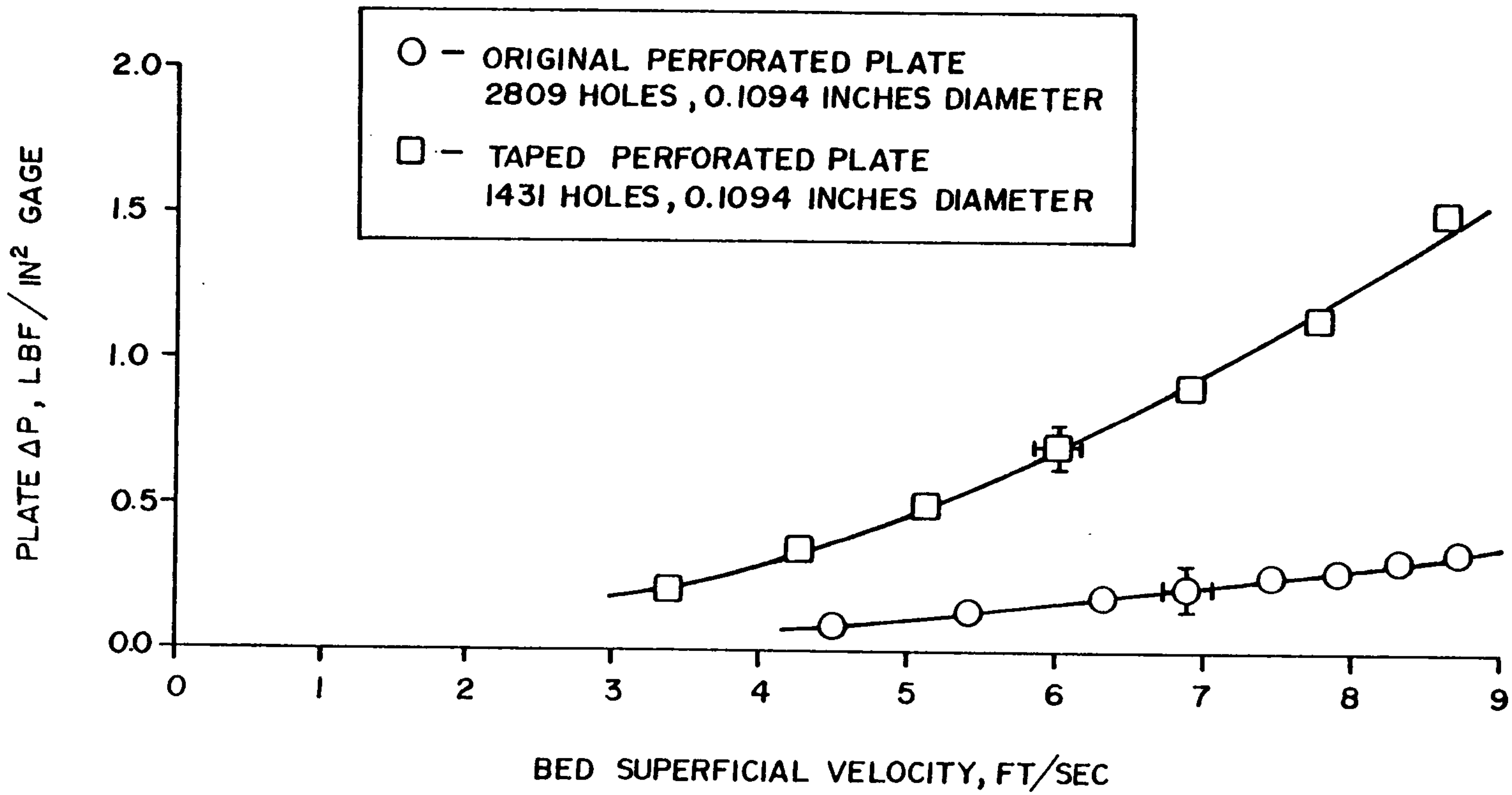

Figure 6.5. Perforated Plate Pressure Drop.

1378 out of the 2809 holes (49.1 percent) were covered. As would be expected, because pressure drop is proportional to the velocity squared, the pressure drop across the plate increased by a factor of four. The pressure drop versus bed superficial velocity performance of the taped perforated plate is also shown in Figure 6.5.

Fluidization

Limestone

The limestone bed material used during all fluidization tests is a nominal 0.125 inch top size double screened limestone supplied gratis by the Franklin Limestone Company of Crab Orchard, Tennessee. The limestone sieve size is stated as 6 by 16, i.e., all material retained on a number 6 sieve or passing a number 16 sieve has been removed. A sieve analysis of the limestone put in the experimental facility is shown in Table 6.1. The weighted average particle diameter, calculated by

$$D_{wt.avg.} = \Sigma[(\text{percentage retained on sieve})(\text{sieve opening diameter})] , \qquad (6.5)$$

is 0.01 inches (2530 μm). The particle or true density of limestone is approximately 170 lbm/ft^3 [93], while the experimentally determined average bulk density of the limestone used is 92 lbm/ft^3.

Table 6.1 also contains a sieve analysis of the limestone after it has been used for approximately 15 hours of testing. It is evident that the limestone particles eroded because the percentage of the larger sieve sizes have decreased while those of the smaller sieve sizes have increased. Most of the erosion occurred during the pneumatic transport and separation-recycle processes rather than

TABLE 6.1

SIEVE ANALYSES OF FRESH AND USED LIMESTONE

Sieve[1]	Sieve Opening[2]	Percent Retained	
		Fresh Limestone	Used Limestone[3]
4	0.1870	0.0	0.0
6	0.1320	4.2	1.0
7	0.1110	31.7	18.0
8	0.0937	45.4	38.3
10	0.0787	11.4	18.0
12	0.0661	5.5	16.5
14	0.0555	0.8	4.0
16	0.0469	0.2	1.5
20	0.0331	0.1	1.6
Pan	0.0000	0.6	1.1

[1] U.S.A. Standard Series.

[2] Approximate opening diameter in inches.

[3] Material which was used for approximately 15 hours of testing.

during the fluidization tests. This conclusion was determined from the amount of dust generated by the respective processes. During the time span represented in Table 6.1, approximately 140 pounds of dust were generated from typical 500 pound limestone bed masses.

Perforated Plate Performance

Fluidization tests were conducted using the perforated plate air distributor with slumped limestone bed heights of 3, 6, and 12 inches. Greater bed heights were not tested initially due to the slugging problems encountered. Many of the results obtained from these early tests were qualitative rather than quantitative because the strip chart recorder and scanivalve unit were not yet in use. Pressures were measured at the plenum box, lower bed, and upper bed pressure taps with water manometers in order to quantify the dynamic performance of the perforated plate and the limestone bed material.

One of the first parameters measured was the minimum fluidization velocity. This velocity is determined experimentally by plotting the pressure drop through the bed as a function of the bed superficial velocity as shown in Figure 6.6. The superficial velocity is the average air velocity in the freeboard region of the bed. The freeboard region is that area above the limestone bed which has the same cross-sectional area as the bed. The velocity which corresponds to the point of intersection of the two distinct slopes in the figure is defined as the minimum fluidization velocity. For the test illustrated the limestone bed height was 12.5 inches. Another test under similar conditions yielded a minimum fluidization velocity of 4.3 ft/sec.

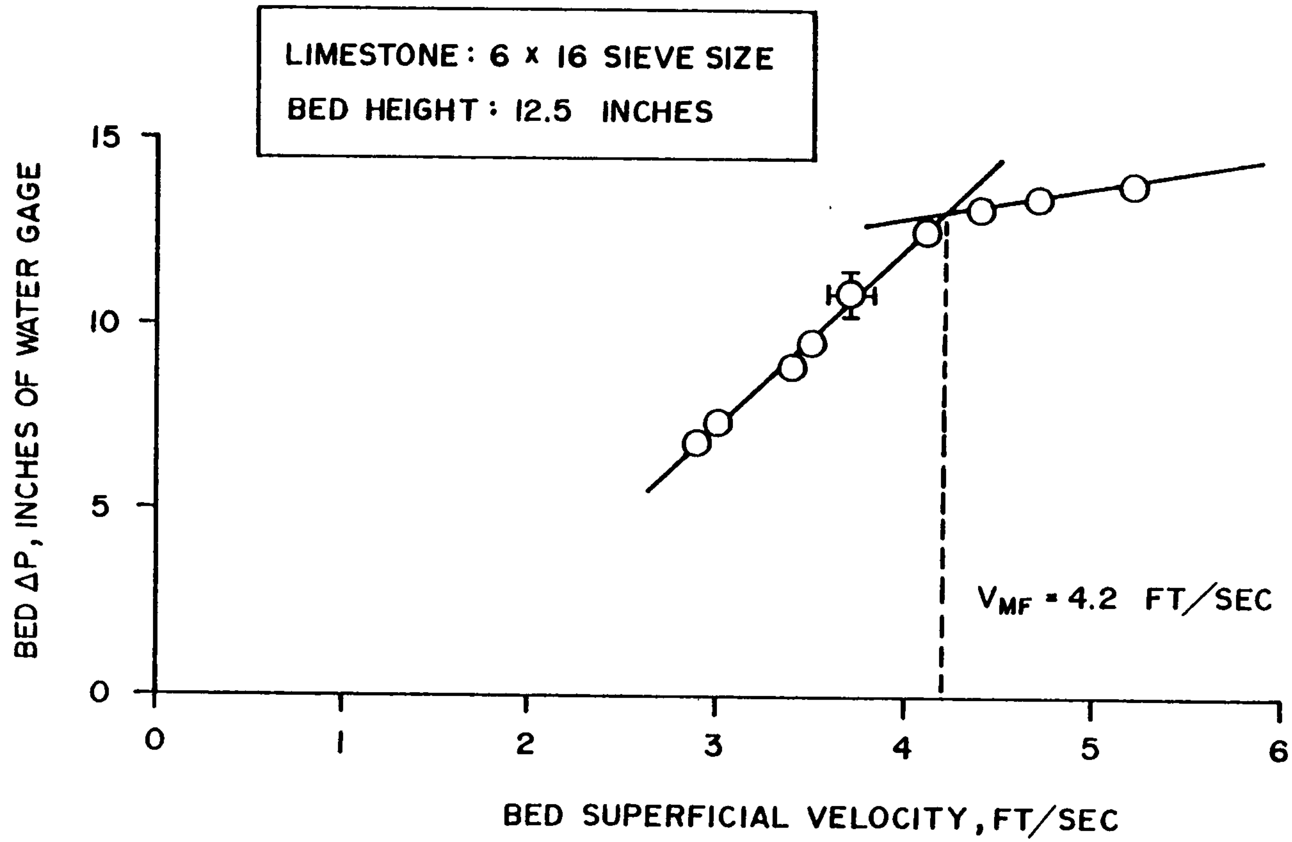

Figure 6.6. Minimum Fluidization Velocity Determination.

The most prominent characteristic of the perforated plate fluidization tests was the violent bed behavior which occurred at superficial velocities between 5 and 8 ft/sec. In this velocity range large bubbles were formed which sometimes appeared to stretch across the entire bed as they rose through the limestone. These large bubbles, or slugs as they are often called, caused the limestone bed to alternately lift and fall with considerable force (a 12 inch bed height contains approximately 360 pounds of limestone). Limestone particles were thrown as high as 3 feet above the bed surface as the bubbles broke through. The magnitudes of the resulting pressure fluctuations through the bed were difficult to determine due to the oscillating liquid levels in the manometers, but they appeared to be $\pm$ 5 inches of water at a superficial velocity of 8 ft/sec.

The behavior of the experimental fluidized bed with the perforated plate distributor was quite consistent with that of a very similar fluidized bed operated by Canada et al. [39]. Both beds have the same cross-sectional areas, air flow range, and temperature range. The particle densities are consistent, although Canada et al. used a single particle size which corresponds to the average of the limestone particle size range given previously. The minimum fluidization velocity measured in both beds is identical. Canada et al. observed basically the same qualitative features that were discussed above. The visually observed pressure fluctuation frequency of 0.8 cycles per second in the experimental bed is comparable to that measured by Canada et al. at a greater bed height. In addition, the bed performance characteristics agree quite well with the correlations of Catipovic et al. [46] which define the bed flow regimes in terms of the particle diameter and the superficial velocity. These correlations accurately predict the transition of the fluidized bed from the slow bubble regime to the rapidly growing bubble regime at approximately 5.5 ft/sec.

As mentioned previously, the perforated plate was modified by taping over half of the holes to see what effect this would have on the fluidization. No significant qualitative changes could be detected, although it would seem reasonable to assume that the bubbles formed by the emerging jets did not coalesce quite as quickly as before. The magnitude and the frequency of the pressure drop fluctuations were essentially the same as those observed with the unmodified perforated plate.

The heat transfer tube assembly was designed and installed in the bed both in an effort to minimize the slugging phenomenon and to more closely model the performance of an actual bed. The presence of the heat transfer tubes in the bed does appear to improve the fluidization performance in that the large slugs of air are broken up as they pass upward through the bed. However, the quantitative changes in the fluidization have not yet been documented. Tests have been performed with the taped perforated plate and the heat transfer tube assembly in which extensive data were recorded. However, complete comparative baseline tests have not been performed using the taped perforated plate with the heat transfer tube assembly removed from the bed.

Experimental Methods

The main parameter used to catalog fluidization data is the bed superficial velocity which is calculated by dividing the air flow from Equation (6.3) on page 83 by the bed cross-sectional area. If the flow is in ft^3/min, then the superficial velocity in ft/sec is

$$V_{sf} = Q_b/240 \ . \tag{6.6}$$

The pressure drop across a coal feeder is an important parameter because it determines the air pumping power required, which affects the efficiency of an actual unit. For the coal feeders tested in the experimental facility, this pressure drop is determined by subtracting the lower bed pressure from the plenum box pressure or by measuring a differential pressure across the two taps. Depending on the location of the coal feeder openings into the bed, part or all of the pressure drop due to the 2.5 inches of limestone below the lower bed pressure tap may need to be subtracted from the measured coal feeder pressure drop.

The bed pressure drop is determined by subtracting the upper bed pressure from the lower bed pressure or by measuring a pressure differential across these two taps. As with the coal feeder pressure drop, sometimes the measured bed pressure drop must be adjusted for the pressure drop across the 2.5 inches of limestone below the lower bed pressure tap.

Theoretically, the frictional pressure drop across a given fluidized bed height is equal to the buoyant weight per unit area of the limestone material. The pressure drop can be expressed simply as

$$\Delta P = \frac{W}{A} = \rho_s \frac{\forall}{A} \frac{g}{g_c} = \rho_s \ H_{fl} \ g/g_c \ . \tag{6.7}$$

By accounting for the buoyant force of the fluidizing gas and for the fact that particles are fluidized rather than a solid mass, the pressure drop across the bed becomes

$$\Delta P = (\rho_s - \rho_g)(1 - \varepsilon)\ H_{fl}\ g/g_c \ . \qquad (6.8)$$

In the latter equation, ε is the voidage fraction of the bed material and is defined as the void volume divided by the total volume. From the definition of the voidage fraction it can be shown that

$$\varepsilon = 1 - \rho_{bulk}/\rho_s \ . \qquad (6.9)$$

Because the bulk density of the limestone in the slumped state has been determined experimentally, Equation (6.9) can be substituted into Equation (6.8) with the slumped height to give

$$\Delta P = \rho_{bulk}(1 - \rho_g/\rho_s)\ H_{sl}\ g/g_c \ . \qquad (6.10)$$

For air fluidized beds of dense particles, the solid density is much greater than the gas density so the theoretical pressure drop across the bed can be approximated as

$$\Delta P = \rho_{bulk}\ H_{sl}\ g/g_c \ . \qquad (6.11)$$

A correction must be made in the bed height used in Equations (6.7) through (6.11) when bed internals are present as these equations are based on a homogeneous bed of limestone material. The two types of internals encountered in the experimental facility are the heat transfer tube assembly and the coal feeders which are tested. (The coal sample probes would have to be considered only if the heat transfer tube assembly was not installed.) The bed internals displace a portion of the limestone in the bed, and thus the apparent bed height must be reduced to account for this. The amount by which the bed height must be reduced when the heat transfer tube assembly is installed is given in Table 6.2, in which the corrections are shown as a function of the bed height. Whether or not a correction is necessary for a coal feeder depends on the volume of limestone it displaces. For example, the pipe grid feeder, discussed in Chapter 7, displaces 0.4 ft^3. This amount is significant because it is equivalent to 1.2 inches of bed height.

Theoretically the pressure drop across a fluidized bed remains constant, although in practice there is some slight variation. However, the pressure drop across a given part of the total bed height does not remain constant. This can be seen from Equation (6.8) on page 96 in which for a given part of the bed height the voidage fraction decreases as the superficial velocity increases, so the pressure drop across the given part of the bed height decreases. However, this decrease in pressure drop across a fixed segment of the bed as the superficial velocity is increased is slight except in the case of a greatly expanded bed. Thus, it is neglected in calculating the pressure drop across the 2.5 inch high portion of material at the base of the bed below the lower bed pressure tap. This pressure drop, calculated theoretically, is 0.13 lbf/in^2 (3.7 inches of water). As mentioned before, the experimentally measured pressure drop across the perforated plate or the coal feeders and that across the total bed may need to be corrected by this amount.

The magnitude of the pressure fluctuations occurring near the base of the bed are indicative of the fluidization. Thus, the lower bed pressure is recorded by the strip chart recorder, which is calibrated in inches of water. A representative lower bed pressure strip chart

TABLE 6.2

BED HEIGHT CORRECTIONS FOR THE HEAT TRANSFER TUBE ASSEMBLY

Apparent Bed Height[1], Inches	Bed Height Reduction, Inches
≤ 8	0.0
9	0.2
10-11	0.4
12	0.6
13-14	0.9
15	1.1
16-17	1.3
18	1.6
19-20	1.8
21	2.0
22-23	2.2
24	2.5
25-26	2.7
27	2.9
28-29	3.2
30	3.4
31-32	3.6
33	3.8
34-35	4.0
36	4.3
≥ 37	4.6

[1]For intermediate heights, e.g., 8.5 inches, estimate the height reduction by linear interpolation.

recording is shown in Figure 6.7. On this chart it can be seen that the pressure fluctuates considerably. The approximate maximum fluctuation (i.e., the largest fluctuation which is repeated) is recorded for each test configuration, and the average fluctuation is recorded at each superficial velocity tested. The average fluctuation is determined by visually estimating the middle position between the smallest and largest fluctuations as shown on the chart in the figure. The fluctuations which are read off the charts are used for comparative purposes, and therefore consistency is more important than absolute accuracy.

The frequency of the pressure fluctuations measured at the lower bed pressure tap is also a characteristic of the fluidization. For frequency measurements the chart speed is increased to obtain resolution between the individual cycles as can be seen on the left portion of the strip chart in Figure 6.7. Each frequency scan covers approximately 10 seconds so that the average frequency can be determined by counting several cycles and dividing by the time interval represented. As was the case with the pressure fluctuation magnitudes, the reading of the frequencies from the strip chart is imprecise, but the frequencies are also used for comparative purposes.

The bed expansion is another indicator of the fluidization. It is defined as the percentage increase in the fluidized bed height over the slumped bed height. The slumped bed height is relatively easy to measure as long as the bed surface is level. However, the fluidized bed height is more difficult to measure as the surface of the bed rises and falls due to the bubbles rising through the bed. To measure the fluidized bed height, the median position of the fluidized bed surface is estimated by observing the maximum and minimum heights. Both the

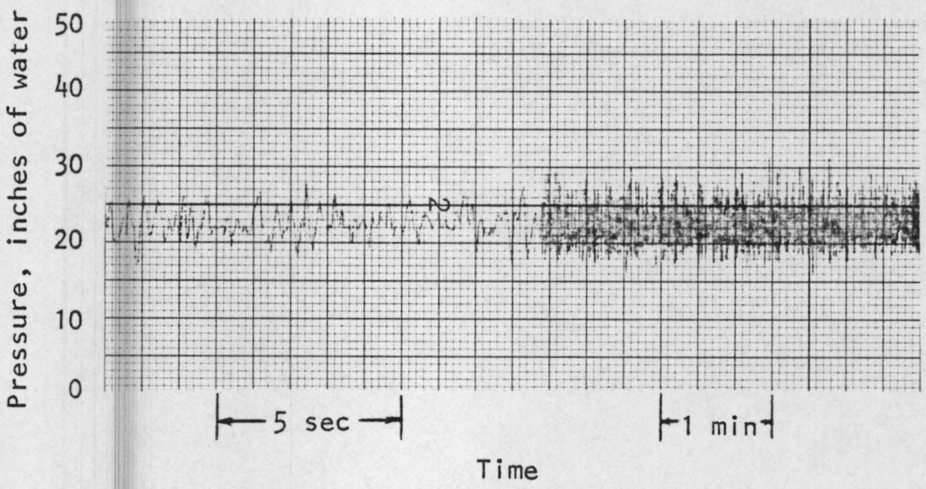

Figure 6.7. Lower Bed Pressure Fluctuations. The average fluctuation is ± 3.2 inches of water and the maximum fluctuation is ± 6.0 inches of water. The frequency is 2.9 cycles per second. Data from the pipe grid feeder: hole pattern II down, 18 inches of limestone (uncorrected), V_{sf} = 8.0 ft/sec.

slumped and the fluidized heights must be corrected for the presence of bed internals when applicable as was done in calculating the theoretical bed pressure drop.

Magnetic Separation

Performance

Although in actual testing the coal feeding and bed sampling processes precede the magnetic separation process, the magnetic separator was tested first because the development of the procedures for the former two processes depended on the separator's operational characteristics. Three tests were conducted on the magnetic separator to determine the number of cycles required to achieve an acceptably low residual concentration of imitation coal in the limestone bed material following coal feeding. For these tests, 230 pounds of limestone were put in the bed. In the first test 21 pounds of imitation coal were fed into the bed. Then, the bed material was repeatedly passed through separation cycles until the calculated concentration of imitation coal remaining in the bed material was approximately one percent. The concentration remaining was calculated by collecting and weighing the removed imitation coal. A sample of the remaining bed material was tested to verify the calculations. This same procedure was repeated twice, except that in the second and third tests the amount of imitation coal fed was decreased slightly to account for the small amount remaining in the bed from the previous test. The results of the three magnetic separator tests are summarized in Tables 6.3 and 6.4. Samples of the separated imitation coal were analyzed and found to contain 2 to 3 percent limestone particles by weight (1.0 to 1.5 percent by volume). This

TABLE 6.3

PERCENTAGE[1] OF IMITATION COAL REMOVED
DURING EACH MAGNETIC SEPARATOR PASS

Pass No.	Test 1	Test 2	Test 3	Average
1	36.1	45.7	46.4	42.7
2	28.4	22.9	21.2	24.2
3	17.8	11.0	14.5	14.4
4	6.5	7.1	7.1	6.9
	88.8	86.7	89.3	88.2

[1]Based on weight.

TABLE 6.4

CALCULATED PERCENTAGE[1] CONCENTRATION OF IMITATION COAL REMAINING IN THE BED MATERIAL AFTER EACH MAGNETIC SEPARATOR PASS

Pass No.	Test 1	Test 2	Test 3	Average
0[2]	8.3	8.4	8.4	8.4
1	4.5	4.7	4.7	4.6
2	2.5	2.8	2.9	2.7
3	1.3	1.8	1.6	1.6
4	0.8	1.2	1.0	1.0
4[3]	0.9	1.1	0.7	0.9

[1]Based on weight.

[2]Initial concentration before any separations.

[3]Measured average concentration of imitation coal in two bed material samples after four separation cycles.

small amount of limestone does not adversely affect the coal feeding tests.

In actual coal feeding tests a smaller amount of imitation coal is fed into the bed, and thus the initial bed concentration is lower. Therefore, the background concentration (i.e., the final concentration of imitation coal after four separations) of 1.0 percent is conservative. Samples taken later after four separation cycles following a standard coal feeding test indicate that the actual background bed concentration ranges from roughly 0.5 to 0.75 percent.

Experimental Methods

Four separation cycles are performed following each coal feeding test. The material is drained from the bed into the upper storage bin and then gravity fed through the magnetic separator. The sliding gate valve is opened to allow a material flow rate of approximately 40 lbm/min (0.5 ft^3/min). After each of the first three separations the material is recycled from the lower storage bin to the upper storage bin. After the fourth separation it is returned to the bed. Normally, the entire process takes approximately an hour, depending on the bed height which is being tested.

Coal Feeding

Performance

Before the first charge of imitation coal was put into the live bin coal feeder hopper, all the material passing a number 100 sieve was removed. This was done because material below this size appeared to be largely either iron particles or plastic particles rather than a combination of both, indicating that the iron particles used to make the imitation coal were in the number 100 to number 150 sieve size range. Table 6.5 shows sieve analyses of the originally crushed imitation coal and of the imitation coal which was put into the live bin coal feeder.

The live bin coal feeder contains a variable speed screw conveyor and is capable of feeding particulate material over a wide range of feed rates. The feed rate corresponding to a specific screw conveyor rotational speed is a function of the bulk density of the material being fed. Thus, the live bin feeder had to be calibrated for the imitation coal. This was done by operating the screw conveyor at a known rotational speed, collecting samples during a timed interval, and then weighing the sample. By repeating this process at several conveyor speeds, the mass feed rate per minute was determined as a function of the rotational speed. The calibration curve for the feeder is shown in Figure 6.8. Repeatability tests were performed with very consistent results.

Before coal feeding tests were performed, the possibility of particle segregation in the bed was anticipated. This segregation is possible because the imitation coal particle density is about half that of the limestone (86 lbm/ft^3 as compared to 170 lbm/ft^3, respectively). However, both visual observations during the tests and vertical bed concentration measurements after the tests revealed that particle segregation due to buoyancy was not a problem. Nevertheless, imitation coal particles were elutriated from the bed. Elutriation is the removal of particles from the bed which have a transport velocity less than or equal that of the exiting air stream. Essentially all imitation coal particles passing a number 30 sieve

TABLE 6.5

COMPARATIVE SIEVE ANALYSES OF IMITATION COAL

		Percent Retained		
Sieve[1]	Sieve Opening[2]	Original 0.25 Inch Crush Material	Material Charged to the Live Bin Coal Feeder	Degraded Material[3]
3/8 in.	0.3750	0.0	0.0	0.0
1/4 in.	0.2500	0.0	0.0	0.0
4	0.1870	0.3	0.3	0.2
8	0.0937	33.7	35.2	45.0
16	0.0469	33.6	35.1	40.7
30	0.0234	16.6	17.3	13.8
50	0.0117	7.6	7.9	0.2
100	0.0059	4.0	4.2	
200	0.0029	2.4	0.0	0.1
325	0.0017	1.2	0.0	
Pan	0.0000	0.6	0.0	

[1]U.S.A. Standard Series.

[2]Approximate opening diameter in inches.

[3]Material which was used for approximately 10 hours of testing.

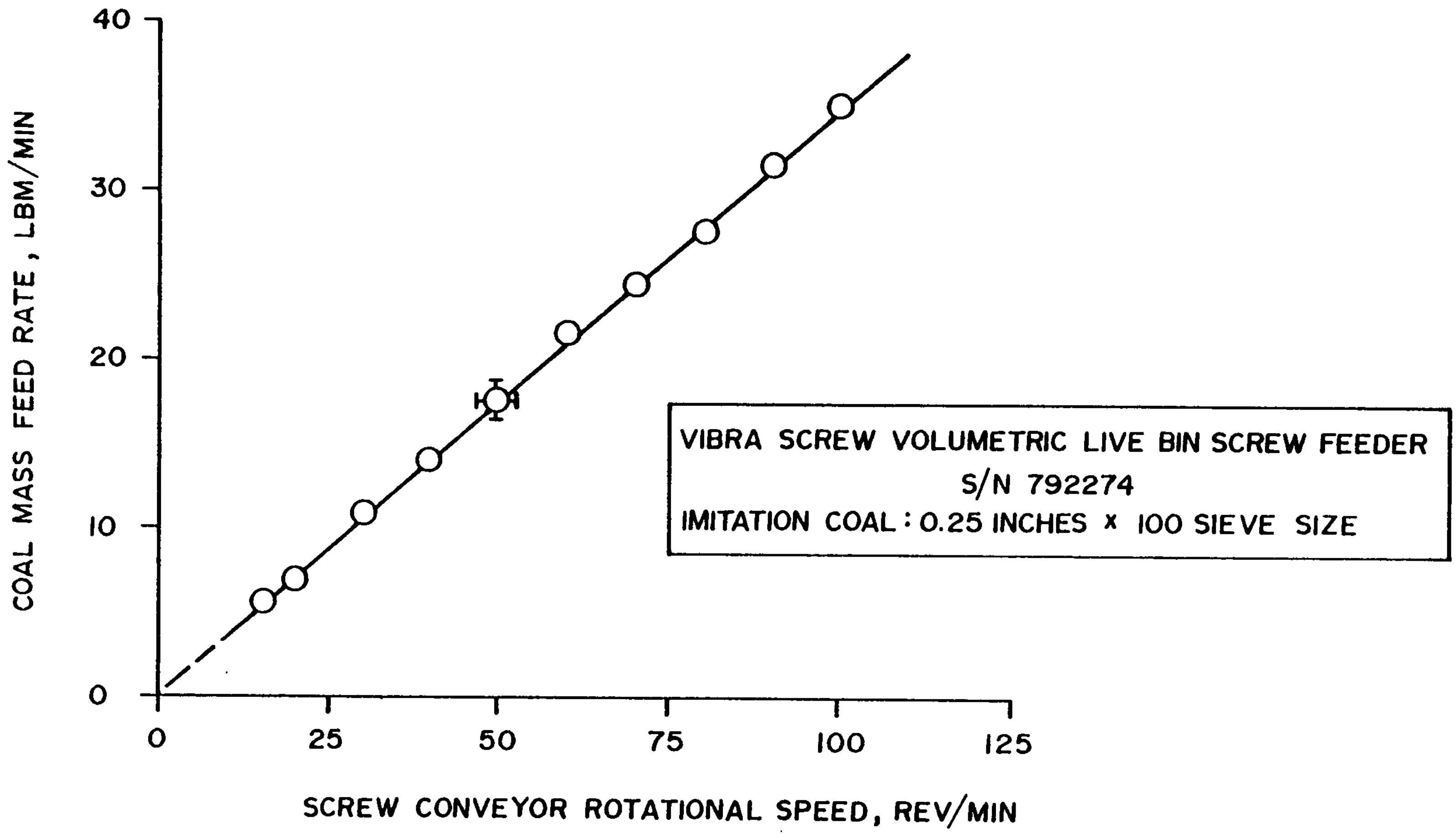

Figure 6.8. Volumetric Live Bin Coal Feeder Calibration Curve.

were elutriated. Also, after the heat transfer tube assembly was installed in the bed, imitation coal particles in the number 20 to number 30 sieve size range were continuously circulated above the bed surface during coal feeding tests. These particles traveled upwards adjacent to the walls parallel to the heat transfer tubes in two mirror image sheets which arched towards the center of the bed above the tubes and then fell back into the bed center. This circulation pattern occurred because the air velocity through the heat transfer tube assembly was high enough to transport these particles. Then, when the air velocity decreased in the freeboard region above the tube assembly, the particles dropped out of the exiting air stream back towards the bed surface. When the bed was shut down after a coal feeding test, there would be a thin layer of the particles on the bed surface.

After the imitation coal had been used in approximately 10 hours of testing, samples were taken from the experimental facility and analyzed. The results of a sieve analysis performed on the samples is shown in Table 6.5 on page 106 under the "degraded material" column. These results confirm that the imitation coal below the number 30 sieve size has been elutriated. They also reveal that the average size of the imitation coal has been decreased by erosion as indicated by the smaller amounts of material retained on the number 4 and the number 30 sieves. The apparent increase in material retained on the number 8 and the number 16 sieves is due to the calculational method. Simply stated, the loss of the particles passing a number 30 sieve cause the remaining particles to comprise a greater percentage of the total sample.

Experimental Methods

The coal feed rate utilized in the coal feeding tests corresponds to the feed rate necessary for combustion with 20 percent excess air in a hot bed. These tests are performed at two basic air flow rates. Full flow coal feeding tests are performed with an inlet fluidization air flow of 1600 ft^3/min and an inlet transport air flow of approximately 200 ft^3/min. Because of the temperature rise across the blower, the resulting bed air flow in full flow tests is approximately 1900 ft^3/min, which corresponds to a superficial bed velocity of 8.0 ft/sec. The coal feed rate for these tests is 14.0 lbm/min. For half flow tests, i.e., a 2:1 turndown ratio, the inlet fluidization air flow is 700 ft^3/min and the inlet transport air flow is again approximately 200 ft^3/min. In this latter case the bed air flow is approximately 950 ft^3/min, which corresponds to a superficial bed velocity of 4.0 ft/sec. For half flow tests the coal feed rate is 7.0 lbm/min.

The transport air flow of 200 ft^3/min mentioned above corresponds to a velocity in the 3 inch coal transport line of approximately 70 ft/sec. This transport velocity for the imitation coal is conservative because its minimum transport velocity was estimated to be 40 to 50 ft/sec using a correlation by Zenz [94] for mixed particle sizes and correlations listed by Jones and Leung [95] for single particle sizes. The actual minimum transport velocity has not been determined experimentally, but at least some of the imitation coal was transported vertically at a velocity of 25 ft/sec in one test. It is not known whether the larger particles dropped out of the flow stream.

Bed Sampling

Performance

The coal sample probe performance tests were conducted with one of the coal feeders which was to be evaluated. The particlar feeder used was the valve cap feeder, described by Henry [91]. Of course, in general it is better not to calibrate a measuring device by using the system which is to be measured. Thus, the initial plan had been to charge the bed with a known imitation coal concentration, and then to fluidize the bed with the perforated plate distributor during the coal sample probe performance tests. However, this method proved to be unfeasible due to the excessive time required, and as it turned out, the valve cap feeder fluidized the bed more uniformly than the perforated plate distributor did.

One of the most difficult problems encountered with the integrated coal feeding evaluation method is the timing of the bed sample collection in relation to the coal feeding process. Part of this difficulty lies in the fact that whereas real coal particles burn in a hot bed and essentially disappear from the system, the imitation coal particles continue to collect in the experimental fluidized bed as coal feeding progresses. Thus, cold model tests intended to be coal feeding tests may become solids mixing tests if caution is not exercised in the evaluation method. The problem of integrating the coal feeding and the sampling is partly due to the uncertainty of the coal particle residence time in a hot bed, i.e., how long the particle remains in the bed before it burns. No conclusive particle residence time data exist, largely because this time depends on the type and size of coal being burned and the furnace conditions.

One possible solution to the coal feeding and sampling dilemma is to feed a large burst of imitation coal into the bed and then take samples almost immediately to minimize the bed mixing that occurs. However, this method is not realistic in terms of the coal/air mixture which is being transported through the coal feeder being tested. Therefore, a decision was made to maintain the proper coal/air mixture as an integral part of the evaluation method.

Sets of tests were conducted with differing coal feeding times, differing coal sample probe opening times, and differing coal sample probe closing times. After examining the results, the sampling method chosen consists of a 30 second coal feeding duration at the proper feed rate with the coal sample probes being open to collect samples during the last 10 seconds of the coal feeding. This amount of coal feeding allows an average imitation coal bed concentration of 1.5 to 2.5 percent to be reached for both half flow and full flow coal feeding tests with bed heights in the range of 1.5 to 2.0 feet. These imitation coal concentrations are significantly above the background bed concentration of approximately 0.5 to 0.75 percent as discussed previously. Also, this combination of times is intended to maximize the coal feeding effect and to minimize the mixing effect.

Several mechanical problems were encountered during the operation of the coal sample probes. These problems arose because of the dusty and gritty environment in which the probes were operated. The first problem occurred when small particles worked into the annular clearance between the inner and outer probe tubes as the inner tube was rotated. This clearance is only 14 mils (0.014 inches), but enough particles got between the tubes to make the probes difficult to operate.

The first solution attempted was to modify the probes so that a purge flow of air could be blown between the tubes and out the compartment openings into the bed. This solution proved to be inadequate as the second and especially the third sample compartments did not receive a sufficient air flow. The second solution tried was the use of a moderately heavy grease in the annulus between the sample probe tubes. This solution was found to work reasonably well, even with only a narrow ring of grease spread adjacent to the three compartments. The grease solution is normally effective for approximately 15 tests. Then when the probes reach the stage of being too tight to turn, they must be disassembled, cleaned, and regreased.

Each coal sample probe must be slid out of and back into its sleeve support between coal feeding tests. The clearance between the probe and its sleeve is only a few mils. A purge flow of air between the two components works quite well in keeping particles from getting into the clearance space and causing binding. However, because both components are aluminum, galling of the contacting surfaces sometimes occurs. The resulting surface scratches must then be removed by sanding, honing, or lapping.

An important test series utilizing the coal sample probes was the evaluation of the electromagnets. In these tests one probe contained six electromagnets, two oriented north pole to south pole in each compartment, while the other probe contained no electromagnets. The double electromagnet configuration yielded the maximum strength magnetic field in each compartment. A power supply provided a 2 ampere current at approximately 20 volts to the six electromagnets connected in parallel. The current to the electromagnets was turned on before the sample probe was opened and off after it was closed. For these tests the sample probes were placed in symmetrical sample port positions.

Many evaluation tests were performed with the electromagnets. The results of three representative tests will be discussed. In the first test the coal feeding and sampling were performed at full flow conditions by the timing procedure outlined previously. For the second and third tests, samples were again taken at full flow, but the material from the first test was in the bed with no magnetic separations or further coal feeding having been performed. The imitation coal concentrations measured in these three tests are shown in Table 6.6. The primary conclusion is that the electromagnets notably increased the amount of imitation coal in the samples. For symmetrically located compartments, the degree of concentration enhancement varied from a multiple of 2.2 to 4.7. However, the fact that the degree of enhancement varied as it did casts some doubt on the validity of the samples collected with the electromagnets. Also, it can be seen that the range of percent variation of the imitation coal concentration from compartment to compartment was approximately twice as large for the probe with the electromagnets. Other data collected in similar tests exhibited the same trends.

Therefore, the electromagnets were not utilized in the subsequent coal feeding tests for two reasons. First, as just described, the use of the electromagnets seemed to increase the inconsistency of the results. Second, samples taken without the electromagnets contained imitation coal concentrations at least twice the background bed concentration level, and this magnitude of difference was considered significant to satisfy statistical sampling considerations.

TABLE 6.6

COAL SAMPLE PROBE ELECTROMAGNET AND REPEATABILITY TEST RESULTS

CFD Parameter[1]	Compartments Without Electromagnets A	B	C	Compartments With Electromagnets A	B	C
			First Test			
%IC	2.6	2.7	1.9	6.8	9.8	6.1
Prb Avg %IC		2.4			7.6	
%IC/Prb Avg %IC	+6.9	+12.7	-19.4	-10.5	+29.9	-19.4
Range of % Variation		32.1			49.3	
			Second Test			
%IC	1.7	2.4	2.1	6.0	10.2	5.4
Prb Avg %IC		2.1			7.2	
%IC/Prb Avg %IC	-17.7	+15.7	+1.7	-16.7	+41.4	-24.8
Range of % Variation		33.4			66.2	
			Third Test			
%IC	2.1	1.9	2.3	4.7	9.0	5.4
Prb Avg %IC		2.1			6.3	
%IC/Prb Avg %IC	+1.0	-9.6	+8.4	-26.6	+41.2	-14.6
Range of % Variation		18.0			67.8	

[1]See Appendix F for an explanation of these labels.

The reason that the electromagnets did not give consistent results became apparent during later testing. The average total sample collected in a coal sample probe compartment had a mass of 70 to 80 grams. However, some sample masses were as low as 40 to 50 grams. These small masses occurred when the probes were closed as a bubble was passing through the compartment. Thus, with the electromagnets used in the compartment, the imitation coal would be preferentially retained while the limestone would be swept out. Such a sample would therefore indicate a higher concentration of imitation coal in the region than actually existed. In retrospect, the electromagnets might well have given more valid results if the absolute mass of imitation coal collected in the sample had been used for comparison between bed regions rather than the percent concentration collected.

The results shown in Table 6.6 also indicate the sampling method repeatability for the probe without the electromagnets, which was the configuration adopted for standard coal feeding tests. The imitation coal concentrations measured in the first test during the coal feeding process were higher than those in the following two tests because the material was allowed to mix 7 minutes before samples were taken in the second test and likewise 7 minutes before samples were taken in the third test. The average concentrations for the second and third test are very consistent, but the individual compartment concentrations show the magnitude of variation which existed in all the tests conducted.

A variation of several tenths of a percent in the imitation coal concentration between compartments is well within reason. Some of the larger individual particles in the samples were weighed, and the limestone particles averaged 0.07 grams apiece while the imitation coal particles averaged 0.05 grams apiece. Because most of the imitation coal sample fractions weighed approximately 1.5 grams, a loss or gain of three large particles would represent a 10 percent variation in the fraction's weight. This loss or gain would furthermore represent a change of about 0.2 percent in the imitation coal concentration in a typical 75 gram sample. Thus, for the relatively small size of the samples collected and the low imitation coal concentrations involved, the apparent variations in the results are less significant than might at first appear.

More than 200 samples have been collected with the coal sample probes and evaluated for imitation coal concentration. Due to the inherent inaccuracies in the sampling method, such as were just described, and to the unrepeating behavior of fluidized beds, no single test results should be viewed with extreme confidence. However, trends can be detected by examining several results obtained during tests of the same configuration of a coal feeder. Most importantly, it is always possible to establish whether the coal concentration in a region is significantly above the bed background concentration. Thus, although the value of the exact concentration measured in a particular bed region may be questionable, it can be known whether the coal feeder under test did or did not deliver a significant amount of coal to the region.

Experimental Methods

For a coal feeding test, the two coal sample probes are inserted into the appropriate sample port positions and then the limestone is put into the bed. After the bed is fluidized the coal feeding process is initiated by turning on the live bin coal feeder which has previously been set to the proper coal feed rate. Twenty seconds after the coal feeding commences both sample probes are opened simultaneously. Ten seconds later the probes are closed and the live bin coal feeder is turned off. After the bed has been drained the sample probes are removed from the bed and the six samples are dumped into individual containers. Each sample is analyzed by using a permanent magnet to separate the imitation coal fraction from the limestone fraction and then weighing the two fractions on a laboratory balance. The imitation coal concentrations in the samples are calculated and compared as described in Appendix F.

For each coal feeder tested, symmetry tests are performed. Simultaneous samples are taken at both the outer and then the inner of the four sample port positions at a given level. Then the sample probes are placed at the two adjacent sample ports on either the left side or the right side of the bed for full flow and half flow coal feeding tests. This whole series of tests is then repeated with the sample probes at a different level of the sample ports if a change in bed height dictates this.

CHAPTER 7

IN-BED PIPE GRID COAL FEEDER

Background

In-bed air distributors and/or coal feeders consist primarily of needles, duct grids, and pipe grids. A distinction is made between this distributor type which extends through the bed walls and those distributors which project through the base of the bed. Examples of the latter type include "buttons", valve caps, bubble caps, tuyeres, and nozzles.

Needles refer to long pipes which project into the active bed region on a downward slope. Material is fed through them into the bed with an assisting air flow. The use of needles and problems experienced with them are discussed in Chapter 1. Despite the significant problems with needles, the Foster Wheeler Boiler Corporation has recommended that they be tested at the Department of Energy's Atmospheric Fluidized Bed Combustion Component Test and Integration Unit at the Morgantown Energy Research Center [96]. Currently the future of this project is uncertain.

Duct grid distributors are similar to the pipe grid distributors described later except that the duct cross section is not circular. A triangular duct arrangement containing an array of downward facing holes has been suggested as a combined air distributor and coal feeder [97]. The triangular shape prevents the deposition of bed material on the top of the duct. However, duct grid distributors suffer the disadvantage of being somewhat difficult to fabricate, particularly in the case of long ducts which must be tapered lengthwise to keep the air velocity above the minimum coal transport velocity.

Pipe grid distributors are most frequently a series of parallel pipes projecting from one or more headers. They have been used for introducing heating or cooling gases into industrial fluidized beds [98]. Some chemical reactor fluidized beds have utilized pipe grids to introduce the reactant gas in processes such as the thermal cracking of naptha and the hydrogen reduction of iron ore [51, p. 86]. Because the primary usage of pipe grid distributors for fluidized beds has been in proprietary industrial processes, the few existing references to these devices are quite sketchy. Volk et al. [53] mention without any elaboration the use of an 8 inch diameter distributor containing 15 holes of 0.25 inch diameter. A double pipe distributor has been reported for use in applications where bed material weeping or drainage is a problem [99]. Brief consideration is given in this latter reference to the selection of hole and pipe sizes and hole spacings for the specific problem of interest. A continuous loop pipe distributor arrangement has been investigated for operation in a fluidized bed afterburner for a radioactive waste incinerator [100]. This configuration is attractive because no dead ends exist where material can accumulate.

Development and Design

The pipe grid distributor was chosen as the type of in-bed feeder combining total air and coal distribution to be evaluated. Needles were rejected because they are a discrete point material injection device of which many would be required to perform the combined functions. A duct grid feeder would likely operate in a similar manner to a pipe grid feeder, but the former is more difficult to analyze and to fabricate.

In the combined total air and coal distribution scheme, the air distribution function is considered to be of foremost significance. A feeder which disperses coal uniformly but which cannot fluidize the bed is certainly not practical. Thus, the development priorities for the pipe grid feeder were to attempt to achieve uniform fluidization first and then to consider modifications which might be necessary to produce uniform coal feeding. Also, a basic philosophy of the overall coal feeder evaluation project has been to keep the coal feeding system designs as simple as possible without compromising the basic idea.

The particular pipe grid configuration selected was determined by the experimental fluidized bed facility geometry and the fluid mechanics governing the flow through the pipes. The basic parameters established were the number of pipes and their orientation, the pipe diameters, the number and spacing of the holes in the pipes, and the hole diameters.

The number of pipes was chosen to be four for reasons including system symmetry, the number of air-material splits required between the source and the bed, and the air flow rate through the system. With two pipes each from opposite sides of the bed in alternating sequence, as shown in Figure 7.1, the problem of balancing the bed in terms of fluidization air and coal feed was greatly diminished. Thus, even if one or more of the air-material splits were uneven or the

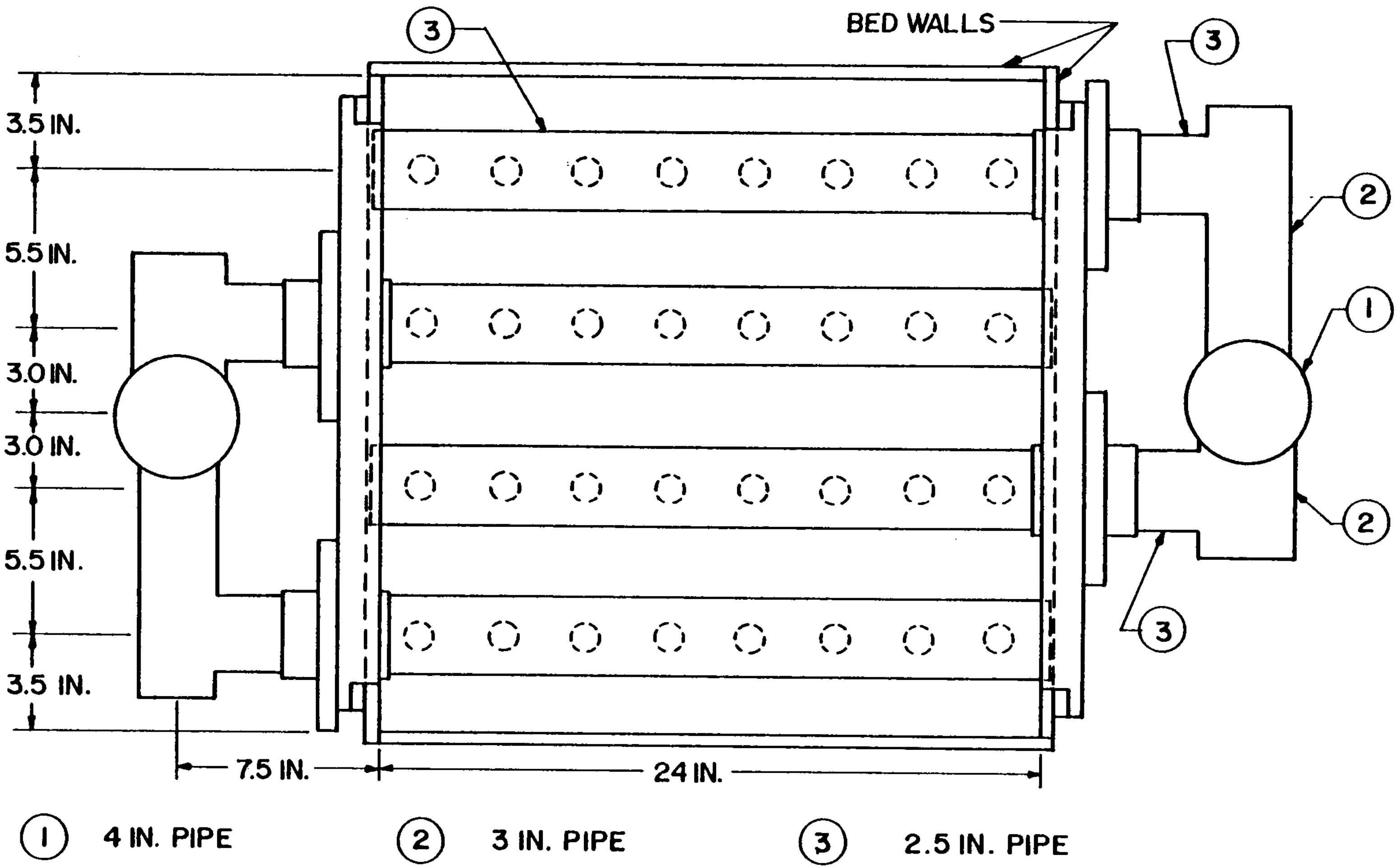

Figure 7.1. Plan View of the Pipe Grid Feeder.

pipe discharges were not uniform along the length, this alternating arrangement of the pipes would average the nonuniformities in a desirable fashion rather than magnifying them.

The diameters of the four pipes were determined by the air flow rate through the system, which dictates the pipe air velocity, and by the bed geometry. The pipe air velocity must exceed the minimum horizontal transport velocity of coal at the lower limit established by the 2:1 velocity turndown ratio. A 3 inch pipe size was initially selected because this size would provide a velocity slightly greater than the minimum required at the reduced flow. For symmetry purposes the four pipes should have been on 6 inch centers, but the rectangular openings in the plexiglass bed test section did not allow sufficient space for such an arrangement with 3 inch pipes. Thus, 2.5 inch pipes were actually used, but even with this reduced diameter the two outer pipes had to be positioned on 5.5 inch rather than 6 inch centers as shown in Figure 7.1. Although the 2.5 inch pipes yield a higher inlet air velocity than is necessary for coal transport, the air velocity theoretically drops below the minimum transport velocity at some axial location in the pipe as air is expelled through the holes. The obvious (although not so easy) solution to this problem is to use a tapered pipe or one which contains consecutive sections of decreased diameter. Due to the short length of the pipes involved combined with the large momentum of the inlet air, uniform diameter pipes were considered satisfactory for this feeder. However, in a large bed, pipe diameter reductions would be necessary for long pipes.

The determination of the number of holes required for each pipe, the hole spacings, and the hole diameters was not a simple problem.

Clearly, the maximum hole diameter is fixed by the pipe diameter and the structural strength required of the pipe. From a fluid mechanics viewpoint, for a given pressure drop the same volume of air can be expelled through many small holes or fewer large ones. However, from a fluidization viewpoint, the hole sizes and proximity are important to jet formation and penetration which lead to bubble development. The available papers [101, 102, 103, 104] on this subject apply primarily to perforated plates and nozzles which utilize upward facing or horizontal holes. Downward facing holes are necessary for pipe grid distributors to prevent the bed material from filling the pipes when the bed is slumped. In addition, because the pressure does change along a pipe as air discharges through the holes, maintaining a uniform discharge flow across each hole requires that either uniform diameter holes be spaced nonuniformly, or non-uniform diameter holes be spaced uniformly. The latter case is preferred for a fluidized bed as it provides an evenly distributed flow throughout the bed.

The calculation of the hole parameters based on fluid mechanics involves the use of perforated pipe or manifold theory. For the specific problem of a manifold which has a large cross-sectional area relative to the collective hole areas and which is fed with high pressure fluid, the problem reduces to one of parallel orifices. However, the more general problem of a manifold with a cross-sectional area on the order of the collective hole area, which is the problem under consideration, is more difficult to solve. Boucher [105] gives an overview of the manifold problem including some practical rules of thumb for design. Senecal [106] points out that a perfectly good solution for the flow in the distributing device can be invalidated by failure to consider the effects of the upstream and downstream flow conditions. This is particularly pertinent in the present case because the flow executes a 90 degree bend just prior to entering the in-bed distributor pipes. Senecal also claims that the problem is complicated by three additional factors. The velocity profile changes at each outlet, the momentum transfer from fluid exiting the pipe to fluid continuing down the pipe is not perfect, and, most important, an error in the orifice flow coefficient, which is difficult to determine, can significantly affect the calculations. Keller [107] and Dow [108] treat the pipe manifold problem both from the theoretical and experimental aspects, particularly as relates to gas flow in a pipe burner. The case of flow in a porous wall pipe, which can be related to the manifold problem, is treated by Olson [109] and Berman [110]. The comprehensive treatment of the manifold problem by Van Der Hegge Zijnen [111] was primarily utilized in the hole diameter calculations, which are outlined in Appendix G.

Two different hole patterns were used in the pipe grid feeder tests. The first configuration, referred to as hole pattern I, consisted of eight uniform diameter holes in each in-bed pipe as shown in Figure 7.2. The second configuration, namely hole pattern II, consisted of eight holes in each in-bed pipe whose diameters varied by 0.0625 inch increments as shown in Figure 7.3.

The finalized pipe grid feeder design incorporated three subsystems. The first subsystem, shown in Figure 7.4, contained the first split of both the fluidization air and the coal/transport air mixture. The fluidization air entered the plenum box from the air intake tee and

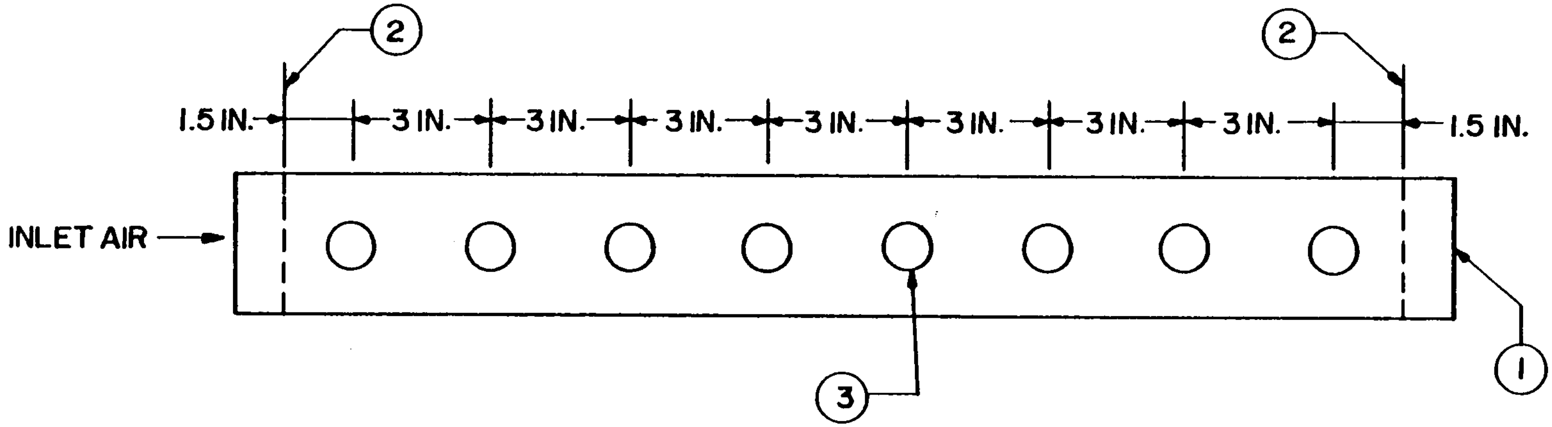

1. 2.5 IN. DIAMETER IN-BED PIPE
2. LOCATION OF BED WALLS
3. 0.875 IN. DIAMETER HOLE - TYPICAL OF ALL

Figure 7.2. Hole Pattern 1.

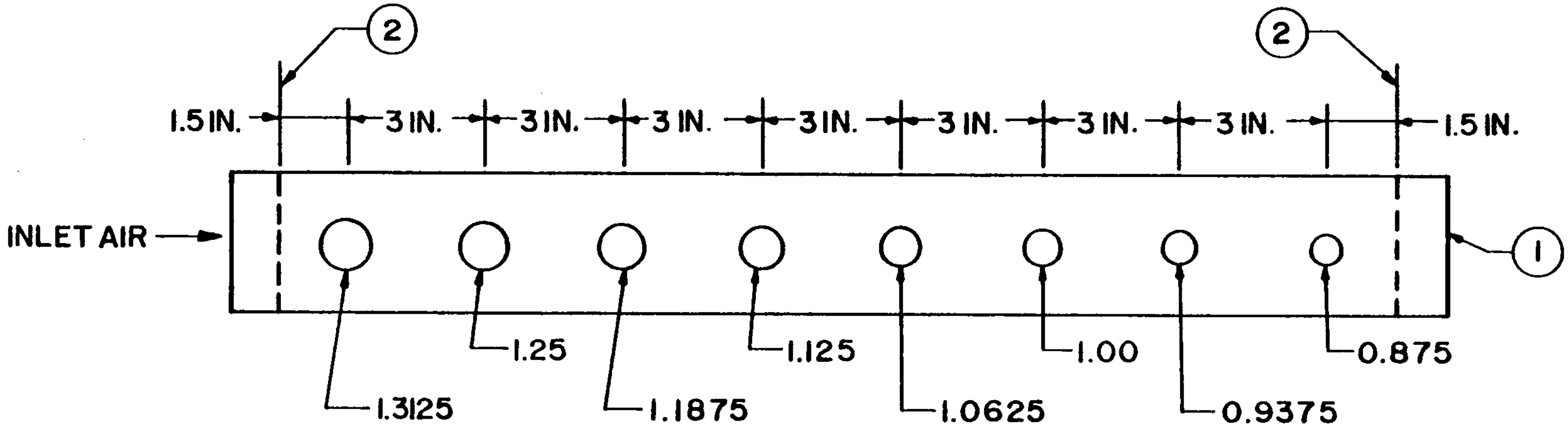

HOLE DIAMETERS IN INCHES

(1) 2.5 IN. DIAMETER IN-BED PIPE

(2) LOCATION OF BED WALLS

Figure 7.3. Hole Pattern 11.

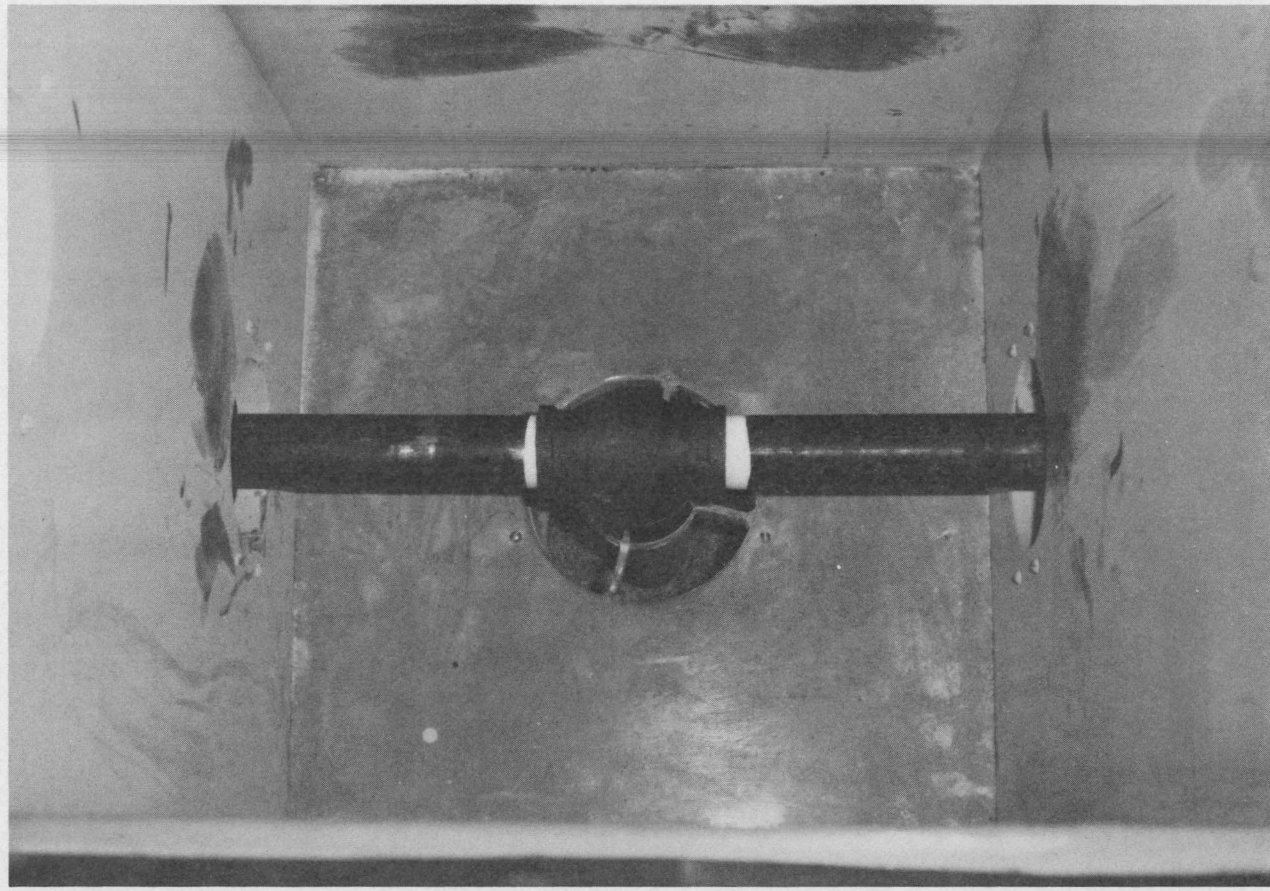

Figure 7.4. Transport Air and Coal Splitter Installed. Top view.

then split as it exited through the two opposing 6 inch openings near the bottom of the plenum box. The coal/transport air mixture entered the plenum box through the 3 inch coal transport line and then split in a standard tee into two 2 inch lines which projected a short distance through the aforementioned 6 inch openings. The second subsystem, shown in Figure 7.5, included two identical sets of polyvinyl chloride (PVC) pipes exterior to the plenum box and the plexiglass bed. The fluidization air and coal/transport air mixture combined in a short section of 6 inch pipe and then passed through a vertical 4 inch pipe. Each half stream (on either side of the plenum box) split again as it passed into horizontal 3 inch pipes as can be seen in Figure 7.1. Each of the final four streams passed through a sharp elbow into 2.5 inch pipes which extended into the plexiglass bed test section. The third subsystem consisted of four 2.5 inch PVC pipes containing the hole patterns, which were located in the bed interior as shown in Figure 7.6. These pipes were installed with threaded connections so that they could be removed for hole size modifications. Each pipe contained a slanted face end plug at the downstream edge of the last hole to prevent a dead end in which coal could collect. Also, each pipe was long enough so that its dead end was supported in a recessed blind hole in the opposite plywood panel.

A solid 0.25 inch thick aluminum base plate supported the limestone bed in all tests with the pipe grid feeder. Also, the heat transfer tube assembly was installed during all tests.

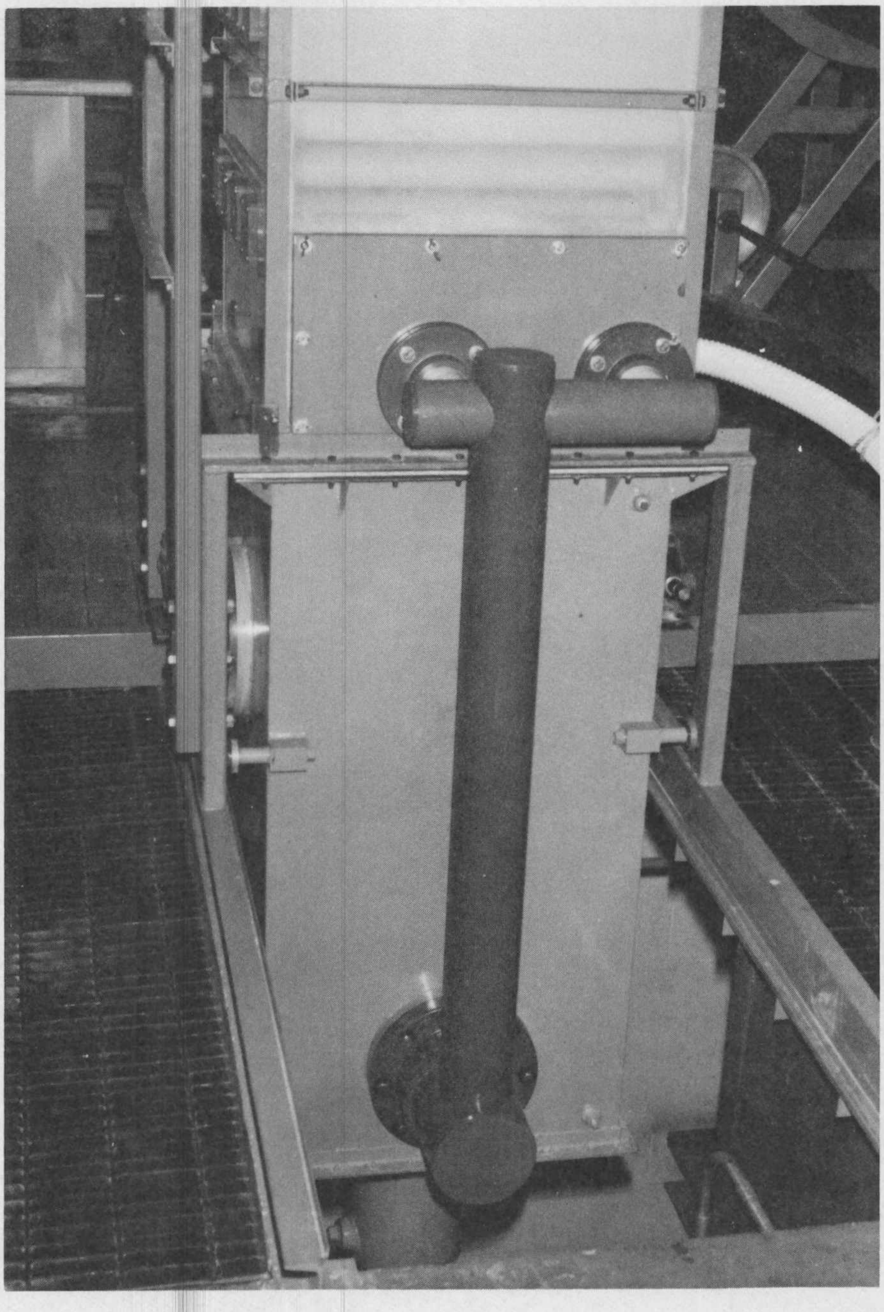

Figure 7.5. Exterior Pipes Installed.

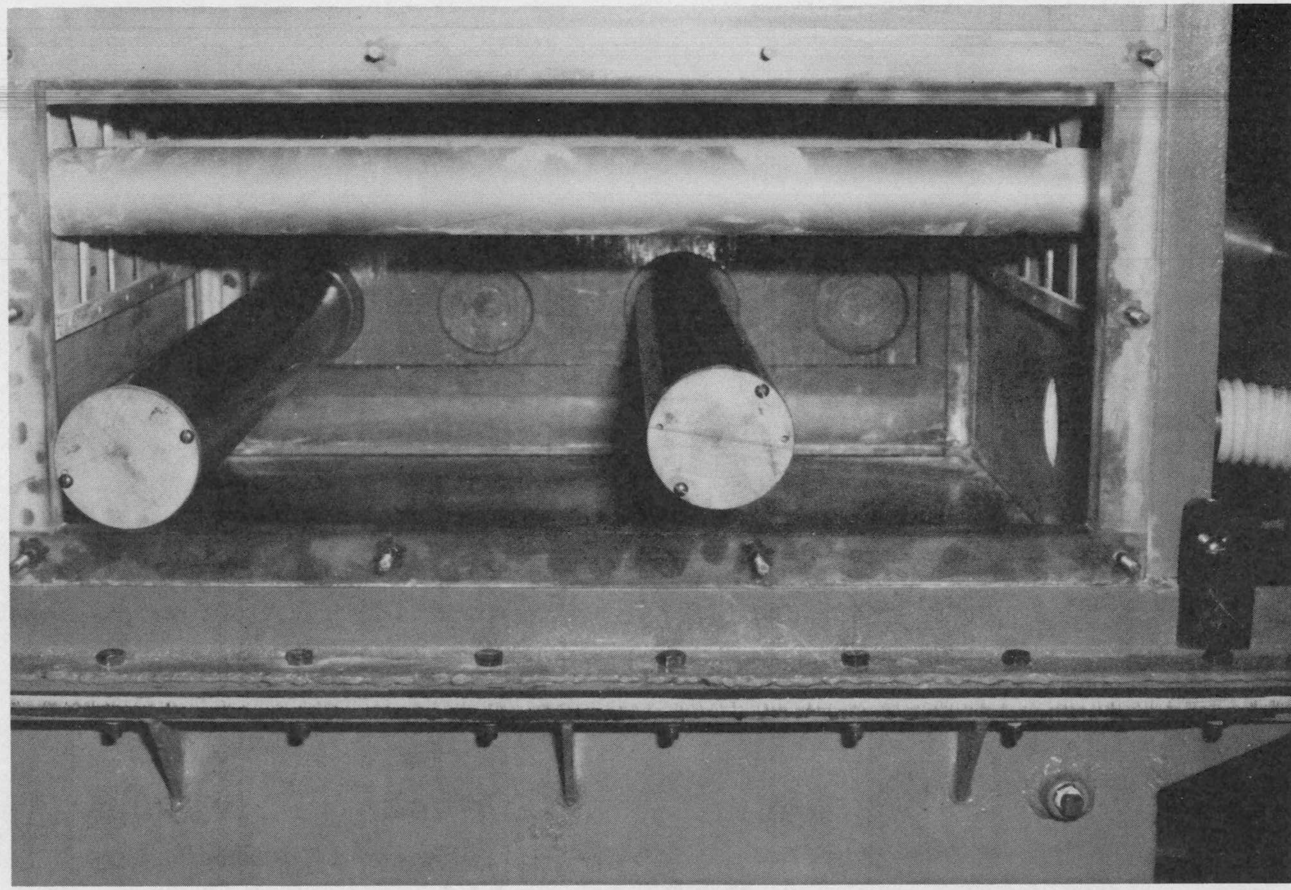

Figure 7.6. Two In-Bed Pipes Installed.

Performance and Results

Introduction

A series of tests were conducted to evaluate the performance of the the pipe grid feeder as both an air distributor and a coal feeder. The parameters which were varied were the bed air flow, the bed height, the in-bed pipe orientation, and the in-bed pipe hole patterns. Experimental measurements were taken to determine the bed superficial velocity, the pressure differentials across the pipe grid feeder and across the bed material, the magnitude and frequency of the pressure oscillations at the base of the bed, the average fluidized bed expansion, and the coal distribution in the bed.

Three sets of tests were performed on the pipe grid feeder. The first test set was performed with hole pattern I turned vertically downward, which put the pipe hole openings 3.25 inches above the base plate. Air flow tests were conducted, then fluidization tests with approximate uncorrected limestone bed heights of 8, 12, and 18 inches, and coal feeding tests with an 18 inch bed height. The second test set was performed with hole pattern I turned vertically upward, which put the pipe hole openings 6.25 inches above the base plate. Air flow tests and fluidization tests with approximate uncorrected bed heights of 12 and 16 inches were conducted. The third test set was performed with hole pattern II turned vertically downward. Air flow tests were conducted, then fluidization tests with approximate uncorrected bed heights of 6, 12, 18, and 24 inches, and coal feeding tests at the 18 and 24 inch bed heights. In each configuration of the three test sets, the range of superficial velocities tested varied from 3.5 to 8.5 ft/sec in approximately 1 ft/sec increments. The reduced data for the tests conducted with the pipe grid feeder are included in Appendix H.

The pipe grid feeder results are compared in the following sections to results obtained with the perforated plate air distributor because the latter is a distributor type which is commonly used in fluidized beds. Air flow, limestone fluidization, and a single coal feeding test were performed with the taped version of the perforated plate under conditions similar to those utilized for the pipe grid feeder tests. The taped perforated plate fluidization results are in Appendix I.

Fluidization

The most noticeable qualitative feature of the hole pattern I down test series was the nonuniform bed fluidization. Unfluidized zones were visible at the entrances of the in-bed feeder pipes. The height of these zones at the bed walls decreased from 4 inches above the base plate at the entrances of the in-bed pipes to 2 inches at the pipe ends. These "dead" zones, along with the visible bed behavior, very clearly indicated that a greater volume of air was being discharged from the downstream holes of the in-bed pipes than from the upstream holes. This nonuniformity of air flow was further confirmed by the unlevel surface of the bed. Limestone tended to pile up over the less active bed regions by being thrown upon them by the more active bed regions. When the bed was drained following fluidization tests, small craters were visible in the 2 inches of limestone remaining below the bed drain hole. These craters, which were sculptured by the air jets from the in-bed pipe holes, were shallowest near the pipe entrance, deepest at the fifth and sixth holes, and intermediate in depth at the seventh and eighth holes (near the pipe dead end). These craters probably indicated to some extent the variation in the air flow pattern, as did another phenomenon discovered when the remainder of the limestone was vacuumed from the bed. The initially shiny aluminum base plate displayed a pattern of frosted circles which correlated with the number and location of the 32 holes in the in-bed pipes. The circles ranged from 2 inches in diameter at the inlet of the pipes to 5.5 inches in diameter at the pipe dead ends. The circles formed by the two outer pipes were slightly larger than those of the two inner pipes, indicating more flow through the outer pipes. The centers of these circles were displaced from the pipe hole centers 1.5 inches downstream indicating that the air exiting the holes had a horizontal velocity component as expected. These frosted circles on the base plate were most likely formed by impinging limestone particles entrained in the air jets emanating from the in-bed pipes.

Complete tests were performed with hole pattern I down because it was unknown at the time whether the subsequent hole pattern modification would improve the fluidization uniformity. As it turned out, hole pattern II down did provide better fluidization, so detailed fluidization characteristics of the hole pattern I down tests are not given. However, the bubble formation by the pipe grid feeder, which is described later, was similar for both hole patterns.

Hole pattern I was tested briefly with the pipes turned vertically upward. This configuration was tested mostly out of curiosity as it would probably not be practical in an actual combusting fluidized bed due to the filling of the feeder pipes with bed material during bed defluidization. The limestone did run into the in-bed pipes during bed filling and slumping, but the length of these pipes was sufficient to prevent the limestone from running into the exterior pipes of the feeder. Sufficient air pumping power was available to blow the limestone out of the in-bed pipes upon blower startup. This clearing process took several minutes, with more time required for greater bed heights. Initially, the air flow was larger at the entrance ends of the in-bed pipes, but as the pipes cleared the flow became larger at the dead ends of the pipes. The pipe clearing process was further indicated by step drops in the plenum box pressure as additional holes were opened. The most notable fluidization features after the pipes had cleared were the spouts of air formed at the downstream ends of the in-bed pipes. These spouts sent continuous sprays of limestone higher than 2 feet into the freeboard region at full flow (superficial velocity of approximately 8 ft/sec). The highest active bed height tested was only 9 inches, leaving 6.25 inches of inactive limestone from the pipe hole openings downward to the base plate.

Hole pattern II was selected in an attempt to correct the nonuniform air distribution of hole pattern I. Due to the apparent inaccuracies in the hole size calculational method of Appendix G, the new hole sizes were based largely on intuition and experience with hole pattern I. Visually, it appeared that the revised hole diameter choices were good. The bed fluidized evenly everywhere except at the region immediately adjacent to the in-bed pipe entrances. This slight nonuniformity was caused by the horizontal velocity component of the air ejecting from the pipe holes. After the bed was drained following fluidization tests, craters in the limestone similar to those of hole pattern I down were observed. These new craters were deepest at the fourth and fifth holes (in the center of the bed). After the remaining limestone was vacuumed from the bed, the frosted circles on the base plate were again apparent. Because the initial pattern had not been removed, the only conclusive change that could be observed was that the smallest circles near the pipe entrances were 0.25 to 0.50 inches larger in diameter. Although the fluidization performance of hole pattern II was definitely better than that of hole pattern I, no means existed by which to prove whether or not the flows from the holes in the in-bed pipes were equal.

The bubbling behavior of the pipe grid feeder was influenced by the presence of the heat transfer tube assembly. Due to the presence of this assembly and of the limestone dust coating on the plexiglass bed walls, bubbles could only be observed near the walls. At the ends of the heat transfer tubes, which were perpendicular to the four in-bed feeder pipes, the bubbles tended to be uniformly small because the tube support structure broke up the bubbles and allowed some of the air to channel up the vertical members. At the walls parallel to the heat transfer tubes, bubbles as large as 1 foot wide could be observed rising through the bed at full flow. These bubbles were actually long and narrow rather than hemispherical as the outer tubes of the assembly were only 2 inches from the bed walls. At the full flow conditions the bubbles threw limestone particles as high as 2 feet into the freeboard region as they burst through the bed surface.

The pressure drop through the pipe grid feeder was determined by measuring the upstream pressure in the plenum box and the downstream pressure at the lower bed pressure tap. The total feeder pressure drop consisted of the drop through the exterior pipes, which split the flow into four streams, and the drop across the four in-bed pipes. The separate pressure drops through these two feeder sections had to be determined concurrently by the calculations outlined in Appendix J. The exterior pipe pressure drop as a function of the bed superficial velocity is shown in Figure 7.7. Equivalent data for both sets of in-bed pipe hole patterns are shown in Figure 7.8. The pressure drop through hole pattern I up was slightly higher than that measured with hole pattern I down, probably due to the location of the lower bed pressure tap. Only the data for hole pattern I down are included in Figure 7.8. In general, hole pattern II had a 25 percent lower pressure drop than hole pattern I. For hole pattern I the pressure drop across the in-bed pipes represented about 45 percent of the total feeder pressure drop, whereas for hole pattern II this value was about 40 percent. The pressure drop across the taped perforated plate, shown in Figure 6.5 on page 88, was very similar to that across the in-bed pipes for hole pattern II.

The amplitudes of the lower bed pressure fluctuations with the three pipe grid feeder configurations were measured and the results are summarized in Table 7.1. These results, as well as those in following tables, have been adjusted by interpolation to consistent superficial velocities. Also, the bed heights given have been corrected for the presence of bed internals as described in Chapter 6. Two conclusions regarding the amplitudes of the pressure fluctuations

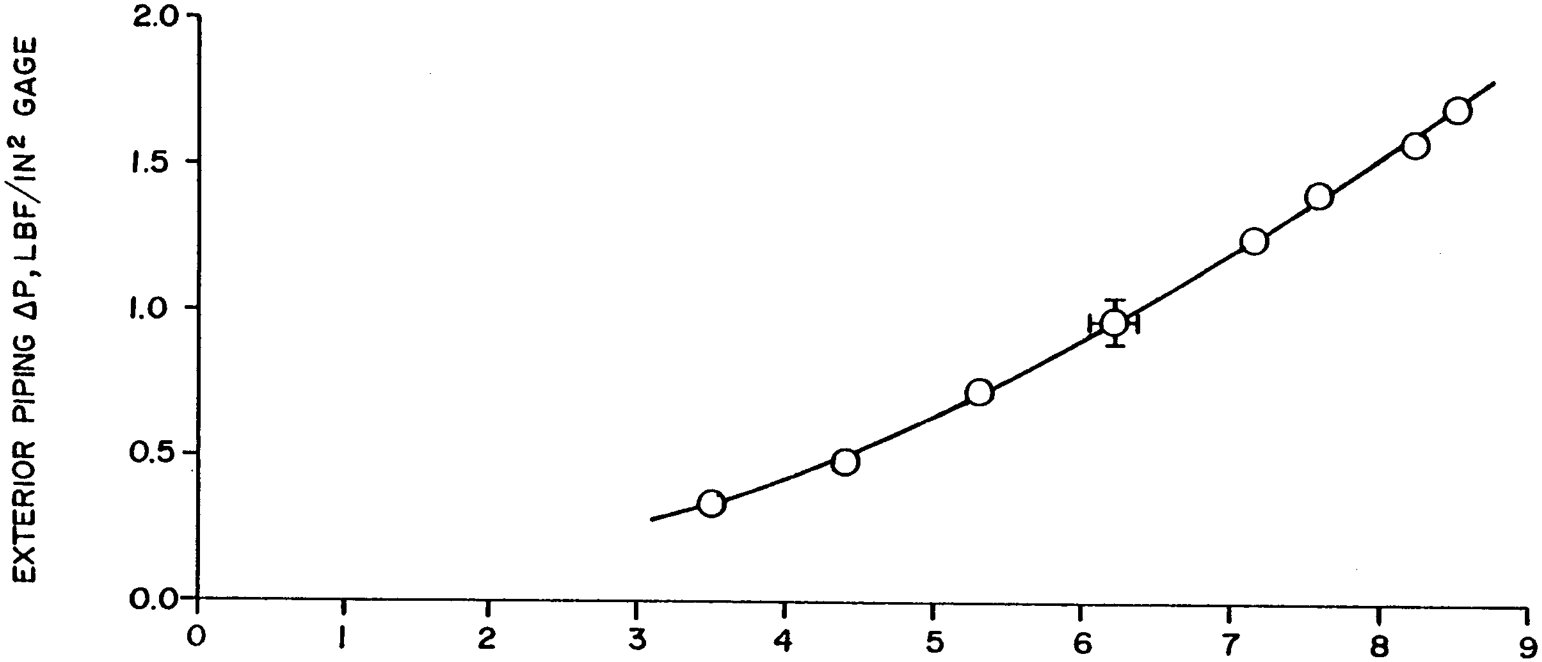

Figure 7.7. Exterior Piping Pressure Drop.

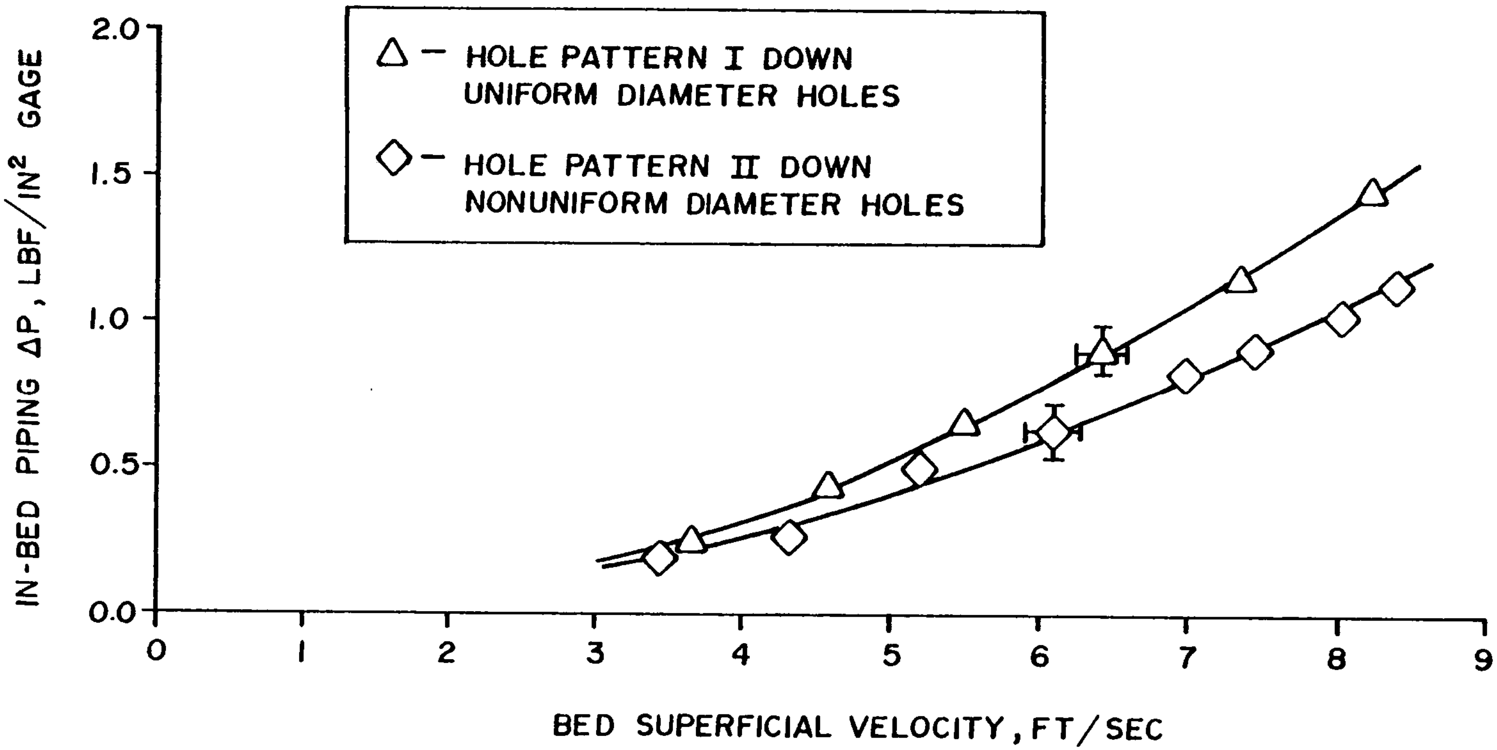

Figure 7.8. In-Bed Piping Pressure Drop.

TABLE 7.1

AMPLITUDES OF THE LOWER BED PRESSURE FLUCTUATIONS WITH THE PIPE GRID FEEDER AND WITH THE PERFORATED PLATE

Superficial Velocity, ft/sec	HPID[1]	HPID	HPID	HPIU	HPIU	HPIID	HPIID	HPIID	HPIID	PP	PP
	5.8[2]	9.8	14.9	4.0	7.3	4.7	10.4	15.4	21.1	9.9	14.1
	Average Amplitudes, ± inches of water										
3.6	0.1	0.2	0.5	0.1	0.3	0.2	0.3	0.6	1.0	0.1	0.1
4.5	0.2	0.4	1.0	0.1	0.4	0.2	0.6	1.2	2.2	0.5	1.5
5.4	0.3	0.7	1.8	0.1	0.5	0.3	1.0	2.0	3.5	1.7	3.3
6.3	0.4	1.2	2.4	0.1	0.5	0.3	1.4	2.5	4.2	2.2	3.9
7.2	0.6	1.4	3.0	0.2	0.6	0.5	1.8	2.8	4.5	3.8	4.4
8.2	1.3	2.2	4.1	0.2	0.7	0.8	2.2	3.2	4.7	4.9	5.5
	Maximum Amplitudes, ± inches of water										
—	2.0	3.2	6.0	0.2	1.4	1.8	3.2	6.0	10.0	9.0	10.0

[1]Configuration: HPID - Hole Pattern I Down, HPIU - Hole Pattern I UP, HPIID - Hole Pattern II Down, PP - Perforated Plate.

[2]Corrected limestone bed height in inches.

are immediately obvious from the table. First, the amplitudes increased with increasing superficial velocity as was expected. Second, the average and maximum amplitudes increased significantly as the bed height increased. The amplitudes of hole pattern I down were consistent with those of hole pattern II down within the measurable accuracy. Hole pattern I up did show a tendency to have lower amplitude fluctuations than the other two configurations, but only two tests were performed on hole pattern I up so no firm conclusions can be drawn. In the latter configuration a minimum of 3.5 inches of limestone was between the active portion of the bed and the lower bed pressure tap, so this slumped limestone may have damped the pressure fluctuations which were measured.

A comparison of the perforated plate pressure fluctuation amplitudes shown on the right side of Table 7.1 with those of the pipe grid feeder reveals that the perforated plate amplitudes were approximately 50 to 100 percent higher. Thus, it is concluded that the pipe grid feeder had a higher quality of fluidization than the perforated plate. The pipe grid feeder appeared to produce smaller bubbles than the perforated plate, and these smaller bubbles percolated up through the bed less violently than the large bubbles or slugs generated by the perforated plate.

The frequencies of the lower bed pressure fluctuations are shown in Table 7.2 for the pipe grid feeder configurations tested. Two general conclusions regarding the frequencies can be drawn. First, the frequency decreased as the bed height increased. Second, in general, the frequencies decreased as the superficial velocity increased. Although the latter decrease was relatively small in

TABLE 7.2

FREQUENCIES OF THE LOWER BED PRESSURE FLUCTUATIONS WITH THE PIPE GRID FEEDER AND WITH THE PERFORATED PLATE

Superficial Velocity, ft/sec	HPID[1]	HPID	HPID	HPIU	HPIID	HPIID	HPIID	HPIID	PP	PP
	5.8[2]	9.8	14.9	7.3	4.7	10.4	15.4	21.1	9.9	14.1
	Frequencies, cycles per second									
3.6	4.0	3.9	-	3.4	-	3.8	3.8	-	-	-
4.5	3.9	3.4	3.3	3.7	4.8	4.0	3.0	2.7	-	1.9
5.4	3.8	3.7	3.1	3.9	5.0	4.0	3.2	2.4	1.9	2.0
6.3	3.9	3.1	2.9	3.8	4.5	4.0	3.0	2.5	1.8	2.0
7.2	3.8	3.0	2.6	3.9	4.2	3.6	2.6	2.5	1.9	1.9
8.2	3.7	2.8	2.7	4.2	4.2	3.0	2.8	-	1.9	1.9

[1]Configuration: HPID - Hole Pattern I Down, HPIU - Hole Pattern I Up, HPIID - Hole Pattern II Down, PP - Perforated Plate.

[2]Corrected limestone bed height in inches.

magnitude, it did occur for the configurations and bed heights tested. A close comparison reveals that hole pattern II down generated slightly higher frequencies than hole pattern I down at the comparable bed heights tested. In the only test with hole pattern I up in which frequencies could be measured, the frequency increased moderately with increasing superficial velocity unlike the other configurations. However, the data taken with hole pattern I up were too limited to establish any trends.

Unlike the pipe grid feeder lower bed pressure fluctuation frequencies, the perforated plate frequencies shown on the right side of Table 7.2 were very consistent for the two bed heights tested. Also, whereas the pipe grid feeder frequencies were in the range of 2.5 to 5.0 cycles per second, all perforated plate frequencies were 2.0 cycles per second or below. The significance to be attached to the frequencies measured is not known. Intuitively, it would seem that lower frequencies would be desirable as these should produce less severe vibrations of the fluidized bed structure.

The percent bed expansion beyond the slumped bed height is recorded in Table 7.3 for two of the pipe grid feeder configurations tested. No data are recorded for the hole pattern I up tests because the spouting of the air through the low bed heights tested did not produce a normal bed expansion. From the table it is apparent that the percent expansion increased as the bed superficial velocity increased. Also, the percent expansion increased modestly with increased bed height. Considering the inherent inaccuracy in measuring the fluidized bed heights, the percent expansions for the two configurations of the pipe grid feeder did not differ significantly.

TABLE 7.3

BED EXPANSIONS WITH THE PIPE GRID FEEDER AND WITH THE PERFORATED PLATE

Superficial Velocity, ft/sec	HPID[1] 5.8[2]	HPID 9.8	HPID 14.9	HPIID 4.7	HPIID 10.4	HPIID 15.4	HPIID 21.1	PP 9.9	PP 14.1
	Bed Expansion, percent								
3.6	0.0	2.4	1.4	2.7	0.8	0.6	6.1	2.5	1.7
4.5	0.0	2.4	6.7	3.2	5.6	7.1	13.0	11.7	7.5
5.4	0.0	5.2	14.5	5.6	9.9	13.0	20.1	19.3	15.7
6.3	8.6	10.6	19.4	15.5	14.7	18.2	25.1	31.6	21.7
7.2	14.8	15.7	25.3	21.4	22.4	26.4	31.0	40.2	30.3
8.2	21.7	27.1	33.0	27.0	28.2	34.4	38.0	55.8	42.3

[1] Configuration: HPID - Hole Pattern I Down, HPIID - Hole Pattern II Down, PP - Perforated Plate.

[2] Corrected limestone bed height in inches.

The perforated plate bed expansion results are shown on the right side of Table 7.3. As with the pipe grid feeder, the perforated plate percent expansion increased with increasing velocity. However, unlike the pipe grid feeder, the percent expansions for the perforated plate decreased with bed height. For a given bed height, the perforated plate gave a greater percent expansion than did the pipe grid feeder. This latter effect was probably due to the larger bubbles or slugs of air which were produced by the perforated plate distributor.

The measured and predicted bed pressure drops for two configurations of the pipe grid feeder and for the perforated plate are shown in Table 7.4. The results of hole pattern I up are not tabulated because the spouting which occurred did not allow a conventional bed pressure drop to be measured. The predicted values, which were calculated from Equation (6.11) on page 96, using the corrected slumped bed height, fell within the range of the measured pressure drops for both distributors.

Coal Feeding

Qualitatively, the most notable feature of the pipe grid coal feeder was the noise made by the imitation coal as it swept through the PVC pipes and impacted the ends of the pipe tees. A related occurrence was the accumulation of static charge on the PVC pipes caused by the plastic imitation coal moving through the pipes. On one occasion a visible and quite strong spark was drawn from the PVC pipes.

Quantitatively, the coal feeding performance of the pipe grid feeder was evaluated with the two coal sample probes using the method

TABLE 7.4

MEASURED AND PREDICTED BED PRESSURE DROPS WITH THE PIPE GRID FEEDER AND WITH THE PERFORATED PLATE

Superficial Velocity, ft/sec	HPID[1] 5.8[2]	HPID 9.8	HPID 14.9	HPIID 4.7	HPIID 10.4	HPIID 15.4	HPIID 21.1	PP 9.9	PP 14.1
	Measured Bed Pressure Drop, lbf/in^2								
3.6	0.15	0.34	0.63	0.12	0.40	0.67	1.01	0.38	0.59
4.5	0.15	0.34	0.66	0.12	0.41	0.70	1.06	0.42	0.66
5.4	0.15	0.35	0.67	0.13	0.41	0.71	1.08	0.45	0.68
6.3	0.16	0.35	0.68	0.13	0.43	0.72	1.10	0.48	0.70
7.2	0.17	0.37	0.69	0.13	0.44	0.75	1.11	0.46	0.72
8.2	0.16	0.40	0.72	0.14	0.46	0.76	1.12	0.48	0.72
	Predicted Bed Pressure Drop[3], lbf/in^2								
-	0.18	0.39	0.66	0.11	0.42	0.69	0.99	0.39	0.62

[1]Configuration: HPID - Hole Pattern I Down, HPIID - Hole Pattern II Down, PP - Perforated Plate.

[2]Corrected limestone bed height in inches.

[3]Using Equation (6.11) on page 96.

outlined in Chapter 6. Coal feeding tests were performed with the hole pattern I down and hole pattern II down configurations of the in-bed pipes, but not with the hole pattern I up configuration. Coal feeding tests were performed with hole pattern I down despite the fact that it did not give uniform fluidization because it was not known at the time whether modifications in the hole pattern would improve the fluidization performance. For both configurations complete coal feeding tests were performed with an uncorrected bed height of 18 inches and with the coal sample probes at the 1 foot level. In addition, a full flow test and a half flow test were conducted with hole pattern II down for an uncorrected bed height of 25 inches with the coal sample probes at the 2 foot level.

The location of the coal sample probe compartments in relation to the distributor holes of the four in-bed pipes are shown in Figure 7.9. Compartments A and C appear to have sampled in-bed pipes 1 and 4 respectively, while the B compartments appear to have received samples combining imitation coal from in-bed pipes 2 and 3. However, with the in-bed pipes turned holes downward, the air and imitation coal had to pass around the outside of these pipes as they proceeded upwards. Thus, the correlation between coal sample probe compartments and the distributor holes sampled should not be extended too far.

The pipe grid feeder coal feeding test results exhibited a considerable range of variation. A complete analysis of a test with reasonably consistent results is illustrated in Table 7.5, while an analysis of a test with inconsistent results is illustrated in Table 7.6. All coal feeding test results are included in Appendix H. The results of symmetry coal feeding tests are compared in Table 7.7. In

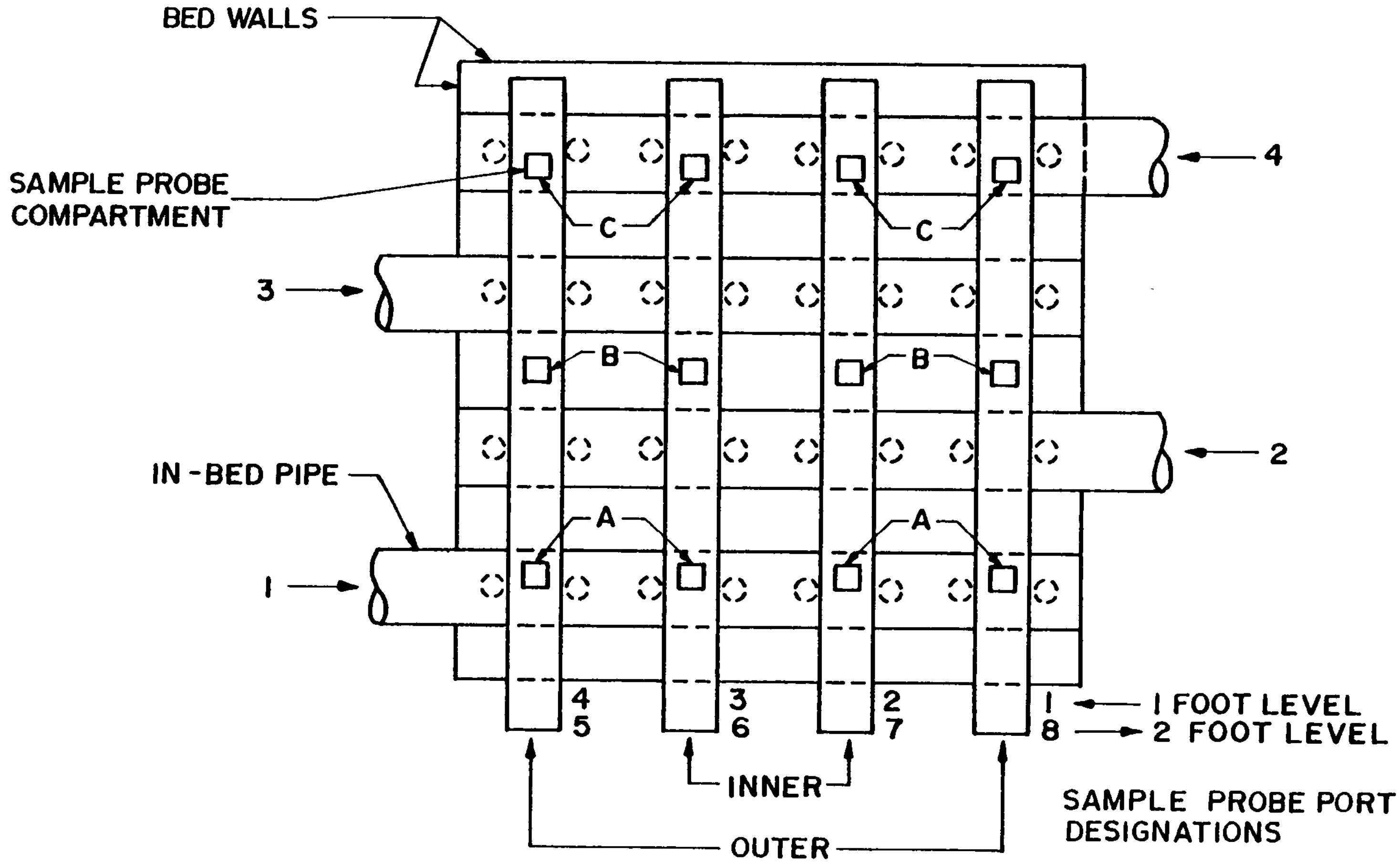

Figure 7.9. Coal Sample Probe Positions with the Pipe Grid Feeder.

TABLE 7.5

TYPICAL CONSISTENT PIPE GRID FEEDER COAL FEEDING TEST RESULTS[1]

CFD Parameter[2]	Compartment of Sample Probe in Port 4				Compartment of Sample Probe in Port 3		
	A	B	C		A	B	C
Limestone, grams	61.77	65.61	77.15		69.57	80.42	57.51
IC, grams	1.43	1.14	1.36		1.49	1.47	0.98
Total, grams	63.20	66.75	78.51		71.06	81.89	58.49
% IC	2.3	1.7	1.7		2.1	1.8	1.7
Prb Avg % IC		1.9				1.9	
% IC/Prb Avg % IC	+19.0	-10.2	-8.9		+13.0	-3.3	-9.7
Tst Avg % IC				1.9			
% IC/Tst Avg % IC	+20.5	-9.1	-7.8		+11.6	-4.4	-10.8

[1]Configuration: Hole pattern II down, 15.4 inches of limestone (corrected), V_{sf} = 7.9 ft/sec.

[2]See Appendix F for an explanation of these labels.

TABLE 7.6

TYPICAL INCONSISTENT PIPE GRID FEEDER COAL FEEDING TEST RESULTS[1]

CFD Parameter[2]	Compartment of Sample Probe in Port 4				Compartment of Sample Probe in Port 1		
	A	B	C		A	B	C
Limestone, grams	54.52	59.36	49.21		54.97	47.96	33.57
IC, grams	1.01	1.06	1.46		1.42	0.86	0.94
Total, grams	55.53	60.42	50.67		56.39	48.82	34.51
% IC	1.8	1.8	2.9		2.5	1.8	2.7
Prb Avg % IC		2.2				2.3	
% IC/Prb Avg % IC	-15.5	-18.5	+33.9		+7.9	-24.5	+16.7
Tst Avg % IC				2.2			
% IC/Tst Avg % IC	-18.9	-21.8	+28.5		+12.3	-21.5	+21.4

[1]Configuration: Hole pattern II down, 15.4 inches of limestone (corrected), V_{sf} = 7.9 ft/sec.

[2]See Appendix F for an explanation of these labels.

TABLE 7.7

SYMMETRY COAL FEEDING TEST RESULTS FOR THE PIPE GRID FEEDER[1,2]

Compartment	Coal Sample Probe Port 4 (I)	4 (II)	3 (I)	3 (II)	2 (I)	2 (II)	1 (I)	1 (II)
C	-34[3,4]	+28[5]	-17	-7	-4	+29	+109	+21
	-8		-11		+6		+18	
B	-4	-22	-3	-7	-7	-25	-33	-21
	-5		-20		-22		-24	
A	-2	-19	+26	-2	+5	+13	-37	+12
	+45		+39		+9		-26	

[1]These tests were performed at full flow conditions with an 18 inch uncorrected bed height.

[2]See Figure 7.9 on page 147 for the port and compartment locations with respect to the in-bed air distributor pipes.

[3]These numbers (percentages) are the % IC/Tst Avg % IC parameter explained in Appendix F.

[4]The numbers to the left of the vertical bars are for hole pattern I down tests.

[5]The numbers to the right of the vertical bars are for hole pattern II down tests.

symmetry tests the two coal sample probes were placed at the outer ports and then the inner ports to determine if the coal distribution in the bed was symmetrical. The primary conclusion is that more coal was distributed near the entrance of the in-bed pipes in the hole pattern I down configuration than at the downstream end. This result appears to contradict the observation that the greatest air flow was out of the downstream end of the pipes. However, the coal particles probably did not accelerate to a high velocity comparable to that of the air after passing through the sharp bend just 9 inches upstream of the beginning of the distributor hole pattern. Thus, with gravity keeping the coal particles near the bottom of the pipes, they would have tended to be swept out the first few holes with the discharging air. The coal distribution from hole pattern II down was less repeating than that of hole pattern I down, although no definite maldistribution characteristics could be detected in the former feeder configuration. However, the range of variation in the distribution of hole pattern II appears to be less than that of hole pattern I. Also, it appears that the concentration of coal was greater above the two outer in-bed pipes (1 and 4) than above the inner pipes (2 and 3) for both configurations. This result is consistent with the observation that the outer in-bed pipes had the higher air flow. The results of standard full flow and half flow tests are summarized in Table 7.8. In these tests both coal sample probes were placed in adjacent ports. The primary conclusion is that the range of variation in the half flow tests was greater than that of the full flow tests.

TABLE 7.8

STANDARD COAL FEEDING TEST RESULTS FOR THE PIPE GRID FEEDER[1,2]

	Coal Sample Probe Port							
Compartment	4		3		4		3	
	Full Flow Tests				Half Flow Tests			
C	+1[3,4]	-8[5]	-36	-11	+45	-16	+7	-1
B	+18	-9	-29	-4	+10	-12	-71	-34
A	+35	+20	+12	+11	+49	+11	-40	+52

[1]These tests were performed with an 18 inch uncorrected bed height.

[2]See Figure 7.9 on page 147 for the port and compartment locations with respect to the in-bed air distributor pipes.

[3]These numbers (percentages) are the % IC/Tst Avg % IC parameter explained in Appendix F.

[4]The numbers to the left of the vertical bars are for hole pattern I down tests.

[5]The numbers to the right of the vertical bars are for hole pattern II down tests.

A single one point coal feeding simulation test was performed with the perforated plate. For the test 7 pounds of imitation coal were piled in the center of the perforated plate and then covered with 16.5 inches of limestone. The fluidization and transport air were turned on and brought up to full flow as rapidly as possible. Samples were taken with the two coal sample probes in the same manner as the other coal feeding tests. The results, which are shown in Table 7.9, were similar in magnitude and degree of variation to those obtained with the pipe grid feeder. Thus, the pipe grid feeder distributed coal with the same order of uniformity as a coal feeder utilizing one feed point for every four square feet of bed area.

Even though the coal feeding test results did not always yield definite conclusions, it can be concluded that at least some coal from the pipe grid feeder reached the coal sample probe compartments in all full flow tests. In fact, except for a few half flow coal feeding samples taken, all measured coal concentrations in the bed were on the order of two to four times the bed background coal concentration of 0.50 to 0.75 percent. Further conclusions and recommendations concerning the pipe grid feeder are included in Chapter 8.

TABLE 7.9

SIMULATED COAL FEEDING TEST RESULTS USING THE PERFORATED PLATE[1]

CFD Parameter[2]	Compartment of Sample Probe in Port 4				Compartment of Sample Probe in Port 3		
	A	B	C		A	B	C
Limestone, grams	29.52	34.19	64.06		72.02	72.43	67.26
IC, grams	0.65	0.39	1.01		1.23	1.03	0.79
Total, grams	30.17	34.58	65.07		73.25	73.46	68.05
% IC	2.2	1.1	1.6		1.7	1.4	1.2
Prb Avg % IC		1.6				1.4	
% IC/Prb Avg % IC	+33.7	-30.0	-3.7		+18.8	-0.8	-17.9
Tst Avg % IC				1.5			
% IC/Tst Avg % IC	+42.4	-25.5	+2.6		+11.0	-7.3	-23.3

[1]Configuration: Taped perforated plate, 15.2 inches of limestone (corrected), V_{sf} = 7.7 ft/sec.

[2]See Appendix F for an explanation of these labels.

CHAPTER 8

CONCLUSIONS AND RECOMMENDATIONS

Specific

The experimental fluidized bed test facility designed and constructed as a part of this thesis project is a useful tool for evaluating combined function total air and coal distributing feeders. The design of the plenum box and lower bed structure allows simple and rapid installation of any below-the-bed or in-bed feeder configuration to be tested. In addition, due to the flexibility incorporated into the experimental facility, it could easily be adapted for use in a variety of fluidized bed research projects including basic fluidization, solids mixing, and conventional coal feeder evaluation studies.

The fluidization evaluation methods developed during the project are a practical means for quantifying fluidization characteristics for comparative purposes. The lower bed pressure fluctuation amplitude and frequency measurements and the percent bed expansion measurements do allow distinctions to be made between the types of fluidization behavior produced by combined function coal feeders. However, these measurements would be more meaningful if the desirable amplitude, frequency, and bed expansion ranges for actual fluidized bed combustors could be established. The proper range determinations will depend on which ones give the best combustion efficiency and sulfur capture results in a hot bed.

If the pressure fluctuation amplitude and frequency measurements from the experimental facility are to be compared with those from other facilities, the amount of damping occurring in the pressure lines between the fluidized bed and the pressure transducers must be established. In this facility these lines are approximately 20 feet in length and contain eight 90 degree bends. Tests should be performed in which the output from tranducers located at the plenum box, lower bed, and upper bed pressure taps is compared to the output of the transducers at the present location. In this way a determination could be made as to whether or not the damping in the pressure lines significantly influences the pressure related measurements.

Consideration should be given to developing other methods for quantifying fluidization performance in the experimental facility. One possibility would be to attach one or more accelerometers to the fluidized bed test section to measure the amount of vibration produced from the fluidization by the various coal feeders. This vibration could be quite significant in a large bed containing tons of limestone. It is possible that the pressure fluctuations measured are directly related to the vibrations produced.

The integrated evaluation method is a relatively quick and easy to perform means for measuring coal feed distribution in a cold model fluidized bed. The imitation coal performs well as a realistic coal substitute material. The magnetic separator is very useful for separating the imitation coal from the limestone as long as a residual coal concentration of approximately 0.75 percent can be tolerated. If it should become necessary to perform tests with lower coal concentrations in the bed, a more efficient (and thus more costly) magnetic separator could be procured and incorporated into the system. The coal sample probes work well as dynamic sample collection devices.

However, the mechanical operating difficulties need to be solved so that the probes do not have to be dissassembled, cleaned, and regreased periodically as is currently necessary. One possible solution might be to install close tolerance nylon or Teflon bushings between the inner and outer probe tubes. These bushings could be fitted around the holes of each probe compartment to reduce the chance of particles becoming trapped between the two tubes. Nylon liners should be installed within the coal sample probe support sleeves to prevent the aluminum galling problem. The time required for evaluating each set of bed material samples collected during the coal feeding tests could be reduced by approximately 30 minutes if a laboratory size high strength magnetic separator was utilized. Currently the imitation coal in the samples is separated from the limestone manually with a permanent magnet.

The integrated evaluation method is more useful for determining the average performance of a coal feeder based on several tests than for measuring the precise performance during a single test. In fact, coal feeding distribution tests in fluidized beds must encompass many tests of the same feeder configuration to achieve valid results due to the changing nature of fluidized beds. The greatest value of the integrated evaluation method is its ability to determine whether a coal feeder distributes coal throughout the bed by being able to distinguish between the local coal concentration and the initial background concentration.

The perforated plate air distributor served the purpose for which it was designed, although its fluidization performance was poorer than that of any coal feeders tested to date (i.e., the valve cap feeder described by Henry [91], the pipe grid feeder described in this thesis, and some feeders currently being tested by Kress). At some time the heat transfer tube assembly should be removed and the perforated plate installed so that complete baseline fluidization tests can be performed with the full instrumentation on-line. By comparing these latter test results with some taken previously with the heat transfer tube assembly installed, the value of the assembly for reducing the slugging behavior of the bed could be determined.

The in-bed pipe grid coal feeder fluidized the bed uniformly after the distributor hole diameters were modified. However, because uniform fluidization requires the balancing of the flow through the distributor holes, it may be difficult to achieve in a large bed containing several long pipes with many holes. The pressure drop through the pipe grid feeder (approximately 3 lbf/in^2 at an 8 ft/sec superficial velocity) was higher than would probably be acceptable in a full size bed due to the air pumping power required. This pressure drop could be reduced in a large bed by using more appropriately sized pipes to lower the air velocities nearer to the required minimum coal transport velocity. In addition, the pressure drop across the in-bed distributor pipes could be lowered by using larger diameter holes. However, the various air/coal flow splitting devices required would still produce a significant pressure drop in a full scale system.

The pipe grid feeder distributed coal to all parts of the bed with moderate variations in the distribution. The hole pattern I down configuration distributed more coal from the upstream holes of the in-bed pipes than from the downstream holes. In some tests the hole pattern II down configuration performed similarly to hole pattern I, while in other tests the coal distribution from hole pattern II appeared to be varied and unrepeating. Possibly a large number of tests on the latter configuration would be required to establish definite distribution characteristics. It should be noted that uniformity of distribution is a relative measurement. Thus, the moderate nonuniformity of coal distribution by the pipe grid feeder may very well be minor in comparison to the distribution provided by some of the fluidized bed coal feeding schemes currently being utilized which have one feed point for every 9 square feet of bed area. In most cases, the degree of coal distribution by these latter feeders has not been quantified.

Preliminary coal distribution tests of a coal feeder such as the pipe grid feeder might be best performed by fixing fabric bags over the outlet of each distributor hole. Thus, the coal collected from each hole could be weighed and the amounts compared. This same procedure could also be used to evaluate the degree of imbalance of air/coal flow splits. Final testing should be performed by taking samples in the bed because the actual bed coal distribution is partially determined by the fluidization performance of the feeder.

The behavior of a combusting fluidized bed is considerably different from that of the cold model experimental fluidized bed. Thus, if the pipe grid feeder concept is adopted, it must be tested in a hot bed under actual operating conditions. One of the important factors to be determined is whether coal will agglomerate within the hot in-bed distributor pipes. The probability that this will occur is low in comparison to other in-bed feeder concepts because the pipe grid feeder utilizes a very dilute mixture of coal in the total fluidization air. In addition, the long term performance of the pipe grid feeder must be established, particularly as related to the thermal stresses of a hot bed and the erosion of feeder components by the particles passing through them.

General

The combined total air and coal distribution concept offers several advantages over other coal feeding methods as discussed in Chapter 1. However, to achieve uniform fluidization in conjunction with the coal feeding process, a combined function feeder requires significantly more coal feed points (which are also air distribution points) per unit bed area than a conventional coal feeder which has separate coal and air feed points. For a combined function feeder, the resulting large number of feed points needed in a full scale bed requires a complex network of pipes and splitting devices to divide the air/coal flow between all the feed points. This large amount of "plumbing" not only increases the complexity and costs of the system, but it also represents a considerable pressure drop which translates into a decreased system efficiency.

The trend during the recent years has been to experiment with successively larger fluidized bed systems. This trend is productive and should continue as it appears that some results obtained from small beds have limited application. Experiments should be performed in realistically designed facilities which utilize the proper particle size distribution and which contain some form of heat transfer tubes as the latter components are an integral part of actual fluidized bed combustors. More hot bed studies must be conducted as the results of these studies are the most useful for evaluating the performance and problems of fluidized bed combustion systems.

A concentrated effort to determine accurate techniques for scaling fluidized bed systems is necessary before full size systems can be designed with confidence. As mentioned previously, the validity of available data is questionable because much of it was generated in small and/or cold model fluidized beds. The determination of proper scaling methods would allow more profitable experiments and test facilities to be developed and designed. The scaling studies proposed by Glicksman [89] appear to be a well-founded approach to the problem. He suggests that three types of scaling experiments need to be performed. Two geometrically similar non-combusting beds, one heated and the other at ambient conditions, should be compared to establish the effects of air density and viscosity on scaling. Then a non-combusting heated bed should be compared to a similar combusting bed to determine the effects of combustion on scaling. Finally, different sizes of geometrically similar ambient temperature beds containing tubes should be compared to account for the wall effect on scaling.

More attention needs to be focused on the flow regimes in which fluidized bed systems operate. The majority of the large particle systems envisioned for fluidized bed combustors operate in the rapidly growing bubble regime (also known as the apparent slug flow regime). The large bubbles and slugging phenomenon associated with this regime have a detrimental effect on the gas-solids contact which is necessary for efficient combustion and sulfur capture. Thus, the turbulent regime should be investigated for fluidized bed combustion systems. This regime is characterized by excellent mixing accompanied by small bubbles or voids. The absence of the slugging phenomenon greatly decreases the amount of vibration that is produced. Certainly, these advantages must be evaluated in light of the higher air pumping power which would be required to reach turbulent regime velocities and the increased bed internals erosion which would likely occur.

The fluidized bed combustion process possesses significant potential for effectively reducing pollutant emissions from coal combustors in the near future. Thus, the organized research and development of this technology should proceed at the most rapid pace affordable.

LIST OF REFERENCES

LIST OF REFERENCES

1. Environmental Protection Agency, "Standards of Performance for New Stationary Sources, Electric Utility Steam Generating Units," 40 CFR Part 60, Cincinatti, OH, effective Sept. 18, 1978.

2. Environmental Protection Agency, "Standards of Performance for New Stationary Sources," Federal Register, Vol. 36, No. 247, Dec. 23, 1971.

3. Babcock and Wilcox, Summary Evaluation of Atmospheric Pressure Fluidized Bed Combustion Applied to Electric Utility Large Steam Generators, Final Report, Vol. 1, EPRI FP-308, Electric Power Research Institute, Palo Alto, CA, Oct. 1976, p. 1-1.

4. Walker, D.J., McIlroy, R.A., and Lange, H.B., "Fluidized Bed Combustion Technology for Industrial Boilers of the Future--A Progress Report," Combustion, Vol. 50, No. 8, Feb. 1979, pp. 26-32.

5. McKenzie, E.C., "Burning Coal in Fluidized Beds," Chemical Engineering, Vol. 85, No. 18, Aug. 14, 1978, pp. 116-127.

6. Suptic, J.M., "Fluidized Bed Combustors," paper presented at the U.S. Department of Energy Fourth Annual Energy Management Symposium, Denver, CO, Sept. 19-21, 1978.

7. Ehrlich, S., "History of the Development of the Fluidized-Bed Boiler," Proceedings of the Fourth International Conference on Fluidized-Bed Combustion, Mitre, McLean, VA, 1976, pp. 15-20.

8. Withers Jr., H.W., and Fox, E.C., "Impact of Revised New Source Performance Standards (NSPS) on Atmospheric Fluidized-Bed Combustion Technology Development," Tennessee Valley Authority, Chattanooga, Nov. 1978.

9. Howe, W.C., "Projects Influencing AFBC of Coal," report by the Radian Corporation for the Energy Research and Development Administration, Sept, 1977.

10. Khan, A.A., Atmospheric Fluidized Bed Combustion Technical Source Book, Union Carbide Corporation, Nuclear Division, unpublished interim report, Feb. 1980.

11. Stoess, Jr., H.A., Pneumatic Conveying, Wiley-Interscience, New York, 1970, pp. 13-19.

12. Wilkerson, H.J., and Krane , R.J., State-of-the-Art Coal and Lime-Stone Feeding for Atmospheric Fluidized Bed Combustion, ME AFBC-79-1, University of Tennessee, Knoxville, 1979.

13. Daw, C.S., et al., "Atmospheric Fluidized Bed Combustion Coal Feeding Test Program," Oak Ridge National Laboratory, Union Carbide Corporation, unpublished paper.

14. Caldwell, L.G., "Some Developments in the Feeding of Coal to Fluidized Bed Combustors," Proceedings of the Conference on Coal Feeding Systems, JPL 77-55, California Institute of Technology, Pasadena, 1977, pp. 653-674.

15. Combustion Engineering Power Systems, Preliminary Design Study for a Fluidized Bed Demonstration Unit, C-E 677, Combustion Engineering, Windsor, CT, June 1978.

16. Mills, D., and Mason, J.S., "Problems of Particle Degradation in Pneumatic Conveying Systems," Stephens, H.S., and Stapleton, C.A., eds., Pneumotransport 4, Fourth International Conference on the Pneumatic Transport of Solids in Pipes, Vol. 1, BHRA Fluid Engineering, Cranfield, England, 1978, pp. F3-27 - F3-36.

17. Kostka, K.S., "Coarse Particle Erosion in Pneumatic Conveyor Bends," Stephens, H.S., and Stapleton, C.A., eds., Pneumotransport 4, Fourth International Conference on the Pneumatic Transport of Solids in Pipes, Vol. 1, BHRA Fluid Engineering, Cranfield, England, 1978, pp. F8-87 - F8-102.

18. Fluidized Combustion Company, Preliminary Design and Cost Estimate for an Atmospheric Fluidized Bed Steam Generator, Vol. 1, FCC 1-77-0103, Fluidized Combustion Company, Apr. 1978, pp. 2-249 - 2-262.

19. Gamble, R.L., "Design of the Rivesville Multicell Fluidized-Bed Steam Generator," Proceedings of the Fourth International Conference on Fluidized-Bed Combustion, Mitre, McLean, VA, 1976, pp. 133-151.

20. Pope, Evans, and Robbins, Interim Report No. 1 on Multicell Fluidized-Bed Boiler Design, Construction and Test Program, PER-570-74, Pope, Evans, and Robbins, New York, Aug. 1974.

21. Branam, J.G., and Rosborough, W.W., "Material Handling Systems for the Fluidized-Bed Combustion Boiler at Rivesville, WV," Proceedings of the Conference on Coal Feeding Systems, JPL 77-55, California Institute of Technology, Pasadena, 1977, pp. 610-614.

22. Tracey, R., Wachtler, F., and Buck, V. "Industrial Application--Fluidized Bed Combustion--Georgetown University," Proceedings of the Fifth International Conference on Fluidized Bed Combustion, Vol. 2., Mitre, McLean, VA, 1978, pp. 61-90.

23. Fraas, A.P., and Holcomb, R.S., "Atmospheric Fluidized Bed Combustion Technology Test Unit for Industrial Cogeneration Plants," Proceedings of the Fifth International Conference on Fluidized Bed Combustion, Vol. 3, Mitre, McLean, VA, pp. 55-69.

24. Beacham, B., and Marshall, A.R., "Experiences and Results of Fluidized Bed Combustion Plant at Renfrew," Journal of the Institute of Energy, Vol. 59, June 1979, pp. 59-64.

25. Modrak, T.M., Morris, T.A., and Lapple, W.C., "EPRI/B&W Fluidized Bed Combustion Development Facility: Initial Test Results," paper presented at the 86th National AIChE Meeting, Houston, April 1-5, 1979.

26. Orr, Jr., C., Particulate Technology, Macmillan, New York, 1966.

27. Romero, J.B., and Johanson, L.N., "Factors Affecting Fluidized Bed Quality," Fluidization, Chemical Engineering Progress Symposium Series, Vol. 58, No. 38, AIChE, New York, 1962, pp. 28-37.

28. Morse, R.D., and Ballou, C.O., "The Uniformity of Fluidization--Its Measurement and Use," Chemical Engineering Progress, Vol. 47, No. 4, Apr. 1951, pp. 199-204.

29. Shuster, W.W., and Kisliak, P., "The Measurement of Fluidization Quality," Chemical Engineering Progress, Vol. 48, No. 9, Sept. 1952, pp. 455-458.

30. Grohse, E.W., "Analysis of Gas-fluidized Solid Systems by X-ray Absorption," AIChE Journal, Vol. 1, No. 3, Sept. 1955, pp. 358-365.

31. Bailie, R.C., Fan, L.T., and Stewart, J.J., "Uniformity and Stability of Fluidised Beds," Industrial and Engineering Chemistry, Vol. 53, No. 7, July 1961, pp. 567-569.

32. Rice, W.J., and Wilhelm, R.H., "Surface Dynamics of Fluidized Beds and Quality of Fluidization," AIChE Journal, Vol 4, No. 4, Dec. 1958, pp. 423-429.

33. Seki, N., Fukusako, S., Torikoshi, K., "Characteristics of Fluidization of a Solid Particle Bed," Transactions of the ASME, Journal of Heat Transfer, Vol. 101, No. 3, Aug. 1979, pp. 386-390.

34. Lirag, Jr., R.C., and Littman, H., "Statistical Study of the Pressure Fluctuations in a Fluidized Bed," Littman, H., et al., eds., Fluidization: Fundamental Studies, Solid-Fluid Reactions, and Applications, AIChE Symposium Series, Vol. 67, No. 116, AIChE, New York, 1971, pp. 11-22.

35. Verloop, J., and Heertjes, P.M., "Periodic Pressure Fluctuations in Fluidized Beds," Chemical Engineering Science, Vol. 29, No. 4, Apr. 1974, pp. 1035-1042.

36. Sutherland, K.S., "Solids Mixing Studies in Gas Fluidised Beds, Part I: A Preliminary Comparison of Tapered and Non-Tapered Beds," Transactions of the Institution of Chemical Engineers, Vol. 39, 1961, pp. 188-194.

37. Rowe, P.N., and Sutherland, K.S., "Solids Mixing Studies in Gas Fluidised Beds, Part II: The Behavior of Deep Beds of Dense Materials," Transactions of the Institution of Chemical Engineers, Vol. 42, 1964, pp. T55-T63.

38. Baeyens, J., and Geldart, D., "An Investigation into Slugging Fluidized Beds," Chemical Engineering Science, Vol. 29, No. 1, Jan. 1974, pp. 255-265.

39. Canada, G.S., McLaughlin, M.H., and Staub, F.W., "Flow Regimes and Void Fraction Distribution in Gas Fluidization of Large Particles in Beds Without Tube Banks," Wen, C.Y., ed., Fluidization: Application to Coal Conversion Processes, AIChE Symposium Series, Vol. 74, No. 176, AIChE, New York, 1978, pp. 14-26.

40. Geldart, C., Hurt, J.M., and Wadia, P.H., "Slugging in Beds of Large Particles," Wen, C.Y., ed., Fluidization: Application to Coal Conversion Processes, AIChE Symposium Series, Vol. 74, No. 176, AIChE, New York, 1978, pp. 60-66.

41. Cranfield, R.R., and Geldart, D., "Large Particle Fluidisation," Chemical Engineering Science, Vol. 29, No. 4, Apr. 1974, pp. 935-947.

42. Babu, S.P., Shah, B., and Talwalkar, A., "Fluidization Correlations for Coal Gasification Materials--Minimum Fluidization Velocity and Fluidized Bed Expansion Ratio," Wen, C.Y., ed., Fluidization: Application to Coal Conversion Processes, AIChE Symposium Series, Vol. 74, No. 176, AIChE, New York, 1978, pp. 176-186.

43. Geldart, D., "Types of Gas Fluidization," Powder Technology, Vol. 7, No. 5, May 1973, pp. 285-292.

44. Yerushalmi, J., et al., "Flow Regimes in Vertical Gas-Solid Contact Systems," Wen, C.Y., ed., Fluidization: Application to Coal Conversion Processes, AIChE Symposium Series, Vol. 74, No. 176, AIChE, New York, 1978, pp. 1-13.

45. Canada, G.S., and McLaughlin, M.H., "Large Particle Fluidization and Heat Transfer at High Pressures," Wen, C.Y., ed., Fluidization: Application to Coal Conversion Processes, AIChE Symposium Series, Vol. 74, No. 176, AIChE, New York, 1978, pp. 27-37.

46. Catipovic, N.M., Jovanovic, G.N., and Fitzgerald, T.J., "Regimes of Fluidization for Large Particles," AIChE Journal, Vol. 24, No. 3, May 1978, pp. 543-547.

47. van Deemter, J.J., "Mixing Patterns in Large-Scale Fluidized Beds," Grace, J.R., and Matsen, J.M., eds., Fluidization, Plenum Press, New York, 1980, pp. 69-89.

48. Broadhurst, T.E., and Becker, H.A., "Onset of Fluidization and Slugging in Beds of Uniform Particles," AIChE Journal, Vol. 21, No. 2, Mar. 1975, pp. 238-247.

49. Kehoe, P.W.K., and Davidson, J.F., "Pressure Fluctuations in Slugging Fluidized Beds," Keairns, D.L., et al., eds., Fluidized Bed Fundamentals and Applications, AIChE Symposium Series, Vol. 69, No. 128, AIChE, New York, 1973, pp. 34-40.

50. Kehoe, P.W.K., and Davidson, J.F., "The Fluctuation of Surface Height in Freely Slugging Fluidized Beds," Keairns, D.L., et al., eds., Fluidized Bed Fundamentals and Applications, AIChE Symposium Series, Vol. 69, No. 128, AIChE, New York, 1973, pp. 41-48.

51. Kunii, D., and Levenspiel, O., Fluidization Engineering, John Wiley and Sons, New York, 1969.

52. Squires, A.M., "Species of Fluidization," Chemical Engineering Progress, Vol. 58, No. 4, Apr. 1962, pp. 66-73.

53. Volk, W., Johnson, C.A., and Stotler, H.H., "Effect of Reactor Internals on Quality of Fluidization," Chemical Engineering Progress, Vol. 58, No. 3, Mar. 1962, pp. 44-47.

54. Harrison, D., and Grace, J.R., "Fluidized Beds with Internal Baffles," Davidson, J.F., and Harrison, D., eds., Fluidization, Academic Press, London, 1971, pp. 599-626.

55. Donlevy, B.T., Measuring Solids Movement in a Large Particle, Air Fluidized Bed: Two New Methods, M.S. Thesis, Oregon State University, Corvallis, 1977, pp. 13-15.

56. Rowe, P.N., et al., "The Mechanisms of Solids Mixing in Fluidised Beds," Transactions of the Institution of Chemical Engineers, Vol. 43, No. 9, 1965, pp. T271-T286.

57. Cranfield, R.R., "Solids Mixing in Fluidized Beds of Large Particles," Wen, C.Y., ed., Fluidization: Application to Coal Conversion Processes, AIChE Symposium Series, Vol. 74, No. 176, AIChE, New York, 1978, pp. 54-59.

58. Babu, S.P., et al., "Solids Mixing in Batch Operated Tapered and Non-Tapered Gas Fluidized Beds," Keairns, D.L., et al., eds., Fluidized Bed Fundamentals and Applications, AIChE Symposium Series, Vol. 69, No. 128, AIChE, New York, 1973, pp. 49-57.

59. Tailby, S.R., and Cocquerel, M.A.T., "Some Studies of Solids Mixing in Fluidised Beds," Transactions of the Institution of Chemical Engineers, Vol. 39, 1961, pp. 195-201.

60. Highley, J., and Merrick, D., "The Effect of the Spacing Between Solid Feed Points on the Performance of a Large Fluidized-Bed Reactor," Littman, H., et al., eds., Fluidization: Fundamental Studies, Solid-Fluid Reactions, and Applications, AIChE Symposium Series, Vol. 67, No. 116, AIChE, New York, 1971, pp. 219-227.

61. Weiner, S.C., Golan, L.P., and Cherrington, D.C., "Solids Mixing and Distribution in a Tube Filled Bed," SAE paper P-78/75, 1978.

62. Hayakawa, T., Graham, W., and Osberg, G.L., "A Resistance Probe Method for Determining Local Solid Particle Mixing Rates in a Batch Fluidized Bed," Canadian Journal of Chemical Engineering, Vol. 42, No. 3, June 1964, pp. 99-103.

63. Fitzgerald, T., Catipovic, N., and Jovanovic, G., "Solid Tracer Studies in a Tube-Filled Fluidized Bed," Proceedings of the Fifth International Conference on Fluidized Bed Combustion, Vol. 3, Mitre, McLean, VA, 1978, pp. 135-152.

64. Potter, O.E., "Mixing," Davidson, J.F., and Harrison, D., eds., Fluidization, Academic Press, 1971, pp. 293-381.

65. Geldart, D., and Cranfield, R.R., "The Gas Fluidisation of Large Particles," Chemical Engineering Journal, Vol. 3, No. 2, Apr. 1972, pp. 211-231.

66. Bowling, K. McG., and Watts, A., "Determination of Particle Residence Time in a Fluidized Bed: Theoretical and Practical Aspects," Australian Journal of Applied Science, Vol. 12, No. 4, Dec. 1961, pp. 413-427.

67. Bowling, K. McG., and Watts, A., "Determination of Residence Time of Particles in Multistage Fluidized Bed Systems," Australian Journal of Applied Science, Vol. 14, No. 1, Mar. 1963, pp. 57-68.

68. Babcock and Wilcox, Conceptual Studies and Preliminary Design of a Fluid Bed Fired Boiler for Service in an Electric Utility, B&W CRD-1006, Babcock and Wilcox, Alliance, OH, Apr. 1978.

69. Babcock and Wilcox, Steam, Its Generation and Use, 39th ed., Babcock and Wilcox, New York, 1978, p. 8-5.

70. Knox, Larry, Tennessee Division of Geology, personal communication, June 1979.

71. Konchesky, J.L., George, T.J., and Craig, J.G., "Air and Power Requirements for the Pneumatic Transport of Crushed Coal in Horizontal Pipelines," Transactions of the ASME, Journal of Engineering for Industry, Vol. 97, Series B, No. 1, Feb. 1975, pp. 94-100

72. Conrad, G.P., "Magnetic Materials," Mantell, C.L., ed., Engineering Materials Handbook, 1st ed., McGraw-Hill, New York, 1958, pp. 8-14 - 8-17.

73. Narcus, H., Metallizing of Plastics, Reinhold, New York, 1960, pp. 165-168.

74. Goldie, W., Metallic Coating of Plastics, Vol. 1, Electrochemical Publications, Middlesex, Eng., 1968, pp. 15, 112-125.

75. McGraw-Hill, "Properties of Conductive Plastics," Electronics, Vol. 22, Oct. 1949, pp. 96-99.

76. Tanner, W.C., "Castable Conductive Plastics," Society of Plastics Engineers Journal, Vol. 15, No. 3, Mar. 1959, pp. 216-219.

77. Gunia, R.B., ed., Source Book on Materials Selection: A Discriminative Selection of Outstanding Articles from the Periodical and Reference Literature, Vol. 2, American Society for Metals, Metals Park, OH, 1977, pp. 400-403.

78. American Society for Testing and Materials, "Coal and Coke," Standards D311-30, D410-38, D431-44, and E11-70, 1978 Annual Book of ASTM Standards, Part 26, ASTM, Philadelphia, 1978, pp. 211-212, 233-237, 449-453.

79. Babcock and Wilcox, Preliminary Design of a 570 MW Atmospheric Fluidized Bed Boiler, Babcock and Wilcox, Alliance, OH, Nov. 1977, p. 4-7.

80. Pryor, E.J., "Magnetic and Electrical Separation," Mineral Processing, 3rd ed., Elsevier, New York, 1965, pp. 571-599.

81. Taggart, A.F., "Electrical Concentration," Elements of Ore Dressing, Wiley, New York, 1951, pp. 44-68.

82. Moskowitz, L.R., "Typical Circuits and Applications," Permanent Magnet Design and Application Handbook, Cahners, Boston, 1976, pp. 210-265.

83. Fitzgerald, T.J., Oregon State University, personal communication with H.J. Wilkerson, May 24, 1979.

84. Wen, C.Y., and Dutta, S., "Research Needs for the Analysis, Design, and Scale-Up of Fluidized Beds," Halow, J.S., ed., Fluidization Theories and Applications, AIChE Symposium Series, Vol. 73, No. 161, AIChE, New York, 1977, pp. 1-8.

85. Lapple, W.C., Generalized Mechanics of Fluid Flow Through Particulate Materials, M.S. Thesis, University of Kansas, Lawrence, May 1957.

86. Horio, M., and Wen, C.Y., "An Assessment of Fluidized-Bed Modeling," Halow, J.S., ed., Fluidization Theories and Applications, AIChE Symposium Series, Vol. 73, No. 161, AIChE, New York, 1977, pp. 9-21.

87. Jackson, R., "Fluid Mechanical Theory," Davidson, J.F., and Harrison, D., eds., Fluidization, Academic Press, London, 1971, pp. 65-119.

88. Boothroyd, R.G., "Similarity in Suspension Flow," Flowing Gas-Solids Suspensions, Chapman and Hall, London, 1971, pp. 102-118.

89. Glicksman, L.R., "Scale-Up of Fluidized Beds," Massachusetts Institute of Technology, Apr. 1979, unpublished proposal.

90. Lackey, M.E., and Withers, H.W., "Cold Slumping Characteristics of a Fluidized Bed," Union Carbide Nuclear Division and the Tennessee Valley Authroity, unpublished report.

91. Henry, R.L., Feeding of Coal and Air to a Fluidized Bed Using Valve Caps, M.S. Thesis, University of Tennessee, Knoxville, Mar. 1981.

92. Wilkerson, H.J., University of Tennessee, Knoxville, "Derivation of Bell Mouth Inlet Mass Flow Rate Equation," unpublished paper, Feb. 1967.

93. Bolz, R.E., and Tuve, G.L., eds., Handbook of Tables for Applied Engineering Science, 2nd ed., CRC Press, Cleveland, 1973, p. 178.

94. Zenz, F.A., "Conveyability of Materials of Mixed Particle Size," Industrial and Engineering Chemistry Fundamentals, Vol. 3, No.1, Feb. 1964, pp. 65-75.

95. Jones, P.J., and Leung, L.S., "Estimation of Saltation Velocity in Horizontal Pneumatic Conveying--A Comparison of Published Correlations," Stephens, H.S., and Stapleton, C.A., eds., Pneumotransport 4, Fourth International Conference on the Pneumatic Transport of Solids in Pipes, Vol. 1, BHRA Fluid Engineering, Cranfield, England, 1978, pp. C1-1 - C1-12.

96. Foster Wheeler Boiler Corporation, "Fuel Feed System Recommendation for the Atmospheric Fluidized Bed Combustion Component Test and Integration Unit at Morgantown, West Virginia," FWBC 3-43-9501, unpublished report, Mar. 1979, pp. 1-2.

97. Withers, Jr., H.W., Tennessee Valley Authority, Chattanooga, personal communication with H.J. Wilkerson, Feb. 6, 1978.

98. Gomezplata, A., and Kugelman, A.M., "Processing Systems," Marchello, J.M., and Gomezplata, A., eds., Gas-Solids Handling in the Process Industires, Marcel Dekker, New York, 1976, p. 151.

99. Rigby, G.R., et al., "New Distributor for Gas Fluidised Beds," Transactions of the Institution of Chemical Engineers, Vol. 55, No. 1, Jan. 1977, pp. 68-70.

100. Rockwell International, "Fluidized Bed Incineration of Radioactive Waste," RFP-2471, Rocky Flats Plant, unpublished report, May 14, 1976, p. 4.

101. Zenz, F.A., "How Flow Phenomena Affect Design of Fluidized Beds," Chemical Engineering, Vol. 84, No. 27, Dec. 19, 1977, pp. 81-91.

102. Merry, J.M.D., "Penetration of Vertical Jets into Fluidized Beds," AIChE Journal, Vol. 21, No. 3, May 1975, pp. 507-510.

103. Zenz, F.A., "Bubble Formation and Grid Design," Institution of Chemical Engineers Symposium Series, No. 30, Institution of Chemical Engineers, London, 1968, pp. 136-139.

104. Babcock and Wilcox, "Air Distributors, Appendix 3D," Summary Evaluation of Atmospheric Pressure Fluidized Bed Combustion Applied to Electric Utility Large Steam Generators: Appendices, Vol. 2, EPRI FP-308, Electric Power Research Institute, Palo Alto, CA, Oct. 1976, pp. 3D-1 - 3D-8.

105. Boucher, D.F., "Fluid and Particle Dynamics," Perry, R.H., and Chilton, C.H., eds., Chemical Engineers' Handbook, 5th ed., McGraw-Hill, New York, 1973, pp. 5-47 - 5-49.

106. Senecal, V.E., "Fluid Distribution in Process Equipment," Industrial and Engineering Chemistry, Vol. 49, No. 6, June 1957, pp. 993-997.

107. Keller, J.D., "The Manifold Problem," Journal of Applied Mechanics, ASME Transactions, Vol. 71, Mar. 1949, pp. 77-85.

108. Dow, W.M., "The Uniform Distribution of a Fluid Flowing Through a Perforated Pipe," Journal of Applied Mechanics, ASME Transactions, Vol. 72, Dec. 1950, pp. 431-438.

109. Olson, F.C.W., "Flow Through a Pipe With a Porous Wall," Journal of Applied Mechanics, ASME Transactions, Vol. 71, Mar. 1949, pp. 53-54.

110. Berman, A.S., "Laminar Flow in Channels with Porous Walls," Journal of Applied Physics, Vol. 24, No. 9, Sept. 1953, pp. 1232-1235.

111. Van Der Hegge Zijnen, B.G., "Flow Through Uniformly Tapped Pipes," Applied Scientific Research, Section A, Mechanics, Heat, Vol. A3, 1951, pp. 144-162.

112. Davidson, J.F., et al., "The Two-Phase Theory of Fluidization and its Application to Chemical Reactors," Lapidus, L., and Amundson, N.R., eds., Chemical Reactor Theory, A Review, Prentice Hall, Englewood Cliffs, NJ, 1977.

113. O'Donnell, W.J., and Langer, B.F., "Design of Perforated Plates," ASME Journal of Engineering for Industry, Transactions of the ASME, Vol. 84, Ser. B, No. 3, Aug. 1962, pp. 307-320.

114. Slot, T, and O'Donnell, W.J., "Effective Elastic Constants for Thick Perforated Plates With Square and Triangular Penetration Patterns," ASME Journal of Engineering for Industry, Transactions of the ASME, Vol. 93, Ser. B, No. 4, Nov. 1971, pp. 935-942.

115. O'Donnell, W.J., "Effective Elastic Constants for the Bending of Thin Perforated Plates With Triangular and Square Penetration Patterns," ASME Journal of Engineering for Industry, Transactions of the ASME, Vol. 95, Ser. B, No. 1, Feb. 1973, pp. 121-128.

116. Kline, S.J., and McClintock, F.A., "Describing Uncertainties in Single-Sample Experiments," Mechanical Engineering, Vol. 75, No. 1, Jan. 1953, pp. 3-8.

117. Holman, J.P., "Analysis of Experimental Data," Experimental Methods for Engineers, 3rd. ed., McGraw-Hill, New York, 1978, pp. 41-87.

APPENDICES

APPENDIX A

EXPERIMENTAL FACILITY OPERATING PROCEDURES

Introduction

These procedures contain the steps necessary to perform the various operations and tests for which the experimental fluidized bed test facility had been designed. They are not rules without exceptions, but rather guidelines for normal operation. The components referred to throughout this appendix are shown schematically in Figure A.1. Most valves and pressure regulators are labeled with a combination of letters and numbers. For directional orientation, the transport air pressure regulator is located southeast of the plexiglass bed test section.

A standard configuration of the facility components is assumed to exist before and after any operations are performed. To prevent unauthorized tampering with the facility, the main electrical switchbox, located on the back of the control panel, is locked and the primary control air valve, CA-1, is closed whenever the facility is not in use. The facility isolation valve, TA-2, is left open except during certain maintenance operations. Therefore, the building air pressure, ranging between 110 and 130 lbf/in^2, is in the lines upstream of the three valves CA-1, TA-1 and the electrical solenoid valve for the baghouse air supply line. Also, a control air pressure of 80 lbf/in^2 is on the blower inlet butterfly valve, FA-1, when TA-2 is open, but this butterfly valve cannot be operated

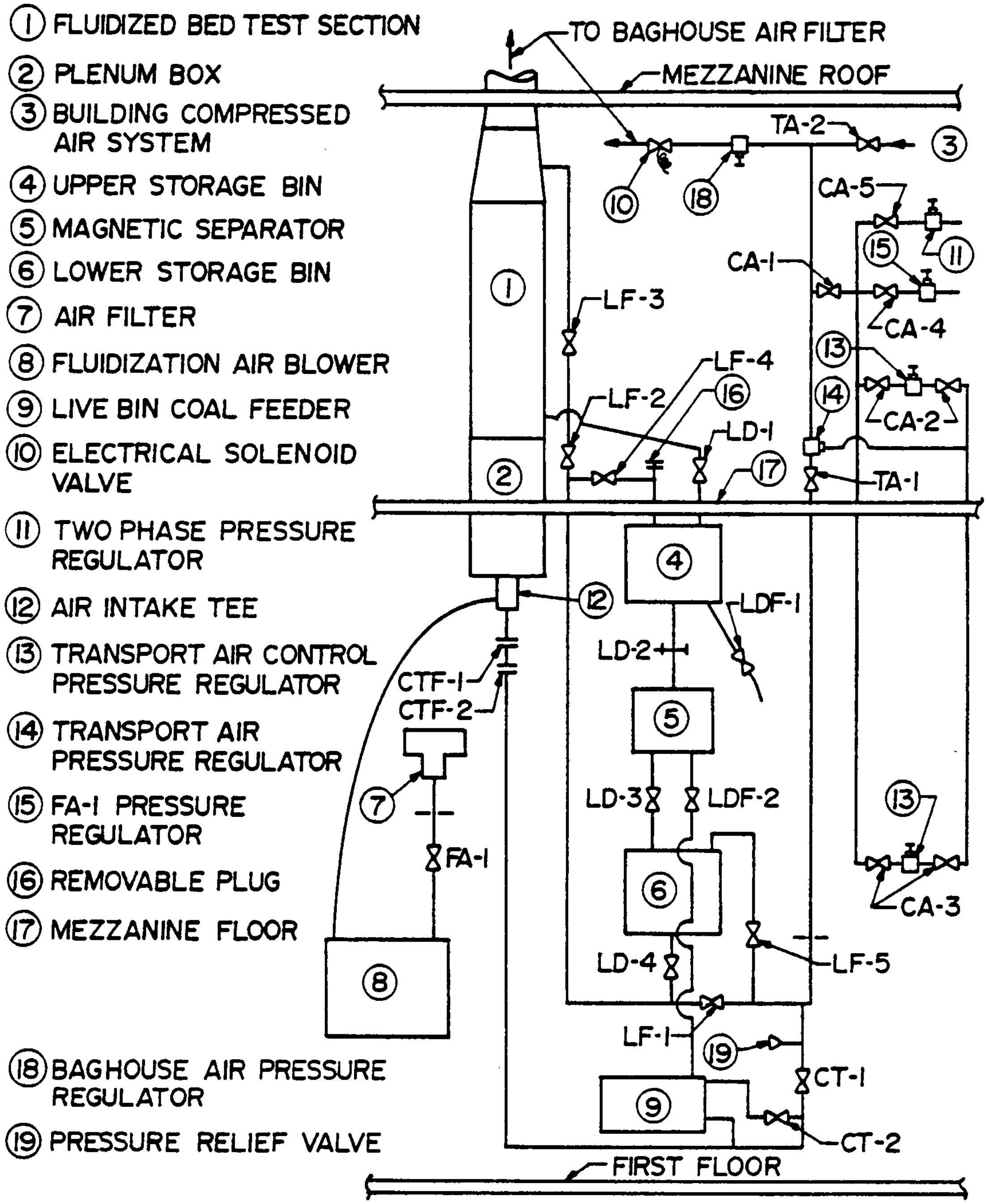

Figure A.1. Experimental Facility Schematic.

unless CA-1 and CA-4 are open. Following any operation all valves and switches are left in the most convenient safe condition, as specified in the procedures, although this may not necessarily be their original position.

Lowering and Raising the Plenum Box

Introduction

The plenum box is lowered and/or raised whenever either the perforated plate, a coal feeder, or the heat transfer tube assembly is removed or installed. The process requires caution because the empty plenum box weighs approximately 200 pounds (and more with a coal feeder installed). Also, the plenum box tends to shift somewhat unpredictably during lowering and raising due to the force applied by the 6 inch flexible line attached to the air intake tee.

Procedure

I. Lowering the plenum box.

1. Drain the material from the bed using the "Bed Material Drain" procedure.
2. Remove the coal sample probes if present.
3. Take off the two plywood side panels.
4. Vacuum any remaining material from the bed.
5. If the heat transfer tube assembly is to be dropped out of the bed, remove the plexiglass sample port plugs and take out the removable heat transfer tubes.

6. Remove the four screws and spacer washers connecting the heat transfer tube assembly to the base plate.
7. Place the wooden support frame across the bed base to catch the heat transfer tube assembly when the plenum box is lowered.
8. Remove the copper tubing pressure line from the upper north 6 inch plexiglass port cover of the plenum box.
9. Remove the double flanged 3 inch pipe section at CTF-1/ CTF-2 from the coal transport line.
10. Bolt a 3 inch blind flange onto CTF-2 to prevent objects from being dropped into the pipe.
11. Clean any particles out of the plenum box wheel tracks. Grease the ends of the wheel axles.
12. Remove the 6 inch plexiglass port covers on the east and west sides of the plenum box.
13. Install the two scissors jacks in the mounting holes in the 4 inch support channels on the east and west sides of the plenum box.
14. Remove the two bolts in the plenum box upper flange above each jack immediately north of the center gusset.
15. Raise both jacks fully and push the top plates toward the center gussets as they approach the plenum box upper flange.

16. Remove the second bolts from the north corners on the east and west sides of the bed and the second bolts from both corners on the south side.
17. Install the 10 inch guide rods in the above four holes.
18. Remove all remaining plenum box support bolts.
19. Lower both jacks simultaneously with 0.75 inch socket and ratchet sets. Proceed slowly and carefully while paying attention to the following actions:
    a. Observe the heat transfer tube assembly as it slides down in the bed to the wooden support frame. Try to keep the base plate level until the three lower tubes contact the support frame. If the heat transfer tube assembly is held up in the bed by wedged particles, chock the space between the three lower tubes and the support frame.
    b. Keep the small clearances between the ends of the wheel axles and the vertical rectangular tube supports as uniform as possible. This requires keeping the two jacks at the same level while lowering them.
    c. Watch the upper north 6 inch plexiglass port cover bolts to make certain that they clear the 4 inch support channel.
    d. If at any time one of the jacks should become unloaded, raise it until it supports weight, and then determine what is hanging up before proceeding.

e. When the plenum box is almost down, watch to make certain that the wheels are dropping into the tracks properly.

20. Once the plenum box is down, continue lowering the jacks until the top plates clear the gussets.
21. Remove the four 10 inch guide rods.
22. Remove the plywood hole cover being very careful not to fall through the hole.
23. Roll the plenum box out from under the bed.

II. Raising the plenum box.

1. If the perforated plate or a coal feeder has been installed, check the orientation of the holes in the base plate to see that they are aligned with the holes in the top flange of the plenum box.
2. Roll the plenum box under the bed.
3. Put the plywood hole cover in place being very careful not to fall through the hole.
4. Install the 10 inch guide rods in the holes referred to in Step I.16.
5. Install the two scissors jacks in the mounting holes in the 4 inch support channels on the east and west sides of the plenum box.
6. Raise the jacks to the upper flange of the plenum box and push the top plates toward the center gussets.

7. Raise both jacks simultaneously with 0.75 inch socket and ratchet sets. Proceed slowly and carefully while paying attention to the following actions:
   a. Keep the small clearances between the ends of the wheel axles and the vertical rectangular tube supports as uniform as possible. This requires keeping the two jacks at the same level while raising them.
   b. Watch the upper north 6 inch plexiglass port cover bolts to make sure that they clear the 4 inch support channel.
   c. When the base plate contacts the heat transfer tube assembly, try to keep it level as it pushes the assembly up into the bed. Be extremely careful to keep the assembly from catching or wedging between the plexiglass walls.
   d. If at any time the load on the jacks should increase, lower them slightly and determine what is hanging up before proceeding.
8. Continue raising the jacks until the bottom plate is snug against the support flanges.
9. Install bolts hand tight in all holes except those containing the guide rods or blocked by the jack top plates. These bolts should not be further tightened because this compresses the two gasket surfaces and makes it difficult to both remove the guide rods and to insert the remaining bolts.

10. Remove the four guide rods and install bolts in these holes.
11. Lower the jacks and install the remaining four bolts.
12. Tighten the bolts in a systematic fashion. This can best be done by having two persons starting at opposite corners and proceeding around the plenum box in the same direction tightening every other bolt. Two or three trips around the plenum box are required to tighten the bolts completely.
13. Remove the jacks.
14. Place the 6 inch plexiglass port covers on the east and west sides of the plenum box.
15. Remove the wooden support frame (and chocks if applicable) from under the heat transfer tube assembly.
16. Use the "2 X 4" wooden blocks to support the heat transfer tube assembly while installing the mounting screws and spacer washers.
17. Replace the plywood side panels.
18. Reconnect the copper tubing pressure line to the north 6 inch plexiglass port cover of the plenum box.
19. Replace the removable heat transfer tubes if necessary and install the coal sample probes as desired.
20. If coal feeding will be performed or transport air will be needed through the plenum box, replace the double flanged 3 inch pipe section in the coal transport line. Otherwise, bolt a 3 inch blind flange onto CTF-1 to seal the plenum box.

Fluidization

Introduction

In the broadest sense, the fluidization process may involve air "fluidization" only, limestone fluidization, or limestone fluidization with coal feeding. Fluidization tests using air only are for the purpose of testing a coal feeding system for air leaks and for evaluating pressure drops in the system. Limestone fluidization tests without and with coal feeding are full scope performance tests of the coal feeding system under consideration.

Limestone fluidization tests are normally initiated after the limestone has been put in the bed, but this is not always the case. The point at which limestone may be added after the blower is running is noted in the following procedure.

Procedure

Note: If only an air "fluidization" test is to be performed, omit the steps preceded by an asterisk (*).

I. System preparation.

1. Check the building air system pressure gauge. A minimum of 80 lbf/in^2 is required for various control pressures.
2. Unlock the electrical switch box on the back of the control panel and close the switch.
3. Begin setting up the strip chart recorder as described in the "Strip Chart Recorder" procedures 1.1 - 1.5. Allow at least 5 minutes of warmup time before proceeding with Step 1.7.

4. Prepare the scanivalve as described in the "Scanivalve System" procedures. If a command is to be automatically repeated (the normal method of operation), enter the command and then leave the scanivalve waiting for the repeat (R) command.

5. Set up the digital thermocouple reader by plugging the power cord into one of the panel outlets, plugging the male jack into the female jack mounted next to the thermocouple switch on the control panel, and pushing in the power ON/OFF button.

6. Place the clock or stopwatch on the control panel desk.

*7. Set up the vacuum cleaner for draining as described in the "Bed Material Drain" procedures.

*8. If a coal feeding test is to be performed, install the coal sample probes and support sleeves in the appropriate sample ports.

9. Close LF-3 and LD-1.

10. Open CA-1 and CA-4 (the latter valve is normally left open).

*11. Open CA-5, check that the appropriate isolation valves for the rotameters are open, set the two phase system pressure regulator to 60 lbf/in^2 (turn clockwise to increase, counterclockwise to decrease), and set the rotameters which will be used to 9 standard cubic feet per hour with the needle valve below each respective rotameter.

12. Turn the FA-1 VPI (Valve Position Indicator) power switch on (leftmost switch on the large electrical box behind the control panel).

*13. Turn the baghouse air supply electrical solenoid valve switch on (third switch from the left on the large electrical box behind the control panel).

14. Fill out the headings on the appropriate test data sheet.

II. Blower start-up.

*1. If the coal sample probes are in place, turn on the bleed air to the support sleeves.

*2. Turn the baghouse controller switch on (second switch from the left on the large electrical box behind the control panel).

3. Start the strip chart recorder by pressing the .25 mm/sec chart speed.

4. Hit the R key (i.e., the repeat command) on the scanivalve to start it.

5. Press the blower START button.

6. Start the clock or stopwatch.

7. When the blower current as shown on the ammeter drops from the pegged position to the surge point, begin opening the FA-1 (inlet butterfly valve) pressure regulator by turning the knob clockwise to the desired position. Observe the FA-1 VPI meter to determine the degree of opening of FA-1, and observe the fluidization air orifice manometer to determine the blower inlet flow.

7. Note: On the "FA-1 control" pressure gauge, less than 3 lbf/in^2 corresponds to a closed butterfly valve (0° on VPI) and 15 lbf/in^2 or greater corresponds to a fully open valve (90° on VPI).

III. Fluidization operation.

Note: If the bed is to be filled with limestone while the blower is running, this is the point at which this operation should take place. FA-1 should be opened approximately 40 degrees when limestone fill is started. It should gradually be opened completely as the bed level builds up.

1. The sole control of the bed during fluidization is the air flow as set with the FA-1 pressure regulator.
2. During a fluidization test various parameters are recorded both manually and automatically. These parameters include such quantities as time, temperatures, pressures or pressure differentials, and bed heights.
3. Any or all of the following activities can be performed as desired while the bed is fluidized:
   a. The addition of transport air and coal feeding as described in the "Coal Transport" procedures.
   b. The collection of imitation coal/limestone samples.
   c. The recording of bed pressure fluctuations as described in the "Strip Chart Recorder" procedures.
   d. The videotaping of the bed fluidization behavior.
   e. The draining of the bed as described in the "Limestone Drain" procedures.

3. Note: Two temperature limits have been set through experience with the system. The blower exhaust air temperature should not exceed 170°F. The plexiglass bed wall temperature should not exceed 130°F. Neither of these temperatures will be reached during normal operation.

IV. Blower shutdown.

1. Close the FA-1 pressure regulator by turning the knob counterclockwise until the blower current drops to the surge point.
2. Press the blower STOP button.
3. Finish closing the FA-1 pressure regulator as rapidly as possible (by turning the knob counterclockwise until it feels loose - do not screw it completely out).
4. Stop the clock or stopwatch.
5. Stop the scanivalve by pressing the HALT button.
6. Stop the strip chart recorder by pressing the STOP button.

*7. Turn the baghouse controller switch off.

*8. Turn the sample probe bleed air off if appropriate.

9. Log the run in the test data notebook.

V. Further testing.

1. Prepare the scanivalve and leave it waiting for the repeat (R) command.
2. Fill out the headings on the appropriate test data sheet.
3. Proceed from Step II.1 through IV.7.

VI. System shutdown.

1. Turn off the strip chart recorder by pressing the POWER button and disconnect the three pressure transducer cables, the thermocouple cable, and the power cord.
2. Disable the scanivalve system (see "Scanivalve System" procedures) and place the canvas dust cover over the teletype.
3. Turn off the digital thermocouple reader by pressing the power ON/OFF button and disconnect the jack and the power cord.

*4. Disconnect the vacuum cleaner hose and power cord.

5. Close CA-5 and CA-1.

*6. Turn the baghouse air supply electrical solenoid valve switch off.

7. Turn the FA-1 VPI power switch off.
8. Open the electrical switch on the box behind the control panel and lock it.
9. Return all mobile equipment to storage.

Limestone Transport

Introduction

The limestone transport process is used to fill the bed to the desired level with limestone. The limestone must be located in the lower storage bin prior to being pneumatically transported into the bed. The air used to transport the limestone is supplied by the building compressed air system and is regulated by the transport air pressure regulator via the transport air control pressure regulator at the first floor control station. For those cases in which the blower must be operating during limestone transport, see Section III of the "Fluidization" procedure.

Procedure

I. Mezzanine operations.

1. Close both CA-2 isolation valves.
2. Isolate the transport air orifice differential pressure manometer. (This is necessary because the volume of air used for limestone transport would cause the differential pressure to exceed the 30 inches of water range of the manometer.)
3. Open CA-1, LF-2, and LF-3.
4. Close LD-1 and LF-4.
5. Open TA-1.

II. First floor operations.

1. Close CT-1, LD-3, and LDF-2.
2. Open LF-1 and LF-5.
3. Isolate the 30 inch manometer.
4. Open both CA-3 isolation valves.
5. Open the transport air control pressure regulator (by turning the knob clockwise) until the transport air control pressure gauge shows about 4 lbf/in^2.

6. Open LD-4 approximately 60 degrees. This allows limestone to drop from the lower storage bin into the 3 inch line and to be transported into the bed.
7. Limestone in the line will cause the pressure drop through the line to increase (as can be seen by observing the transport air pressure gauge). The transport air pressure should be kept about 2 lbf/in^2 when limestone is in the line. The transport air control pressure regulator can be opened further to obtain this pressure if necessary.
8. For maximum limestone transport, LD-4 can be opened to approximately 75 degrees. Observe the transport air pressure and open the pressure regulator further if necessary to maintain 2 lbf/in^2.
9. If slugging or choking of the limestone in the transport line should occur (this will be evident due to the change in motion induced sound coming from the 3 inch line and by noting that the pressures on both gauges are either fluctuating widely or are the same):
   a. Close LD-4 carefully and then close LF-5.
   b. Open the transport air control pressure regulator enough to blow out the line.
   c. Close the regulator partially until the transport air control pressure shows approximately 4 lbf/in^2.
   d. Open LF-5.
   e. Open LD-4 as was done initially to resume limestone transport.

10. When the desired amount of limestone is in the bed, carefully close LD-4 to stop the limestone flow from the lower storage bin.
11. After waiting about 15 seconds to let the 3 inch line clear out, close the transport air control pressure regulator (by turning the knob counterclockwise until it feels loose - do not screw it completely out).
12. Close the upper CA-3 isolation valve, let the transport air control pressure go to zero, and then close the lower CA-3 isolation valve.

III. Mezzanine operations.

1. Close TA-1.
2. Close CA-1 if the system will not be operated further.

Coal Transport

Introduction

The coal transport process is used to pneumatically convey imitation coal into the limestone bed through a coal feeder. The imitation coal is metered by the live bin coal feeder into the 3 inch coal transport line. The transport air is supplied by the building compressed air system and is regulated by the transport air pressure regulator via the transport air control pressure regulator at the mezzanine control panel. Coal transport must only be performed while the limestone bed is being fluidized or when the bed is empty of limestone.

Procedure

I. First floor operations.

1. Close LF-1 and LF-5.
2. Open CT-1 and CT-2.
3. Check that the double flanged section at CTF-1/CTF-2 is installed.
4. Check that both CA-3 isolation valves are closed.

II. Mezzanine operations.

1. Check that TA-1 and the CA-2 isolation valves are closed.
2. Check that the tygon pressure lines from the transport air orifice are connected to the proper 30 inch manometer in the bank.

   Note: Normally the blower is not on during the preceding steps unless the bed has been filled with limestone while the blower is operating. However, the bed must be fluidized before the following steps are taken.
3. Set the FA-1 pressure regulator to achieve the desired blower flow rate (turn the knob clockwise to increase the flow, counterclockwise to decrease it). This blower flow rate must be added to the transport air flow rate to determine the total flow rate to the bed.
4. Open both CA-2 isolation valves.
5. Open the transport air control pressure regulator (by turning the knob clockwise) until the transport air control pressure matches the transport air pressure.

   Note: This is done to keep the transport air pressure regulator from bleeding when TA-1 is opened.

6. Open TA-1.

7. Open the transport air control pressure regulator until the desired flow rate is achieved as indicated by the differential pressure on the transport air orifice manometer. Note: This differential pressure must be greater than 9 inches of water to provide the approximate minimum transport velocity of 45 ft/sec for the imitation coal. A conservative setting of 20 inches of water is normally used (corresponds to a flow of 200 ft^3/min and a transport velocity of 70 ft/sec).

8. Flip the "Coal" Feeder switch to ON.

   Note: If the feed rate (and thus the speed) of the live bin coal feeder is to be changed, it must be done while the feeder is operating. The FAST or SLOW buttons on the "Coal" Feed Rate switch are depressed to change the feed rate as desired. NEVER operate the live bin coal feeder unless the transport air is on or the spout of the feeder is over an open container.

9. When the proper amount of time has elapsed, flip the "Coal" Feeder switch to OFF.

10. After allowing about 15 seconds for the coal transport line to clear, turn down the transport air flow (by turning the transport air control pressure regulator knob counterclockwise) until the transport air control pressure and the transport air pressure match.

11. Close TA-1.

12. Close the transport air control pressure regulator (by turning the knob counterclockwise until it feels loose - do not screw it out completely).

13. Close the upper CA-2 isolation valve, let the transport air control pressure go to zero, and then close the lower CA-2 isolation valve.

Bed Material Drain

Introduction

The bed material drain process is used to remove bed material following a limestone fluidization test (which may include coal feeding). The material is drained from the plexiglass bed test section to the upper storage bin through the 2 inch flexible drain line. Normally the bed is drained with the blower on as this keeps the bed material surface level while material is removed. The portable vacuum cleaner is used to assist the process by drawing a vacuum on the upper storage bin. It is possible to drain the bed without the blower being on, but in this case the material must be scooped to the 2 inch drain outlet or first collected in the vacuum cleaner and then dumped into the upper bin.

Procedure

I. Before the bed is fluidized.

   1. Check that LF-4, LD-1, LD-2, and LDF-1 are closed.

   2. Remove the 3 inch plug in the recycle line tee above the upper storage bin. Install the vacuum cleaner hose adapter in its place.

3. Connect the flexible vacuum cleaner hose to the adapter.

4. Plug the vacuum cleaner power cord into a remote outlet. Do not use a panel outlet as this will overload the circuit.

II. While the bed is fluidized (when draining is desired).

1. Open LD-1.

2. Flip the toggle switch on the vacuum cleaner to ON.

3. When the bed material has essentially quit draining turn the vacuum cleaner toggle switch to OFF.

III. After bed fluidization has been terminated.

1. If desired, finish cleaning out the bed as follows:

a. For below-the-bed feeders or the perforated plate, remove one of the two plywood side panels. Screw the short flexible hose into the inside of the 2 inch drain hole. Turn on the vacuum cleaner and clean out the bed with the hose. When cleaning is complete, turn off the vacuum cleaner, remove the vacuum cleaner hose from the adapter, remove the short flexible hose, and replace the plywood side panel.

b. For in-bed feeders, remove the 6 inch plexiglass plug on the east side of the bed. Use the vacuum cleaner hose and attachments to clean out the bed through the 6 inch port. When finished, turn off the vacuum cleaner, remove the motor head, and dump the tank contents into the upper storage bin through a funnel in the 3 inch recycle line tee. Replace the 6 inch plexiglass plug

2. Replace the 3 inch plug in the recycle line tee.

3. Periodically clean the vacuum cleaner filter and filter protector bag.

Separation-Recycle

Introduction

The separation-recycle process separates the imitation coal from the limestone following a coal feeding test. The mixed material is gravity fed from the upper storage bin into the magnetic separator from which limestone falls into the lower storage bin and imitation coal falls into the live bin coal feeder hopper. Tests have shown that acceptable separation of the imitation coal and limestone requires four passes of the material through the magnetic separator. Thus, the material is recycled from the lower storage bin back to the upper storage bin by pneumatic transport between the separation processes.

Procedure

I. Mezzanine operations.

   1. Check that both CA-2 isolation valves are closed.
   2. Open CA-1, TA-1, LD-1 and LF-4.
   3. Close LF-2 and LF-3.

II. First floor operations.

   1. Check that LD-4 and CT-1 are closed.
   2. Open LF-1, LF-5, LD-3, and LDF-2.
   3. Turn the magnetic separator on by pressing the START button on the electrical box mounted above the magnetic separator motor.

4. Open LD-2, the sliding gate valve, 0.5 inches. Gauge the opening with the marked metal strip lying under LD-2. Slide the gate valve slowly and carefully to prevent overshooting of the specified opening.

5. When all the material has drained out of the upper storage bin, open LD-2 slowly to approximately 8 inches. Then close LD-2 with short, jerking motions. These actions will remove the material resting on top of the gate valve. (Completion of material drainage from the upper storage bin will be apparent due to the lack of noise produced by the material in motion.)

6. Turn off the magnetic separator by pressing the STOP button on the electrical box.

7. Close LD-3 and LDF-2.

8. To recycle the material, follow "Limestone Transport" procedures II.3 - II.12. Note that the material is going into the upper storage bin rather than the bed.

9. Repeat the above Steps II.1 to II.8 three times. This is necessary to achieve sufficient separation of the limestone and imitation coal. After the fourth magnetic separation leave the limestone in the lower storage bin prior to being transported into the bed.

III. Mezzanine operations.

1. Close TA-1.

2. Close CA-1 if the system will not be operated further.

Strip Chart Recorder

Introduction

The Gould Brush 2400 four channel strip chart recorder can be used to record a wide variety of analog-type signals depending on the kind of amplifier modules utilized. In the present application it records three gauge pressures with bridge amplifier modules and one temperature with a thermocouple amplifier module. The pressure signals are monitored by diaphragm pressure transducers containing strain gauge circuits. The temperature signal is a millivolt current generated by an iron-constantan thermocouple.

The recording chart contains four strips or sections. Each sectional width contains 50 small blocks each 1 millimeter square and 10 large blocks each 5 millimeters square. The chart drive runs at a variety of speeds ranging from 0.05 millimeters/second to 200 millimeters/second. The 12 total speeds are attained by dividing each of the 6 basic speeds by a factor of 100.

Procedure

I. Preparation.

1. Plug the power cord of the unit into a panel outlet.
2. Connect the female plugs on the three amplifier cables (no.'s 1, 2, and 3) to the male plugs on the three pressure transducer cables using the numbered labels to match the corresponding sets of plugs.
3. Connect the male end of the thermocouple jack (wired into the thermocouple switch) with the female jack on the back of the thermocouple amplifier (no. 4).

4. Press the power button to turn the unit on.
5. Check the settings of the calibrate knobs to ascertain that they agree with the prior calibration settings. (See Section IV for calibration.) Also, check the vernier settings if the zero suppression function is to be used. At this point the volts switches must be off. (See Section V for zero suppression setting.)
6. Allow at least 5 minutes for the unit to warm up before proceeding with the following steps.
7. After making sure that the % load full scale or degrees full scale switches on the four amplifiers are off, press one of the chart speed buttions (0.05 mm/sec is recommended). Zero each chart pen to the right side of its chart section with the position knob above each chart.
8. For amplifier/transducer combinations 1, 2, and 3 in turn; disconnect the tygon tubing pressure line from the fitting at the end away from the pressure transducer, turn the % load full scale switch in steps from 500 to 20 and zero the pens as necessary with the balance knob, and reconnect the tygon tubing as it was initially (increase the chart speed to 1 or 2 mm/sec momentarily while zeroing the pens).
9. Set the appropriate % load full scale on each amplifier. For limestone fluidization tests, 100 or 50 is normally appropriate on amplifiers 1 and 2, while 20 is satisfactory for amplifier 3. For air tests, smaller values may be appropriate.

10. Turn the thermocouple amplifier (no. 4) to the 100 degrees full scale position. No further actions are necessary if the amplifier has been previously adjusted (as described in Section IV).

11. Turn on the timer if desired by flipping the toggle switch on the rear of the recorder. (Often the timer switch is left on at all times.) For the given chart speeds, a time interval of ten seconds has been set. A change in this interval requires an internal adjustment.

II. Operation.

1. Prior to starting a test, press the appropriate chart speed button. For normal pressure and temperature recording, 0.25 mm/sec is satisfactory.

2. The chart recorder is now in operation. The mark event buttons can be pressed to make small horizontal tic marks on either the left or right side of the chart paper. The right one is better because the left one conflicts with the timer tic marks. A felt tip pen can be used to write notes on the chart paper.

3. To record the frequency of pressure fluctuations, set the chart speed at 5 mm/sec for at least 5 seconds.

4. When a test is over, stop the strip chart recorder by pressing the stop button.

5. If another test is to be run, return to Step II.1 and proceed.

III. Termination.

1. Turn the three % load full scale switches and the degrees full scale switch to off.
2. Press the power button to turn the unit off.
3. Disconnect the three pressure transducer plugs and the thermocouple jack.
4. Unplug the power cord.
5. Cover the unit with the plastic dust protector.

IV. Calibration of the bridge amplifiers.

Note: The bridge amplifiers need only be calibrated once for a given set of pressure transducers. After the calibration is performed, the numerical readings on the calibrate knobs should be recorded so that they may be reset if necessary. The amplifiers are calibrated such that the strip charts can be read directly in inches of water. Therefore, a 60 inch water manometer is used in the calibration process. Repeat the following steps for each amplifier/ transducer set.

1. Install tygon tubing with a tee fitting between the bottom of the manometer and the pressure transducer. Make certain that the top of the manometer is open to atmosphere.
2. Prepare the strip chart recorder by performing Steps I.1 - I.8.
3. Make sure that the zero suppression volts switch is off.
4. Set the % load full scale switch to 50.

5. Use a rubber squeeze bulb or lung power to put a pressure slightly greater than 50 inches of water on the manometer and transducer. Pinch or fold the tubing to maintain the pressure.
6. Decrease the pressure to 50 inches of water.
7. Rotate the calibrate knob until the pen is at full scale.
8. Turn the % load full scale switch to 100 and then 200 and ascertain that the chart readings are correct.
9. Check the amplifier at intermediate pressures to verify linearity.
10. Lock the calibrate knob and record the setting.

V. Zero suppression of the bridge amplifiers.

Note: The zero suppression function is used to subtract out the static part of a pressure trace and then expand the dynamic part of the trace for better resolution. This is done essentially by moving the zero position off scale. The bridge amplifier must be calibrated (see IV) before zero suppression is set.

1. Prepare the strip chart recorder by performing Steps I.1 - I.8.
2. Turn the % load full scale switch to a position greater than the pressure to be suppressed.
3. Put the pressure to be suppressed on the transducer (such as is done in Steps IV.1 and IV.5).
4. Set the volts switch and turn the vernier knob to bring the chart pen to the right side of the chart. This point now has the value of the suppressed pressure. Lock the vernier knob and record the numerical reading.

4. Note: The plus (+) side of the volts switch moves the pen to the right, and the minus (-) side moves the pen to the left. The 0.1 position suppresses ten times the value suppressed by the 0.01 position.

5. Once set, the zero suppression function can be switched in or out with the volts switch as desired while the chart is running. The same value is suppressed on any of the % load full scale positions.

VI. Setting the thermocouple amplifier.

Note: The thermocouple amplifier (No. 4) is set to record Fahrenheit temperatures from 70 degrees to 170 degrees. Other ranges can be set by properly modifying the following steps.

1. Prepare the strip chart recorder by performing Steps 1.1 - 1.7 and prepare the digital thermocouple reader by performing Step 1.5 of the "Fluidization" procedure. Turn the thermocouple switch on the control panel to position 1.

2. The t.c. open light indicates (when on) that either the thermocouple jack is not plugged into the amplifier or there is an open circuit in the thermocouple or lead wires.

3. Turn the degrees switch to F (Fahrenheit).

4. Turn the sensitivity knob to the fully clockwise position. Note: Setting the sensitivity knob to other positions allows different values of degrees full scale than those given by the degrees full scale switch.

5. Turn the degrees full scale switch to 100 (corresponds to 100 Fahrenheit degrees full scale).

6. Turn the deg X 100 switch to +2.5 and set the vernier knob on 2.80. This zero suppresses the scale by 70 degrees. Lock the vernier knob.

   Note: The formula for the value to be zero suppressed is (deg X100) multiplied by (the vernier reading divided by 10). In this case, (2.5 X 100)(.280) = 70 degrees. The plus (+) side of the deg X 100 switch moves the pen to the right, while the minus (-) side moves the pen to the left.

7. Check the thermocouple amplifier settings by comparing readings on the strip chart to the digital thermocouple reader. Use a heat lamp to change the temperature on the thermocouple.

   Note: If desired, the zero suppression can also be set in this manner by heating the thermocouple to the temperature to be suppressed. Then bring the chart pen to the right side of the strip chart with the deg X 100 switch and the vernier knob. Lock the vernier knob.

8. No future adjustments to the thermocouple amplifier are necessary unless this setting is to be changed.

General Note: For further information on the Gould Brush 2400 strip chart recorder or its amplifiers consult the following Gould Operating and Service Manuals.

1. "2400 Series Recorders - All Models"
2. "D.C. Bridge Preamplifier - Model 13 4615 30"
3. "Thermocouple Amplifier - Model 13 4615 4X"

Scanivalve System

Introduction

The Scanivalve System is a microprocessor which controls a scanivalve connected to a pressure transducer and a teletype. The scanivalve is a mechanism containing 48 pressure ports which can be scanned consecutively. The pressure at each port is "read" by the pressure transducer and the resulting signal is interpreted by the microprocessor and printed by the teletype. Only one pressure transducer can be installed for use at a given time, but the three available transducers have ranges of -1 to + 1 lbf/in^2 gage, - 10 to + 10 lbf/in^2 gage, and - 14.7 to + 100 lbf/in^2 gage respectively. A differential pressure can be measured by utilizing the center tap of the scanivalve, but this dictates that the center tap be the reference pressure for all 48 ports. Thus, if more than one differential pressure is needed, the center tap should be left open to atmosphere for the reference, and each pressure measured will be a gage pressure. Thus the resulting gage pressures can be algebraically added to determine the pressure differential.

The scanivalve operating program for the microprocessor can be loaded manually from the keyboard or from paper tape, the latter method being easier and quicker. Once loaded, the program will be retained in memory as long as there is electrical power to the unit. If a power interruption occurs, however, the program must be reloaded; a process that requires approximately 2 minutes using the tape.

Procedure

I. Loading the scanivalve operating program from tape.

1. Ensure that the power cord is plugged into an outlet.

2. Flip the toggle switch on the right side to ON.

3. Turn the teletype knob (located on the lower right front corner of the keyboard) to LINE.

4. Depress the ODT button (located on the right side).

   Note: Whenever the ODT button is depressed, the contents of six storage registers will be printed. These can be ignored.

5. Press the B key.

6. Manually load and start the paper tape at the teletype tape reader (lower left hand corner) by inserting the tape in the direction of the arrow on the plastic hatch, closing this hatch, and flipping the tape reader switch to START.

7. Each "page" of the program is entered separately, so when the tape stops press the B key again until all the program is read in (requires three additional presses of the B key).

8. When the tape stops a few inches from the end, flip the tape reader switch to STOP.

9. Open the plastic cover and remove the tape.

II. Initializing the scanivalve operating program.

Note: If the tape was just read in, the scanivalve is ready to respond to keyboard inputs. This condition can be ascertained by noting that the small red light above the HALT and ODT buttons is on. However, following a depression of HALT button, the scanivalve will not respond to keyboard inputs and the light is off. In this latter case, to start the program, depress the ODT button (the contents of the six registers will be printed).

1. The type of transducer being used must be entered. Type 5S, the teletype will line-feed (LF) and carriage-return (CR), and then type 317/. The teletype will print a three digit number, which is the value currently stored in memory location 317. Immediately after this number, type the three digit number corresponding to the transducer being used and then press CR:

Transducer	Number
1 lbf/in^2 gage	001
10 lbf/in^2 gage	002
100 lbf/in^2 gage	003

Note: Once entered, this information need not be reentered unless the power has been off or another type of transducer has been installed. (The default value is 002.)

2. A repeat (R) command is available which causes the microprocessor to continuously repeat the previously executed command. (See III.3 for a description of the available commands.) If this command is to be used, a time interval

must be entered into the microprocessor. This time interval is the amount of time between the completion of a command and the initiation of the next repeat of this command. It is not the time required for a repeat cycle (i.e., the time from the start of a command to the start of the repeat of the command). Thus if each repeat cycle is to have a fixed length of say, 30 seconds, the time interval to be entered is 30 seconds minus the time required to scan the 48 ports and type the requested pressures. This latter time is best determined by clocking the actual operation. The time interval must be entered in octal form (base eight) and must consist of three digits (leading zeroes are used if necessary). This time interval is stored in two locations, with the value in the first location (004) being simply a multiplier of the value in the second location (006). Thus, to store whole minutes, enter the octal equivalent of the number of minutes in the first location and enter 60 seconds (074 in octal) in the second location. To store minutes and seconds or seconds only, enter an appropriate multiplier in the first location (often this is 001), and then enter the number of seconds or seconds to be multiplied in the second location. Thus, to enter a time interval, type 7S, the teletype will LF-CR, type 004/, three digits will be typed, type three digits representing the number of whole minutes or the multiplier in octal form, CR, type 006/, three digits will be typed, type three digits representing the number of seconds or the value to be multiplied in octal form, and CR. The three digits printed by the teletype following each slash (/) were the values stored in the registers. They can be followed by a CR if no change is to be made.

Note: As with the transducer type number, this time interval will be stored until the power to the microprocessor is turned off or another time interval is entered. (The default value is one minute.)

III. Running the scanivalve operating program.

Note: If the power to the microprocessor has not been off since the initialization in part II was performed, this is the normal starting point for a scanivalve operation.

1. If the teletype knob is at OFF or LOCAL, turn it to LINE.

   Note: Turning this knob to LINE, OFF, or LOCAL does not affect the storage of the scanivalve operating program in the microprocessor. It only affects the teletype. In the LINE mode the teletype is connected to the microprocessor, while in the LOCAL mode it is not.

2. If the red light is not on, depress the ODT button and the contents of the six storage registers will be printed. When the light is on, type 7S, the teletype will LF-CR, and then type 127G. The dash (-) indicates that the microprocessor is ready for a command.

3. The available commands are:

a. \$ -- \$ After typing the first \$, a heading or message of any length can be typed. Typing the second \$ causes the microprocessor to respond with a dash in anticipation of another command.

b. # The scanivalve prints all port pressures from 01 to 48.

c. Caa,bb(CR) The scanivalve prints all port pressures from aa to bb where aa and bb are two digit numbers ranging from 01 to 48.

d. Saa,bb,..(CR) The scanivalve prints all port pressures aa, bb, ... discretely where aa, bb, ... are two digit numbers ranging from 01 to 48.

e. I The scanivalve increments to the next port and prints the pressure at that port.

f. H The scanivalve homes to port 48 but no pressures are printed.

g. R The scanivalve will continuously repeat the previously executed command. The repeat cycles are separated by the time interval stored in 11.3.

4. When the pressure scanning and recording are finished:

a. If the repeat (R) command was used, the HALT button must be depressed to stop the execution of the command.

4. b. If the repeat (R) command was not used, it is possible to leave the system waiting for another command (i.e. the last character printed was a dash). However, if desired, the HALT button may be depressed.

5. Turn the teletype knob to OFF.

6. Normally, the toggle switch is left in the ON position so that the scanivalve operating program will be retained in memory. However, if the scanivalve system will not be used for several days, the power should be turned off.

General Note: Further instructions and explanations of this system are contained in the "Scanivalve Operating Program (SVOP)" booklet. This booklet includes information on calibration, programming the microprocessor, and other items not necessary for the normal operation of the scanivalve system.

APPENDIX B

PERFORATED PLATE DESIGN

A perforated plate, or multiorifice plate, is an air distributor consisting of a pattern of holes in a metal plate. This type of distributor has been used extensively in fluidized beds due to its low cost and simple fabrication requirements. However, the design of perforated plates still remains an art as well as a science.

Several references to perforated plate design exist in the literature, a few of which will be mentioned. Kunii and Levenspiel [51, pp. 86-90, 463] propose a simplified design procedure which they claim gives results very similar to those from more rigorous design procedures. An example using the simplified design procedure is included as well as some experimental distributor performance data from operating units. Davidson et al. [112, pp. 638-644] propose a more sophisticated design method, but they utilize bed operational parameters which are difficult to determine a priori. However, they do include some experimental data which support their method. Pope, Evans and Robbins [20, pp. 63-79] performed tests with a distributor plate containing nozzles and then generalized their results to apply to any distributor containing orifices. Similarly, Babcock and Wilcox [68, pp. 3-57 - 3-61] extrapolated results from bubble cap air distributor tests to construct correlations for perforated plate design. Khan et al. [10, pp. 2.1.3-1 - 2.1.3-31] provide a good summary of several types of distributor design procedures. They include the work by the Institute of Gas Technology, which contains an extensive distributor design procedure and an example illustrating this procedure.

The purpose of the perforated plate in this project has been to serve as a basic air distributor for the test facility to provide fluidization results which could be compared with those of the coal feeders tested. Thus, because the perforated plate was to be only a minor part of the total coal feeder evaluation project, it was designed in a somewhat simplistic manner. The decision to use a simple design method was influenced by the fact that the design methods referred to previously do not give consistent results.

A perforated plate can be treated as a matrix of parallel orifices with the total flow divided equally among the orifices. The discharge equation for a single orifice is

$$q = KA\left(\frac{2\Delta P}{\rho g_c}\right)^{1/2} . \tag{B.1}$$

For n holes of diameter d, the total flow is

$$Q = \frac{K n\pi d^2}{4}\left(\frac{2\Delta P}{\rho g_c}\right)^{1/2} . \tag{B.2}$$

Thus, the number of holes required to produce a given pressure drop in terms of the hole diameter is

$$n = \frac{4Q}{K\pi d^2}\left(\frac{\rho g_c}{2\Delta P}\right)^{1/2} . \tag{B.3}$$

To solve Equation (B.3), the total air flow, air density, perforated plate pressure drop, individual hole diameter, and orifice flow coefficient must be specified. The basic design parameters chosen for the fluidized bed test facility were a nominal bed flow of 1800 ft^3/min

at a blower outlet pressure of 3.5 lbf/in^2 gage. This bed flow is equivalent to a superficial velocity of 7.5 ft/sec. For calculational purposes, an air density of 0.073 lbm/ft^3 is assumed.

Most of the previously mentioned references recommend that the air distributor pressure drop be 10 to 30 percent of the bed pressure drop and that it fall in the range of 4 to 20 inches of water. For the originally planned slumped bed height of 34 inches, the bed pressure drop would be approximately 50 inches of water. Thirty percent of this value is 15 inches of water, which falls into the specified range. The actual design pressure drop chosen was 16 inches of water so that for a 2:1 velocity turndown ratio, the distributor pressure drop would be 4 inches of water. This design pressure drop of 16 inches of water is the same value used by Pope, Evans, and Robbins [20, pp. 73-74] and Combustion Engineering [15, p. 21] in their perforated plate designs.

The individual hole diameter is a function of the limestone particle size range used and the size of the air jets to be generated. The limestone particle size distribution, shown in Table 6.1 on page 90, restricts the maximum hole diameter to approximately 0.11 inches to prevent excessive limestone drainage through the perforated plate when the bed is slumped. The hole diameter choice dictates the number of holes which will be required to produce a specified pressure drop. The resulting spacing between the holes is important from the aspect of jet penetration theory [102, 103, 104]. According to this theory, if the holes are too closely spaced, then the bubbles formed by the emerging air jets will coalesce prematurely into large slugs, or pockets, of air.

The choice of the orifice flow coefficient is the least well-defined step in the design procedure. Certainly, a matrix of holes in a flat plate would be expected to behave somewhat differently from a group of individual parallel pipes containing orifices. Also, the holes themselves are not true sharp-edged orifices because their length dimension, discussed later, is greater than their diameter. Somewhat arbitrarily, a flow coefficient of 0.61 was chosen. Intuitively, it was believed that the perforated plate would produce an even greater pressure drop than the orifice analogy predicted. Thus, in addition to choosing a relatively small flow coefficient, a countersink for each hole was incorporated into the design in an attempt to further reduce the pressure drop across the perforated plate.

Several hole diameters were substituted into Equation (B.3) to determine the number of holes and thus the hole spacings required. Primarily due to the number of holes to be drilled and the limestone particle size range, a hole diameter of 0.1094 inches was selected. From Equation (B.3) the number of holes required for this diameter is 2790. The closest number of holes needed to produce a square pattern is 2809. With these holes in a 53 by 53 matrix, the hole center-to-center spacing is 0.453 inches. Preliminary estimates using the jet penetration theory equations indicated that a hole spacing of approximately 2 inches should be used for the flow conditions under consideration. However, this latter spacing seems unreasonably large for the small hole size, so the spacing of 0.453 inches was used.

Aluminum was chosen as the plate material because it would be easier to drill the holes in aluminum than in steel. Although some information exists concerning the structural strength of perforated plates [113, 114, 115], the calculations appear to be rather complicated. Thus, approximate calculations were made using plate theory equations by treating the perforated plate as a solid square plate with clamped edges. The assumption of a solid plate is reasonable in this case because the area factor (ratio of hole area to plate area) of 0.046 is small. For a 0.25 inch thick aluminum plate with a limestone loading of 1200 pounds, the maximum deflection is 0.06 inches at the center, and the maximum bending stress is approximately 6000 lbf/in^2. The deflection is within the acceptable limit, and the stress is well below the maximum allowable stress for the 2024-T351 material used.

APPENDIX C

BELL MOUTH INLET VOLUMETRIC FLOW RATE EQUATION

Wilkerson [92] showed that the mass flow rate through a bell mouth inlet can be determined from the ambient conditions and from the static pressure at the bell mouth throat. The derivation of the appropriate equations is based on compressible flow principles. After the mass flow rate has been determined, the volumetric flow rate can be easily obtained by applying the continuity equation.

Consider the bell mouth inlet shown in Figure C.1 where the ambient conditions are denoted by the subscript ∞ and the throat conditions by the subscript 1. In the derivation, static conditions

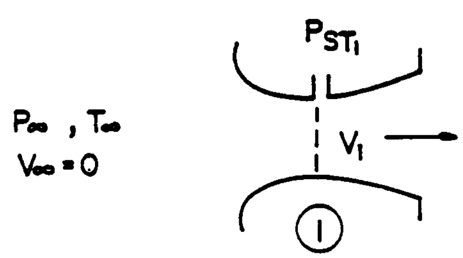

Figure C.1. Bell Mouth Inlet Parameters.

will be denoted by the subscript st, and total conditions will be denoted by the subscript t.

From the one dimensional continuity equation for steady flow, the mass flow rate through the throat can be expressed as

$$\dot{m}_1 = \rho_1 Q_1 = \rho_1 A_1 V_1 \ . \tag{C.1}$$

The density at the throat is given by the ideal gas equation in terms of static conditions as

$$\rho_1 = \frac{P_{st_1}}{R\,T_{st_1}} \ . \tag{C.2}$$

From compressible flow theory the Mach number at the throat is defined in terms of static conditions as

$$M_1 = \frac{V_1}{c} = \frac{V_1}{(k\,g_c\,R\,T_{st_1})^{1/2}} \ . \tag{C.3}$$

Equations (C.1), (C.2), and (C.3) can be combined to express the mass flow rate through the throat as

$$\dot{m}_1 = P_{st_1} A_1 M_1 \left(\frac{kg_c}{R\,T_{st_1}}\right)^{1/2} = \frac{P_{st_1} A_1}{T_{t_1}^{\ 1/2}} M_1 \left(\frac{kg_c}{R}\,\frac{T_{t_1}}{T_{st_1}}\right)^{1/2} \ . \tag{C.4}$$

From the thermodynamics of compressible flow, for isentropic flow along a streamline the pressure and temperature are related in terms of static and total conditions by

$$\frac{T_{t_1}}{T_{st_1}} = \left(\frac{P_{t_1}}{P_{st_1}}\right)^{(k-1)/k} . \tag{C.5}$$

In addition, the total pressure in compressible flow is defined as

$$P_{t_1} = P_{st_1}\left(1 + \frac{k-1}{2} M_1{}^2\right)^{k/(k-1)} . \tag{C.6}$$

By substituting Equations (C.5) and (C.6) into Equation (C.4), the mass flow rate can now be expressed as

$$\dot{m}_1 = A_1 P_{t_1}\left\{\frac{2g_c}{RT_{t_1}}\left(\frac{k}{k-1}\right)\left[\left(\frac{P_{st_1}}{P_{t_1}}\right)^{2/k} - \left(\frac{P_{st_1}}{P_{t_1}}\right)^{(k+1)/k}\right]\right\}^{1/2} . \tag{C.7}$$

For a bell mouth inlet, the total temperature at the throat is equal to the ambient temperature, i.e., $T_{t_1} = T_\infty$, and the total pressure at the throat is only very slightly less than the ambient pressure so equality can be assumed, i.e., $P_{t_1} = P_\infty$. Also, for steady flow the mass flow rate is a constant, i.e., $\dot{m}_1 = \dot{m}$. Making these substitutions into Equation (C.7) gives

$$\dot{m} = \frac{A_1 P_\infty}{T_\infty{}^{1/2}}\left\{\left(\frac{2g_c k}{R(k-1)}\right)\left(\frac{P_{st_1}}{P_\infty}\right)^{2/k}\left[1 - \left(\frac{P_{st_1}}{P_\infty}\right)^{(k-1)/k}\right]\right\}^{1/2} . \tag{C.8}$$

By measuring the bell mouth throat static pressure relative to the ambient pressure with a manometer, the manometer deflection can be expressed as

$$s = P_\infty - P_{st_1} \tag{C.9}$$

from which

$$\frac{P_{st_1}}{P_\infty} = \frac{P_\infty - s}{P_\infty} = 1 - \frac{s}{P_\infty} \ . \tag{C.10}$$

Thus, the mass flow becomes from Equations (C.8) and (C.10)

$$\dot{m} = \frac{A_1 P_\infty}{T_\infty^{\ 1/2}} \left(1 - \frac{s}{P_\infty}\right)^{1/k} \left\{ \left(\frac{2g_c k}{R(k-1)}\right) \left[1 - \left(1 - \frac{s}{P_\infty}\right)^{(k-1)/k}\right] \right\}^{1/2} \ . \tag{C.11}$$

From Equations (C.1) and (C.2) the volumetric flow rate can be expressed in terms of the mass flow rate as

$$Q_\infty = \frac{\dot{m}}{\rho_\infty} = \frac{\dot{m}\, R\, T_\infty}{P_\infty} \ . \tag{C.12}$$

Therefore, by substituting Equation (C.11) into Equation (C.12), the volumetric flow rate becomes

$$Q_\infty = A_1 \left(1 - \frac{s}{P_\infty}\right)^{1/k} \left\{ \left(\frac{2g_c k\, R\, T_\infty}{k-1}\right) \left[1 - \left(1 - \frac{s}{P_\infty}\right)^{(k-1)/k}\right] \right\}^{1/2} \ . \tag{C.13}$$

Substituting in values of k and R for air, g_c, and the throat area of the bell mouth inlet (15.3 in^2), the volumetric flow rate in ft^3/min for T_∞ in degrees Rankine and P_∞ and s in consistent units becomes

$$Q_\infty = 698.73 \left(1 - \frac{s}{P_\infty}\right)^{.714} \left\{ T_\infty \left[1 - \left(1 - \frac{s}{P_\infty}\right)^{.286}\right] \right\}^{.5} \ . \tag{C.14}$$

APPENDIX D

EXPERIMENTAL UNCERTAINTY ANALYSIS

The uncertainty analysis method proposed by Kline and McClintock [116], which is further described and illustrated by Holman [117], has been used to calculate second order uncertainties in the experimentally determined quantities in this thesis. This method is applicable when the calculated result C is a known function of the independent variables a_1, a_2, a_3, ..., a_n such that

$$C = C(a_1,\ a_2,\ a_3,\ \ldots,\ a_n)\ . \tag{D.1}$$

Suppose w_c is the uncertainty in the result and w_1, w_2, ..., w_n are the uncertainties in the experimentally determined independent variables. Then the second order uncertainty in the calculated result is

$$w_c = \left[\left(\frac{\partial C}{\partial a_1} w_1\right)^2 + \left(\frac{\partial C}{\partial a_2} w_2\right)^2 + \ldots + \left(\frac{\partial C}{\partial a_n} w_n\right)^2\right]^{1/2} . \tag{D.2}$$

The experimental measurements which were performed during the reported tests are summarized in Table D.1. The instruments used for these measurements are listed along with the instrument measurement range and the instrument least count as determined by the scale on which the measurements were observed. The table only includes measurements which were used in the calculation of pertinent experimental results and thus excludes such measurements as the blower amperage and differential pressure and the two phase pressure measurement system flow and pressure.

The uncertainties in the experimentally determined variables employed in the analysis were based on the instrument least counts,

TABLE D.1

EXPERIMENTAL MEASUREMENTS

Measurement	Instrument		
	Identification	Range	Least Count
Fluidization air orifice ΔP	Water manometer, scv[1]	0-30 in. of water	0.1 in. of water
Transport air orifice ΔP	Water manometer, scv	0-30 in. of water	0.1 in. of water
Temperatures - fluidization and transport air inlet, bed freeboard air	Iron-constantan thermocouples, Omega Model J2165A T/C Reader, S/N 590018	Variable	1°F
Ambient air pressure	Mercury barometer	25.5-32.7 in. of Hg	0.01 in. of Hg
Pressures - plenum box, lower bed, upper bed	Statham Labs Transducers Model P6-5, 2D-350, S/N's 3233, 3765, 3772; Brush 2400 Strip Chart Recorder Model 2007-4404-00, S/N 00357, scv	Recorder: 0-5, 10, 20, 50, 100, or 200 in. of water	0.1, 0.2, 0.4, 1.0, 2.0, or 4.0 in. of water
Coal feed rate	Tachometer, Reliance Electric Co., S/N GE-18829	0-155 rev/min	5 rev/min
Coal or limestone weight	Ainsworth Electronic Balance Model A-4, S/N 57917	0-160 grams	0.0001 grams

[1] The scanivalve system was also used to record the pressure(s).

repeatability test data when available, and calibration data when available. The basic uncertainties utilized, which are believed to be conservative, were 0.2 inches of water for water manometer readings, 1 degree Rankine for inlet air temperatures, 0.02 inches of mercury for the ambient air pressure, and 0.4 to 2.0 inches of water for system air pressures depending on the strip chart recorder scale used.

The bed average superficial velocity is the parameter used to categorize fluidized bed data. Thus, uncertainty analyses were performed at average superficial velocities of 3.6 and 8.3 ft/sec. These average superficial velocities represent bed air flow rates of 860 and 1990 ft^3/min, respectively, which are termed reduced flow and full flow. Because the transport air flow rate utilized in the tests was approximately 200 ft^3/min, the respective fluidization air flow rates were 660 and 1790 ft^3/min.

The fluidization air inlet flow rate is measured with the 6 inch orifice and a water manometer. This orifice was calibrated by the use of a bell mouth inlet device using

$$Q_\infty = A_1\left(1 - \frac{s}{P_\infty}\right)^{1/k} \left\{\left(\frac{2g_c k R T_\infty}{k-1}\right) \left[1 - \left(1 - \frac{s}{P_\infty}\right)^{(k-1)/k}\right]\right\}^{1/2} , \qquad (D.3)$$

which is developed in Appendix C. Based on a throat area uncertainty of 0.25 in^2, the uncertainty in the fluidization air inlet flow is 4.6% (30.4 ft^3/min) at reduced flow and 1.7% (30.8 ft^3/min) at full flow. The magnitude of uncertainty incurred in reading flow rates from the resulting calibration curve is significantly less than the uncertainty of the flow rates themselves.

The transport air inlet flow rate is measured with the 3 inch orifice and a water manometer. This orifice was designed according to ASME standards as described by Henry [91], but it was not calibrated. Rather, the flow rate is calculated from

$$Q = KA \left(2g \, \Delta s \; \frac{\rho_w R_a T_a}{P_a} \right)^{1/2} , \qquad (D.4)$$

which is developed in Appendix E. A relatively large uncertainty of 0.05 was used for the orifice flow coefficient, while the area uncertainty used was 0.006 in^2 and the water density uncertainty was 0.2 lbm/ft^3. The resulting transport air inlet flow rate uncertainty at 200 ft^3/min is 7.7% (15.4 ft^3/min).

Both the fluidization and transport air inlet flow rates must be corrected to the bed conditions due to the pressure and temperature changes which occur. The appropriate relation is

$$Q_b = Q_i \left(\frac{T_b}{T_i} \right) \left(\frac{P_i}{P_b} \right) . \qquad (D.5)$$

The bed temperature uncertainty used was 2.5°R and the bed pressure uncertainty used was 0.014 lbf/in^2 (corresponds to 0.4 inches of water). For both reduced and full fluidization air flow rates and for the transport air flow rate, the increase in uncertainty due to the pressure and temperature changes is less than 0.1%. Thus, when the fluidization and transport air flow rates are combined as corrected bed air flow, the reduced flow uncertainty is 5.4% (46.1 ft^3/min) and the full flow uncertainty is 2.4% (47.5 ft^3/min).

The bed average superficial velocity is calculated from the bed flow rate and the bed area using

$$V_{sf} = \frac{Q_b}{L^2} \; . \qquad (D.6)$$

An uncertainty of 0.125 inches was used for the measurement of the inside bed dimension. In average superficial velocity determinations for test conditions not utilizing transport air, at reduced flow (2.75 ft/sec) the uncertainty is 4.75% (0.13 ft/sec) and at full flow (7.5 ft/sec) it is 2.1% (0.16 ft/sec). In average superficial velocity determinations for test conditions utilizing transport air, the uncertainty at reduced flow (3.6 ft/sec) is 5.5% (0.20 ft/sec) and at full flow (8.3 ft/sec) it is 2.6% (0.22 ft/sec).

The uncertainty in the volumetric live bin coal feeder calibration curve was determined from the calibration test results. The least count of the screw conveyor tachometer was used to determine the rotational speed uncertainty of 2.5 rev/min. Repeatability tests indicated a feed rate uncertainty of 0.25 lbm/sec at low feed rates (20 rev/min) and an uncertainty of 0.5 lbm/sec at high feed rates (80 rev/min).

The uncertainties in the limestone and imitation coal weights from bed material samples were discussed in Chapter 6. Because no calculations were performed on these measurements, the uncertainty analysis of this appendix is not applicable.

The experimental data graphs in this thesis contain the uncertainty bands which have been calculated. These uncertainty bands are not significantly larger than the plotting symbols employed except in the case of the transport air flow rate.

These calculated uncertainties are to be applied to average measurements and not discrete measurements. For example, at full flow conditions utilizing transport air, local superficial velocities in the bed freeboard region might vary by as much as 1 ft/sec at a given time. However, the experimentally determined superficial velocity is believed to be the average value of these local velocities within an uncertainty of ± 0.22 ft/sec.

APPENDIX E

TRANSPORT AIR VOLUMETRIC FLOW RATE EQUATION

The transport air flow is measured with an orifice, designed and constructed by recommended procedures, which is located in the 3 inch supply line and connected to a water manometer. The manometer and orifice equations are used to derive an equation relating the manometer deflection and the transport air flow.

A schematic of the orifice and manometer configuration is shown in Figure E.1. Letting the subscript a represent air and w represent

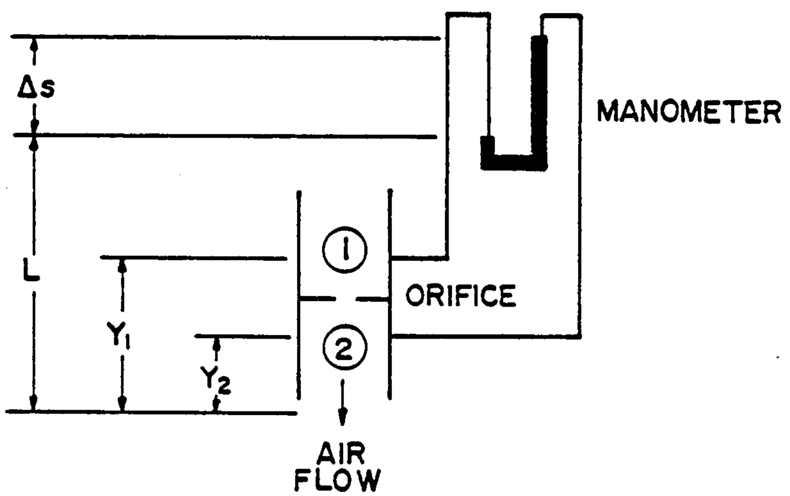

Figure E.1. Transport Air Orifice and Manometer Configuration.

water, the manometer equation written from point 1 to point 2 is

$$P_1 - (L - y_1 + \Delta s)\ \gamma_a + \Delta s\ \gamma_a - \Delta s\ \gamma_w + (L - y_2 + \Delta s)\ \gamma_a = P_2\ . \qquad (E.1)$$

This equation can be rearranged to give

$$\left(\frac{P_1}{\gamma_a} + y_1\right) - \left(\frac{P_2}{\gamma_a} + y_2\right) = \Delta s\left(\frac{\gamma_w}{\gamma_a} - 1\right)\ . \qquad (E.2)$$

The two terms on the left are the piezometric head, Δh, so

$$\Delta h_a = \Delta s\left(\frac{\gamma_w}{\gamma_a} - 1\right)\ . \qquad (E.3)$$

The flow through an orifice in terms of the piezometric head is given by the orifice equation,

$$Q = KA\ (2g\,\Delta h)^{1/2}\ . \qquad (E.4)$$

Substituting Equation (E.3) into Equation (E.4) gives

$$Q = KA\left[2g\,\Delta s\left(\frac{\gamma_w}{\gamma_a} - 1\right)\right]^{1/2}\ . \qquad (E.5)$$

Using the ideal gas equation,

$$\rho_a = \frac{P_a}{R_a T_a}\ , \qquad (E.6)$$

and the definition of fluid specific weight ($\gamma = \rho g$), Equation (E.5) can be written as

$$Q = KA\left[2g\,\Delta s\left(\frac{\rho_w R_a T_a}{P_a} - 1\right)\right]^{1/2} . \tag{E.7}$$

The orifice was designed with a diameter ratio of 0.6 so that for the range of air flows to be measured the orifice flow coefficient would be an essentially constant value of 0.65. Substituting the known quantities (orifice hole diameter is 1.8 inches and 85°F is a reasonable average water temperature) into Equation (E.7) gives the flow in ft^3/min as

$$Q = \left[\Delta s\left(58.7\,\frac{T_a}{P_a} - 2.5\right)\right]^{1/2} , \tag{E.8}$$

for Δs in inches, T_a in degrees Rankine, and P_a in lbf/in^2 absolute. The 2.5 term in this expression can be neglected as its contribution to the flow calculated is less than 0.1 percent. This term follows from the -1 term of Equation (E.3) which is negligible in this case because $\gamma_w >> \gamma_a$. Thus, the transport air flow measurement equation becomes

$$Q = 7.66\left(\frac{T_a\,\Delta s}{P_a}\right)^{1/2} \tag{E.9}$$

for the units specified for Equation (E.8).

APPENDIX F

PRESENTATION OF COAL FEEDING TEST RESULTS

The terms used in the presentation of coal feeding results in the various tables in this thesis are described herein. Each of these terms refers to a specific "CFD Parameter" or Coal Feeding Distribution Parameter.

The "Compartment" letters identify the three sample collection spaces in each coal sample probe. The "Port" refers to the number of the sample port into which a coal sample probe was inserted for the test. The location of the compartments and ports are shown in Figure 7.9 on page 147.

The measurements resulting from a coal feeding test are the weights in grams of the limestone and imitation coal (IC) in each of the coal sample probe compartments. The "% IC" is simply the percent of imitation coal by weight in the total sample (includes the limestone and the imitation coal) from a single compartment.

The "Prb Avg % IC" is the average of the imitation coal percentages for the three compartments of a single coal sample probe. The "% IC/Prb Avg % IC" is the percent variation between the probe average imitation coal percentage and a compartment imitation coal percentage, using the probe average as the base. The total variation in these last quantities for a single sample probe is referred to as the "Range of % Variation."

The "Tst Avg % IC" is the average of the imitation coal percentages for the six compartments of both coal sample probes in a test. The "% IC/Tst Avg % IC" is the percent variation between the test average imitation coal percentage and a compartment imitation coal percentage, using the test average as the base.

The calculation results just explained are used to compare the compartmental imitation coal percentages from a single test. They are used primarily to establish the variation between the six individual samples from the two coal sample probes. However, as discussed in Chapter 6, the coal feeding results from any one test must not be overemphasized. Rather, several tests of the same feeder and bed configuration must be compared for meaningful conclusions to be drawn. The "% IC/Tst Avg % IC" parameters of several tests can be compared to determine if certain regions of the bed typically contain more or less imitation coal. The comparison of the actual imitation coal percentages of one coal feeding test with those of another normally does not lead to valid conclusions. First, the background imitation coal percentage varies somewhat from test to test. This variation occurs because more of the bed material is drained after some tests than after others and also because the amount of bed material mixing allowed before initiating coal feeding and sampling varies from test to test. Second, tests with differing slumped bed heights have different average imitation coal percentages within the bed following a coal feeding test.

APPENDIX G

PIPE MANIFOLD FLOW THEORY AND CALCULATIONS

A theoretical equation to predict the hole diameters necessary to insure uniform discharge from holes in a pipe containing a fluid flowing along the axis can be derived in a manner similar to the method used by Van Der Hegge Zijnen [111]. This method assumes the quantities initially known are the pipe diameter and length, the number of holes and their spacing, the pipe inlet fluid pressure and velocity, and the pressure exterior to the pipe. These parameters are illustrated in Figure G.1.

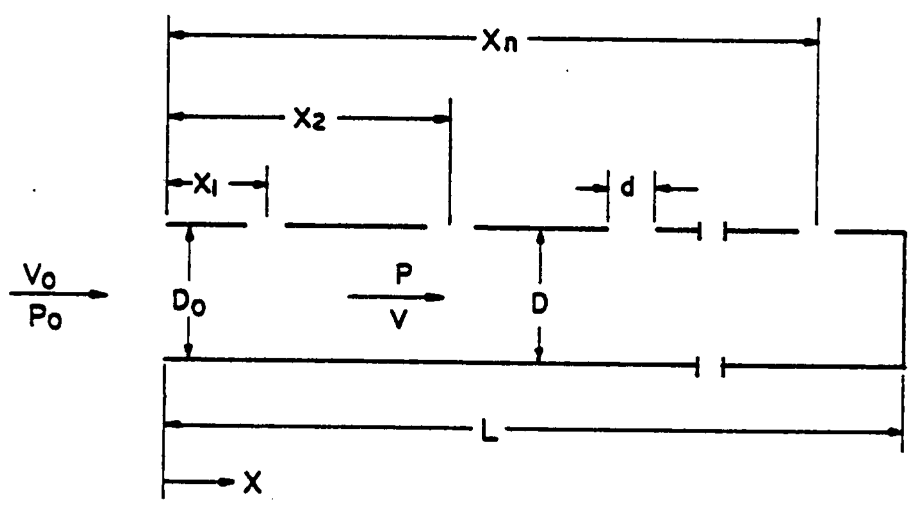

Figure G.1. Pipe Manifold Parameters.

The rate of pressure change in the flow direction can be expressed as

$$dP = - \frac{d(b\,\rho\,V^2)}{2g_c} - f\,\frac{dx}{D}\,\frac{\rho\,V^2}{2g_c} \; . \tag{G.1}$$

The first term on the right corresponds to the effect on the pressure of the fluid deceleration in the pipe due to the decreasing fluid mass resulting from fluid discharge through subsequent holes. This Bernoulli-type term is negative because a pressure increase corresponds to a velocity decrease. The variable b is the pressure recovery factor, which has a value less than one. The second term corresponds to the effect of the pipe friction of the fluid on the pressure. This term is also negative because friction causes a pressure decrease in the flow direction. The above equation can be rearranged to give

$$\frac{d}{dx}\left(P + \frac{b\,\rho\,V^2}{2g_c}\right) = -f\,\frac{1}{D}\,\frac{\rho\,V^2}{2g_c} \; . \tag{G.2}$$

For turbulent flow in smooth pipes, the pipe friction can be expressed in terms of the Reynolds number as

$$f = \frac{.316}{Re^{1/4}} \qquad \text{for} \qquad 4000 < Re < 100000. \tag{G.3}$$

Assuming a uniform discharge along the pipe (which actually treats the pipe as having a continuous slot--probably a reasonable assumption for many closely spaced holes), the local fluid velocity can be expressed as

$$V = V_o\;(1 - \frac{x}{L}) \; , \tag{G.4}$$

and the velocity gradient becomes

$$\frac{dV}{dx} = - \frac{V_o}{L} . \tag{G.5}$$

Recalling that the Reynolds number is defined as

$$Re = \frac{VD}{\nu} , \tag{G.6}$$

Equations (G.3), (G.4), and (G.5) can be substituted into Equation (G.2) to give, after some manipulations,

$$\frac{dP}{dx} = \frac{\rho V_o^2}{2g_c} \left[\frac{2b}{L} \ (1 - \frac{x}{L}) - .316 \ Re_o^{-1/4} \ \frac{1}{D} \ (1 - \frac{x}{L})^{7/4} \right] . \tag{G.7}$$

Integrating this equation along the pipe length and using the boundary condition that the pressure is P_o at the pipe entrance location x_o yields

$$P = P_o + \frac{\rho V_o^2}{2g_c} \left\{ \frac{2bx}{L} \ (1 - \frac{x}{2L}) + .115 \ Re_o^{-1/4} \ \frac{L}{D} \left[(1 - \frac{x}{L})^{11/4} - 1 \right] \right\} . \tag{G.8}$$

Van Der Hegge Zijnen [111] uses an exponent of 5/4 rather than 11/4; apparently a typographical error. With P and P_o as gage pressures, if the pressure exterior to the pipe is taken to be atmospheric, then P actually represents the differential pressure across an orifice at location x (commonly denoted ΔP).

The discharge from each hole in the pipe is given by the orifice equation

$$q = KA \left(\frac{2\Delta P}{\rho g_c} \right)^{1/2} . \tag{G.9}$$

For inlet flow Q_o in a pipe with uniform discharge through n holes of diameter d, this equation becomes

$$\frac{Q_o}{n} = \frac{K\pi d^2}{4}\left(\frac{2\Delta P}{\rho g_c}\right)^{1/2} . \qquad \text{(G.10)}$$

Since ΔP is known at each hole position x from Equation (G.8), the respective hole diameters can be calculated from

$$d = \left[\frac{4Q_o}{nK\pi(2\Delta P/\rho g_c)^{1/2}}\right]^{1/2} . \qquad \text{(G.11)}$$

Two things should be noted before calculations employing these equations are considered. First, the use of a smooth pipe equation to calculate the pipe friction is valid because plastic pipe was used. However, the actual Reynolds numbers for the experimental conditions ranged from 130000 to 270000. These values are slightly above the validity range for the pipe friction Equation (G.3), but the error introduced is small (as can be determined by a Moody Chart inspection). A pipe friction relation does exist for the range of Reynolds numbers encountered, but it is cumbersome to use because the pipe friction value cannot be solved for explicitly. Second, the assumption of uniform discharge along the pipe introduces error of unknown magnitude. It appears to be a reasonable approach because the velocity does vary in a continuous manner as the discharge holes are not points but rather are two dimensional. Also, the same average velocity would be calculated in those pipe manifold solution methods which treat each hole discretely.

An iterative process can be performed with Equations (G.8) and (G.11) in which for given inlet conditions the number of holes in the pipe can be varied to examine the effect on the hole diameters. A series of such calculations indicated that 8 holes would give roughly 1 inch diameter holes. This choice would put the holes on 3 inch centers due to the 24 inch length of the in-bed distributor pipes. This combination of hole number, diameters, and spacings was considered reasonable for a 2.5 inch diameter pipe and for the bed area the air from each hole would be required to fluidize.

When the design calculations were first performed, some errors were made in choosing the inlet conditions, so the original hole diameters were determined to be in a small range around 0.875 inches rather than on the order of 1 inch diameter as they should have been. Because the total variation in the hole diameters calculated was approximately 0.06 inches, it was felt that the probable inaccuracies in the calculations did not justify the time consuming process of boring the holes to the exact diameters calculated. Thus, the first set of holes were all drilled 0.875 inches in diameter. This combination of uniform diameter holes was dubbed hole pattern I.

As described in Chapter 7, hole pattern I failed to fluidize the bed uniformly. Thus, a new hole pattern was chosen partly on the basis of revised calculations and largely on the basis of the experience with the first pattern. The hole nearest the pipe dead end was left at 0.875 inches diameter, but each succeeding hole diameter along the pipe was increased by 0.0625 inches over the diameter of the preceding hole. This new set of hole diameters was dubbed hole pattern II.

Several differential pressure and hole diameter results calculated from Equations (G.8) and (G.11) are tabulated in Table G.1. Also included in the table are the diameters for hole patterns I and II. In all of the calculations the following values were used: $\rho = 0.07$ lbm/ft^3, $\nu = 2.01 \times 10^{-4}$ ft^2/sec, L = 2.0 ft, D = 0.194 ft, b = 0.9, K = 0.62, and n = 8. The calculations termed full flow represent a bed superficial velocity of 8.2 ft/sec, which was the average velocity measured during limestone fluidization tests. The values used for this condition were Q = 1975 ft^3/min, Q_o = 494 ft^3/min, V_o = 280 ft/sec, and $Re_o = 2.7 \times 10^5$. Calculations termed half flow represent a bed superficial velocity of 4.3 ft/sec, which was characteristic of the 2:1 velocity turndown fluidization tests. The values used for this condition were Q = 1034 ft^3/min, Q_o = 259 ft^3/min, V_o = 146 ft/sec, and $Re_o = 1.4 \times 10^5$.

The first set of calculated differential pressures and diameters in Table G.1 are for full flow at 0.20 lbf/in^2 gage inlet pressure. These are the conditions which should have been used for the initial design calculations. This inlet pressure was obtained from the rule of thumb stating that the distributor pressure drop for a fluidized bed should be approximately 10 to 30 percent of the bed pressure drop [68, p. 3-57; 112, pp. 638-639]. The pressure drop across 18 inches of limestone, which was the most frequently used bed height in the tests, is approximately 1 lbf/in^2. Thus, taking 20 percent of 1 lbf/in^2 gives the 0.20 lbf/in^2 used. Returning to the first set of data in the table, although the calculated differential pressure increases along the pipe by a factor of about 2.5 due to the pressure regain from deceleration,

TABLE G.1

CALCULATED[1] PIPE MANIFOLD DIFFERENTIAL PRESSURES AND HOLE DIAMETERS[2]

Hole No.	Position[3]	Actual Hole Diameter		P_o=0.20 lbf/in^2, Full Flow		P_o=0.05 lbf/in^2, Half Flow		P_o=1.13 lbf/in^2, Full Flow	
		Pattern I	Pattern II	Diff.Press.	Diameter	Diff.Press.	Diameter	Diff.Press.	Diameter
1	1.5	0.875	1.313	0.26	1.280	0.07	1.304	1.19	0.875
2	4.5	0.875	1.250	0.37	1.174	0.09	1.190	1.30	0.856
3	7.5	0.875	1.188	0.46	1.109	0.12	1.123	1.39	0.841
4	10.5	0.875	1.125	0.54	1.067	0.14	1.078	1.47	0.830
5	13.5	0.875	1.063	0.60	1.038	0.16	1.048	1.53	0.821
6	16.5	0.875	1.000	0.65	1.018	0.17	1.027	1.58	0.815
7	19.5	0.875	0.938	0.68	1.006	0.18	1.014	1.61	0.811
8	22.5	0.875	0.875	0.70	1.000	0.18	1.008	1.63	0.809

[1] Using Equations (G.8) and (G.11).

[2] Differential pressures are in lbf/in^2 gage and hole diameters are in inches.

[3] Distance, in inches, of the hole center from the pipe entrance.

the variation in the calculated hole diameters from the largest to the smallest is only on the order of 0.25 inches.

The second set of calculated differential pressures and diameters in Table G.1 are for half flow at a 0.05 lbf/in^2 gage inlet pressure. The percent increase in the differential pressure along the pipe and the variation in hole diameters are of about the same magnitude as those of the first set. However, each respective hole diameter calculated at half flow is slightly larger than the calculated diameter at full flow. Therefore, the hole diameters are a function of the inlet pipe conditions. This conclusion is also apparent from Equation (G.8) in which the local differential pressure is a function of the inlet pressure, velocity, and fluid properties. Thus, theoretically, a given set of hole diameters will yield uniform flow at only one set of inlet conditions. However, from a practical viewpoint, the degree of nonuniformity is quite small judging from the slight difference in hole diameters (less than 0.025 inches) predicted for full flow versus half flow conditions.

The third set of calculated differential pressures and diameters in Table G.1 are for full flow at an inlet pressure of 1.13 lbf/in^2 gage, which was the actual inlet pressure measured at full flow with hole pattern II in place. It is interesting to note that the hole diameters predicted in this case are not too different from the uniform hole diameters of hole pattern I. In fact, the total hole area for hole pattern I is only 10.5 percent higher than that of these holes. However, at equivalent full flow conditions, hole pattern I produced a measured differential pipe pressure of 1.45 lbf/in^2 whereas these calculations would predict this differential to be less than

1.13 lbf/in^2. Thus, the error in these calculations is approximately 30 percent. The underprediction by the theoretical equations of the pipe pressure differential is also observed by comparing the diameters of hole pattern II to those in the first set of calculated data in the table. Although the individual hole areas are distributed differently for these two cases, the total hole areas differ by less than 3 percent. Yet the difference between the inlet pressure measured with hole pattern II and that used in the calculations is approximately 0.9 lbf/in^2. So, to reiterate, the theoretical equations predict hole diameters that are too small for a given pipe differential pressure, or equivalently, the measured pipe differential pressure is significantly larger than that predicted for a given set of hole diameters.

Much simpler calculations than those just described predict that hole pattern I will not fluidize the bed uniformly for the given inlet flows. Boucher [105] gives two rules of thumb to determine if the maldistribution of flows from a perforated pipe with uniform diameter holes will be less than plus or minus 5 percent of the total flow. These rules state that the ratio of the inlet stream kinetic energy to the total pressure differential across the distributor pipe and the ratio of the pipe friction loss to the total pressure differential across the distributor pipe should both be equal to or less than 0.1. Using experimental measurements, the kinetic energy ratio is 0.53 at full flow conditions and 0.43 at half flow. Thus, this is an example of the case discussed by Senecal [106] in which the largest discharge is near the dead end of the perforated pipe because momentum and kinetic energy dominate. Using experimental measurements the pipe friction ratio at full flow conditions is 0.06 and at half flow it is

0.13. Thus, the effect of pipe friction on flow maldistribution is negligible at full flow and small at half flow.

The manifold flow theory was not as fully researched or developed as might have been possible. In the interest of time and due to the experimental nature of the project, it was judged to be profitable to employ intuition and experience in conjunction with the theoretical results when choosing the hole diameters. The goal of the project has been to build and test a coal feeder; not to investigate the theoretical aspects of pipe manifold flow.

APPENDIX H

PIPE GRID FEEDER REDUCED EXPERIMENTAL DATA

The following tables contain reduced experimental air flow, fluidization, and coal feeding data measured during the pipe grid feeder tests, which included all three configurations of the in-bed pipes. The heat transfer tube assembly was installed during these tests. The limestone bed heights are the corrected slumped heights. For hole pattern I up the bed height given is the height of material above the in-bed distributor pipe holes. The feeder and bed differential pressures are the measured values, and thus contain the effect of the 2.5 inches of limestone below the lower bed pressure tap for the hole pattern I down and the hole pattern II down configurations.

TABLE H.1

PIPE GRID FEEDER AIR FLOW

Hole Pattern I Down		Hole Pattern I Up		Hole Pattern II Down		In-Bed Pipes Removed	
Superficial Velocity ft/sec	Feeder ΔP lbf/in^2	Superficial Velocity ft/sec	Feeder ΔP lbf/in^2	Superficial Velocity ft/sec	Feeder ΔP lbf/in^2	Superficial Velocity ft/sec	Exterior Piping ΔP[1] lbf/in^2
3.7	0.62	3.4	0.58	3.5	0.53	3.5	0.42
4.6	0.97	4.3	0.93	4.3	0.74	4.4	0.64
5.5	1.43	5.2	1.36	5.2	1.21	5.3	0.96
6.4	1.93	6.1	1.85	6.1	1.57	6.2	1.29
7.4	2.48	7.0	2.35	7.0	2.04	7.2	1.68
7.5	2.56	7.3	2.53	7.4	2.29	7.6	1.89
8.2	3.04	8.2	3.08	8.0	2.57	8.2	2.14
				8.4	2.79	8.5	2.29

[1] Includes the expansion loss from the 2.5 inch pipe into the bed.

TABLE H.2

PIPE GRID FEEDER HOLE PATTERN I DOWN WITH A 5.8 INCH BED HEIGHT

Superficial Velocity ft/sec	Feeder ΔP lbf/in^2	Bed ΔP lbf/in^2	Lower Bed Press. Fluct. $\pm$ inches of water	Lower Bed Press. Freq. cycles/sec	Bed Expansion %
3.6	0.62	0.15	0.1	4.0	-
4.5	0.97	0.15	0.2	3.9	-
5.4	1.43	0.15	0.3	3.8	-
6.3	1.92	0.16	0.4	3.9	8.6
7.3	2.52	0.16	0.6	3.9	17.2
8.3	3.02	0.16	1.4	3.7	22.4

TABLE H.3

PIPE GRID FEEDER HOLE PATTERN I DOWN WITH A 9.8 INCH BED HEIGHT

Superficial Velocity ft/sec	Feeder ΔP lbf/in^2	Bed ΔP lbf/in^2	Lower Bed Press. Fluct. $\pm$ inches of water	Lower Bed Press. Freq. cycles/sec.	Bed Expansion %
3.6	0.65	0.34	0.2	3.9	2.4
4.5	1.00	0.34	0.4	3.4	2.4
5.5	1.44	0.35	0.7	3.7	5.5
6.4	1.94	0.35	1.3	3.0	11.2
7.3	2.46	0.37	1.4	3.0	16.3
8.1	2.90	0.39	2.0	2.9	23.1
8.2	3.03	0.40	2.2	2.8	27.1

TABLE H.4

PIPE GRID FEEDER HOLE PATTERN I DOWN WITH A 14.9 INCH BED HEIGHT

Superficial Velocity ft/sec	Feeder ΔP lbf/in^2	Bed ΔP lbf/in^2	Lower Bed Press. Fluct. $\pm$ inches of water	Lower Bed Press. Freq. cycles/sec	Bed Expansion %
3.5	0.65	0.63	0.4	-	2.0
4.4	0.97	0.66	0.9	3.3	7.4
5.3	1.42	0.67	1.5	3.1	16.8
6.3	1.91	0.68	2.3	2.9	22.1
7.1	2.36	0.69	3.0	2.6	28.2
7.8	2.77	0.70	3.0	2.8	34.2
8.1	2.90	0.72	3.5	2.7	36.2

TABLE H.5

PIPE GRID FEEDER HOLE PATTERN I UP WITH A 3.6 INCH BED HEIGHT

Superficial Velocity ft/sec	Feeder ΔP lbf/in^2	Bed ΔP lbf/in^2	Lower Bed Press. Fluct. $\pm$ inches of water	Lower Bed Press. Freq. cycles/sec	Bed Expansion %
3.7	0.68	0.09	0.1	-[1]	13.9[2]
4.6	0.98	0.08	0.1	-	20.8
5.6	1.48	0.07	0.1	-	31.9
6.5	1.95	0.07	0.1	-	31.9
7.5	2.60	0.06	0.2	-	20.8
8.3	3.10	0.06	0.2	-	6.9

[1]The pressure fluctuations were negligible with the low bed height.

[2]The bed expansions have very little meaning due to the spouting which occurred at the low bed height.

TABLE H.6

PIPE GRID FEEDER HOLE PATTERN I UP WITH A 7.3 INCH BED HEIGHT

Superficial Velocity ft/sec	Feeder ΔP lbf/in^2	Bed ΔP lbf/in^2	Lower Bed Press. Fluct. $\pm$ inches of water	Lower Bed Press. Freq. cycles/sec	Bed Expansion %
3.7	0.68	0.27	0.3	3.4	5.5
4.6	1.02	0.27	0.4	3.7	5.5
5.6	1.45	0.26	0.5	4.0	11.0
6.5	1.88	0.26	0.5	3.7	16.6
7.5	2.49	0.25	0.6	4.0	23.4
8.4	3.02	0.24	0.7	4.3	23.4

TABLE H.7

PIPE GRID FEEDER HOLE PATTERN II DOWN WITH A 4.7 INCH BED HEIGHT

Superficial Velocity ft/sec	Feeder ΔP lbf/in^2	Bed ΔP lbf/in^2	Lower Bed Press. Fluct. $\pm$ inches of water	Lower Bed Press. Freq. cycles/sec	Bed Expansion %
3.6	0.52	0.12	0.2	-	2.7
4.5	0.83	0.12	0.2	4.8	3.2
5.5	1.22	0.13	0.3	5.0	5.9
6.4	1.65	0.13	0.3	4.4	16.7
7.3	2.10	0.13	0.5	4.2	22.0
7.6	2.28	0.14	0.6	4.6	24.7
8.3	2.63	0.14	0.8	4.1	27.4

TABLE H.8

PIPE GRID FEEDER HOLE PATTERN II DOWN WITH A 10.4 INCH BED HEIGHT

Superficial Velocity ft/sec	Feeder ΔP lbf/in^2	Bed ΔP lbf/in^2	Lower Bed Press. Fluct. $\pm$ inches of water	Lower Bed Press. Freq. cycles/sec	Bed Expansion %
3.6	0.53	0.40	0.3	3.8	0.8
4.4	0.80	0.41	0.5	4.0	5.1
5.4	1.18	0.41	1.0	4.0	9.9
6.3	1.59	0.43	1.4	4.0	14.7
7.2	2.06	0.44	1.8	3.6	22.4
7.4	2.15	0.44	1.9	3.4	24.3
8.2	2.59	0.46	2.2	3.0	28.2

TABLE H.9

PIPE GRID FEEDER HOLE PATTERN II DOWN WITH A 15.4 INCH BED HEIGHT

Superficial Velocity ft/sec	Feeder ΔP lbf/in^2	Bed ΔP lbf/in^2	Lower Bed Press. Fluct. $\pm$ inches of water	Lower Bed Press. Freq. cycles/sec	Bed Expansion %
3.6	0.47	0.67	0.6	3.8	0.6
4.5	0.83	0.70	1.2	3.0	7.1
5.4	1.21	0.71	2.0	3.2	13.0
6.3	1.58	0.72	2.5	3.0	18.2
7.3	2.09	0.75	3.0	2.7	27.3
8.2	2.57	0.76	3.2	2.8	34.4

TABLE H.10

PIPE GRID FEEDER HOLE PATTERN II DOWN WITH A 21.1 INCH BED HEIGHT

Superficial Velocity ft/sec	Feeder ΔP lbf/in^2	Bed ΔP lbf/in^2	Lower Bed Press. Fluct. $\pm$ inches of water	Lower Bed Press. Freq. cycles/sec	Bed Expansion %
3.4	0.56	1.00	0.7	-	4.7
4.2	0.79	1.05	1.7	2.8	10.2
5.1	1.12	1.08	3.2	2.4	18.5
6.0	1.53	1.09	4.0	2.5	23.2
6.9	1.94	1.11	4.5	2.6	28.9
7.8	2.36	1.11	4.5	2.4	36.5

TABLE H.11

PIPE GRID FEEDER COAL FEEDING

Hole Pattern	Corrected Limestone Bed Height inches	Superficial Velocity ft/sec	% IC							
			Port	Compartment			Port	Compartment		
				A	B	C		A	B	C
I Down	14.9	8.0	4	2.45	2.39	1.65	1	1.58	1.68	5.23
I Down	14.9	7.8	4	3.18	2.09	2.01	1	1.61	1.67	2.58
I Down	14.9	7.8	3	2.29	1.76	1.52	2	1.91	1.70	1.74
I Down	14.9	7.8	3	2.91	1.67	1.87	2	2.29	1.62	2.21
I Down	14.7	7.7	4	2.87	2.50	2.14	3	2.39	1.52	1.36
I Down	14.5	3.9	4	1.85	1.38	1.81	3	0.74	0.36	1.34
II Down	15.4	8.2	3	1.48	1.40	1.41	2	1.72	1.13	1.95
II Down	15.4	7.9	4	1.82	1.75	2.88	1	2.52	1.76	2.72
II Down	15.4	7.9	4	2.26	1.71	1.73	3	2.10	1.80	1.68
II Down	15.4	4.0	4	1.09	0.86	0.83	3	1.50	0.65	0.97
II Down	21.1	7.9	5	2.07	1.19	1.28	6	1.23	1.39	1.39
II Down	21.1	4.0	5	0.57	0.75	1.08	6	0.64	0.57	0.40

APPENDIX I

TAPED PERFORATED PLATE REDUCED EXPERIMENTAL DATA

The following three tables contain reduced experimental fluidization data measured during tests of the taped perforated plate air distributor. The heat transfer tube assembly was installed during these tests. The limestone bed heights are the corrected slumped heights. The plate and bed differential pressures are the measured values, and thus contain the effect of the 2.5 inches of limestone below the lower bed pressure tap.

The air test results for the taped perforated plate are plotted in Figure 6.5 on page 88. The simulated coal feeding test results, including an analysis, are in Table 7.9 on page 154.

TABLE I.1

TAPED PERFORATED PLATE WITH A 10.3 INCH BED HEIGHT

Superficial Velocity ft/sec	Plate ΔP lbf/in^2	Bed ΔP lbf/in^2	Lower Bed Press. Fluct. $\pm$ inches of water	Lower Bed Press. Freq. cycles/sec	Bed Expansion %
3.6	0.32	0.38	0.1	-	2.5
4.5	0.49	0.42	0.5	-	11.7
5.4	0.64	0.45	1.7	1.9	19.3
6.4	0.81	0.48	2.2	1.8	33.0
7.3	1.06	0.46	4.0	1.9	41.1
7.8	1.17	0.48	4.5	2.0	49.2
8.3[1]	1.31	0.48	5.0	1.9	57.4
8.7[1]	1.44	0.47	4.5	1.6	62.9

[1] These velocities may be incorrect due to a possible error in the transport air flow measurement.

TABLE I.2

TAPED PERFORATED PLATE WITH A 15.2 INCH BED HEIGHT

Superficial Velocity ft/sec	Plate ΔP lbf/in^2	Bed ΔP lbf/in^2	Lower Bed Press. Fluct. $\pm$ inches of water	Lower Bed Press. Freq. cycles/sec	Bed Expansion %
3.6	0.32	0.59	0.1	-	1.7
4.6	0.45	0.67	1.7	1.9	8.1
5.5	0.65	0.68	3.5	2.0	16.6
6.4	0.83	0.70	4.0	2.0	22.3
7.4	1.01	0.73	4.5	1.9	32.3
7.8	1.15	0.71	5.0	1.8	38.0
8.4[1]	2.07	0.72	5.7	1.9	44.4

[1] This velocity may be incorrect due to a possible error in the transport air flow measurement.

TABLE I.3

TAPED PERFORATED PLATE WITH A 16.0 INCH BED HEIGHT

Superficial Velocity ft/sec	Plate ΔP lbf/in^2	Bed ΔP lbf/in^2	Lower Bed Press. Fluct. $\pm$ inches of water	Lower Bed Press. Freq. cycles/sec	Bed Expansion %
3.4	0.32	0.59	0.1	-	1.7
4.3	0.50	0.66	0.2	-	6.8
5.2	0.65	0.72	3.0	1.8	14.3
6.2	0.88	0.72	3.8	2.0	23.8
7.2	1.10	0.73	4.5	2.0	29.3
8.3[1]	1.64	0.75	5.0	2.0	38.1

[1]This velocity may be incorrect due to a possible error in the transport air flow measurement.

APPENDIX J

PIPE GRID FEEDER PRESSURE DROPS

The expected pressure drop through the pipe grid feeder exterior pipes (upstream of the in-bed pipes) can be calculated for comparison with the measured pressure drop. This pressure drop is a combination of the pipe friction losses and the fitting losses (the so called minor losses).

The pipe friction losses for turbulent flow can be calculated from the relation

$$\Delta P = f \frac{L}{D} \frac{\rho V^2}{2g_c} . \tag{J.1}$$

By calculating the flow Reynolds number,

$$Re = \frac{VD}{\nu} , \tag{J.2}$$

and noting that PVC pipes are classified as smooth pipes, the friction factor f can be obtained from the Moody Chart or from one of the several published correlations for smooth pipes.

The minor losses can be calculated from the relation

$$\Delta P = K' \frac{\rho V^2}{2g_c} \tag{J.3}$$

where the loss coefficient K' can be obtained from a reference with tabulated values.

The pipe friction and minor losses for the pipe grid feeder exterior pipe section were calculated at flows of 1057 ft^3/min (termed half flow) and 1975 ft^3/min (termed full flow). These two flow rates correspond to bed superficial velocities of 4.4 ft/sec and 8.25 ft/sec, respectively. Summarized, the exterior pipe losses calculated were:

	Half Flow	Full Flow
Friction Losses, lbf/in^2	0.04	0.12
Minor Losses, lbf/in^2	0.47	1.64
Total Losses, lbf/in^2	0.51	1.76

To see how these calculated losses compared with the measured losses, air flow tests were performed with the in-bed pipes removed. However, in order to compare the two sets of losses, the expansion loss from the 2.5 inch pipes into the bed had to be taken into account. This loss is a type of minor loss also, so Equation (J.3) was used with a loss coefficient of 0.99. For half flow conditions the expansion loss was calculated to be 0.18 lbf/in^2 while at full flow it was 0.62 lbf/in^2.

The calculated expansion losses were added to the previously given exterior pipe losses. These two sets of combined losses can then be compared to the total losses measured as follows:

	Half Flow	Full Flow
Calculated Losses, lbf/in^2	0.69	2.38
Measured Losses, lbf/in^2	0.67	2.16
Percent Difference, %	3.0	10.2

The calculated values compare well with the measured values, especially considering the number of fittings and short pipe segments involved. Because it is not known whether one or both of the calculated values, i.e., exterior pipe loss and/or expansion loss, is in error, a set of correction factors was generated which reduces both losses proportionately to give the proper total measured loss. Then, expansion losses were calculated and corrected for all of the flow conditions under which air tests were performed. The corrected expansion losses were subtracted from the total losses measured with the in-bed pipes removed to give the best estimate of the actual pressure drop through the exterior pipes. These are the values which are plotted as a function of the bed superficial velocity in Figure 7.7 on page 137.

Therefore, by being able to estimate the pressure drop through the exterior pipes at the various flow conditions, these pressure drops could then be subtracted from the total pressure drop measured across the pipe grid feeder with the in-bed pipes installed to give the pressure drop across the in-bed pipes themselves. These latter values are plotted as a function of bed superficial velocity for hole patterns I and II down in Figure 7.8 on page 138.

It should be noted that the calculations for predicting the pressure drops across the in-bed pipes, outlined in Appendix G, were not nearly as accurate as these calculations for the exterior pipes. The inlet pressure for the in-bed pipes used in that appendix were determined by subtracting the exterior pipe pressure drop, as calculated above, from the measured plenum box pressure.

VITA

Gary David Knox was born on March 26, 1954, in Columbia, Tennessee, as the second of three children. He accepted Jesus Christ as personal Lord and Savior on March 22, 1964. After attending schools in Columbia through the twelfth grade, he graduated from Central High School in May 1972. During these years he worked part-time on the family farm on which he was raised. In September 1972 he entered Tennessee Technological University and in June 1978 received a Bachelor of Science degree in Engineering Science. During this time he worked a total of two years as a cooperative education student at the United States Government's Savannah River Plant and Savannah River Laboratory in Aiken, South Carolina. In June 1978 he entered the Graduate School of the University of Tennessee, Knoxville, under a Hilton A. Smith graduate fellowship. He held a graduate research assistantship during the work on this thesis and then received the Master of Science degree in Mechanical Engineering in March 1981.

The author is a member of the American Society of Mechanical Engineers, Tau Beta Pi, Phi Kappa Phi, and Mortar Board and was included in the 1976 edition of Who's Who in American Colleges and Universities. He will be employed by Sverdrup/ARO at the Arnold Engineering Development Center following graduation.

He is happily married to the former Melissa Grove of Dunlap, Tennessee.